Supplement of the Progress of Theoretical Physics, No. 16, 1960

Heavy Primary Cosmic Radiations

——*Prince Albert Project*——

H. AIZU,* Y. FUJIMOTO, S. HASEGAWA, M. KOSHIBA,+
I. MITO,** J. NISHIMURA and K. YOKOI

Institute for Nuclear Study, University of Tokyo, Tokyo
**Department of Physics, Rikkyo University, Tokyo*++
***Department of Physics, Konan University, Kobe*

Contents

+ On leave to University of Chicago, Illinois, U. S. A.
++ On leave to North-Western University, Illinois, U. S. A.

Abstract

A systematic investigation on the heavy primary cosmic radiation is made on the basis of extensive analysis of the Prince Albert Stack. The experimental methods used in nuclear emulsion work for the determination of the charge and energy of the heavy primary are critically discussed and summarized.

The experimental result described here is the first, and to date the only one, to give information on the rigidity spectrum of various components of heavy primaries in the low rigidity region. The general shape of the spectrum, common to all components, is found to have a broad maximum which falls around 2.2 Gv with a width of about 0.6 Gv.

The flux values above the atmosphere of the various components are as follows (in units of particles/m²•sec•sterad.):

	$1.3<R<2.7$ Gv	$R>2.7$ Gv
He	40.6 ±5.2	81.1 ±7.2
L	1.15±0.13	1.61±0.15
M	3.64±0.32	6.39±0.80
H	1.24±0.16	1.87±0.18.

The effect of solar activity on the heavy primary cosmic radiation is discussed on the basis of the observations by the present authors compared with others.

Our knowledge of the chemical composition of heavy primaries and its comparison with the astrophysical data on the abundance of various elements enable us to discuss the origin of cosmic rays. The chemical composition of heavy primaries has the following remarkable features:

(i) Fe group elements are overabundant as compared with their abundance in usual stars.

(ii) C is overabundant in C, N and O group elements as compared with usual stars.

(iii) Ne is underabundant when compared with its abundance in stars and, at the same time, the abundance of Ne is comparable to that of Mg.

(iv) On the whole, it is very similar to that of planetary nebulae up to elements of $Z\sim14$.

This fact as well as the consideration about the production efficiency of the cosmic ray particles makes it very plausible to consider that the main contribution to the cosmic ray component up to $Z\sim14$ seems to come from late-stage giant stars whereas supernovae account for the component of $Z\gtrsim20$.

Introduction

For hundreds of years, astronomers have been observing the celestial bodies only through the optical telescopes. Only quite recently the solar and the cosmic radio waves have been discovered, and the observations using these waves are giving us much information as to the mechanism of the solar burst, the structure of the spiral arm of the galaxy and so on.

At present we have the third method to explore our universe besides these optical and radio wave observations. This is the investigation of the cosmic rays.

In 1949, Minneapolis group[0001] first discovered the existence of the heavy primaries in the cosmic radiation using nuclear emulsion exposed at high altitude by a huge plastic balloon. After this discovery, the importance of the cosmic rays in understanding cosmic phenomena has been widely recognized. Cosmic rays are now known to be composed not only of protons but also of nuclei of various elements, He, Li, Be, and so on. Under the present experimental limitations it is confirmed that cosmic rays contain almost every element in the periodic table up to the iron group. It is probable that they should contain heavier elements, too, but with much smaller abundances.

These particles are precious samples of matter of our universe carried to the earth from far outside of the solar system. Their chemical composition and isotopic abundance tell us stories of the element synthesis which occurred in the source of cosmic rays. Since the element synthesis is understood to be necessarily followed by the stellar evolution, these pieces of information will show what part of the life history of a star is closely connected with the cosmic rays. Hayakawa and his collaborators have already pointed out that supernova would be mostly responsible for cosmic ray production.[0002]

The energy spectrum and the time variation of the intensity of heavy primaries give us another important information. One can guess from them how the particles are accelerated, decelerated and scattered in their long traversal through the stellar atmosphere, the interstellar space and the interplanetary space. Properties of magnetohydrodynamic behavior of plasma clouds occupying these spatial regions will be made clear through such investigations.

Unfortunately, only little is known about the energy spectrum of heavy primaries. Most of the works carried out so far were concerned with the flux measurements of various heavy primary components in a restricted narrow energy range, say, from one Gev/nucleon to ten Gev/nucleon. Systematic investigations have not been made either in the higher or in the lower energy region of heavy primaries excepting the α-particle component. This situation makes our understandings of cosmic ray phenomena very unsatisfactory.

An extensive study of heavy primaries, particularly in the lower energy region, has been carried out since 1957 by the collaboration work of the cosmic ray group of Institute for Nuclear Study, Tokyo and of the University of Chicago. This project is called "the Prince Albert Project",[0003] as the balloon exposure was made at Prince Albert, Canada, geomagnetic latitude 61°N. Because of the high geomagnetic latitude and the high altitude balloon flight, observations could be made down to very low energy, for example, 115 Mev/nucleon for α-particles, 220 Mev/nucleon for C

nuclei. Thus it is now possible to make a systematic investigation of energy spectra of various heavy primary components in the energy region of several hundred Mev/nucleon and higher.

This article is intended to cover a review of information on heavy primary experiments, particularly on our collaboration work, the Prince Albert Project. Chapter 1 is devoted to the experimental technique of emulsion work applied to the determination of charge and energy of the heavy primaries. Details are given on ionization and velocity measurements which are necessary for the investigation on non-relativistic tracks. In Chapter 2, the whole experimental results of the Prince Albert Project are presented together with a review of results by other authors in the Gev/nucleon energy region. Experimental results obtained at the balloon altitudes have to be corrected for the interactions in the residual atmosphere. Furthermore, correction is necessary for the interaction in the interstellar space when one wants to see the heavy primaries at the origin. § 1 of Chapter 3 gives a description of such correction procedures.

Finally at the rest of Chapter 3, the astrophysical significance of the information from heavy primary experiment is discussed.

The Prince Albert Project revealed several interesting properties of the heavy primaries.

All components of heavy primaries, alpha, light, medium and heavy nuclei, appear to have the rigidity spectrum of the same shape. This spectrum is found to have a broad maximum around 2.2 Gv with a half width of about 0.6 Gv. Furthermore, comparison of our data with other observations seems to suggest the existence, at the concerned energy region, of large time variation of the flux connected with the variation of the solar activity. With this new information on the energy spectrum, together with the data of element abundances and the time variation, we discuss the origin of cosmic rays, the acceleration mechanism, and the modulotion effect of solar activity.

Chapter 1. Experimental Procedures

Prince Albert Project was started in 1957 to see the detailed features of charge distribution and energy spectra of the heavy primaries, especially at the low energy side. As we are mainly concerned with the low energy heavy primaries, the energy and the charge must be measured simultaneously, and this makes our analysis more complicated than in the case of relativistic particles. The analysis was made combining the several methods usually adopted in the heavy primary investigations; and in some cases new techniques had to be developed for the analysis.

Here we will give the general review of the exposure, scanning and

the other problems involved in the heavy primary work, and finally discuss the techniques for charge and energy determination of heavy primaries referring to the case of our Prince Albert Project.

§ 1·1. Exposure

1·1·1. *Apparatus of exposure*

In order to make observations of heavy primaries the exposure must be made at a very high altitude, because they are easily destroyed by collisions with atmospheric nuclei. High altitude observation is all the more necessary both in the case of very heavy nuclei which have a shorter absorption mean free path and in the case of Li, Be and B which arise mainly from the fragmentation of heavier nuclei.

Most of the observations made so far, including ours in Prince Albert Project, were carried out by means of balloon-borne nuclear emulsions. Vehicles other than balloons will become as important, if they ensure as long enough flight and as sure recovery of instruments.

There have been some experiments with instruments other than nuclear emulsions.[1101] They are the combination of the Čerenkov counters and the scintillators, and sometimes the combination of the other devices. Superiority of the nuclear emulsions in the research of heavy primaries is, however, indisputable at present: as it enables us to observe several qualitatively different phenomena at the same time which reflect different natures of one and the same incident nucleus, we are in a position to determine its charge and energy with a greater certainty than with any other apparatus.

Expected flux values

For the design of the emulsion experiment, the number of the heavy primary tracks which will be observed in a certain size of emulsion stack is an important problem. As an illustration, we describe here the case of a stack containing 100 emulsion sheets, 600 μ in thickness with top edge length 10 cm, exposed for ten hours in the vertical orientation of the emulsion sheets at certain altitudes and geomagnetic cutoffs. Then we can evaluate the number of the heavy primary tracks which pass the top edge satisfying the following conditions that are usually accepted.

(1) Track length per plate should be larger than 3 mm.

(2) Zenith angle should be smaller than 30°.

These flux values are evaluated using the data reported till now, and the results are shown in Fig. 1·1·1 for the stacks exposed on a day of minimum solar activity at various altitudes and geomagnetic cutoffs.

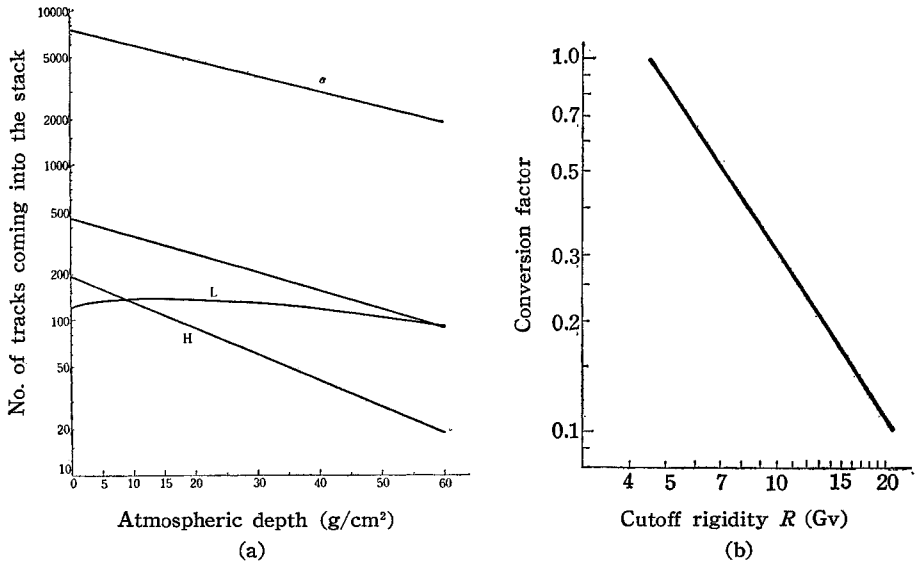

Fig. 1•1•1. Fig. 1•1•1(a) gives the expected number of heavy primary tracks at various atmospheric depths coming into an emulsion stack containing 100 emulsion sheets, each 600 μ in thickness with top edge 10 cm, exposed in the vertical orientation of the emulsion sheets at the location with geomagnetic cutoff rigidity of 4.5 Gv (geomagnetic latitude ~41°) for 10 hours. Only the tracks which satisfy the following scanning criteria are considered:

(i) Track length per plate should be larger than 3 mm.
(ii) Zenith angle should be smaller than 30°.

The expected number of tracks at other locations can be obtained by multiplying the conversion factors given in Fig. 1•1•1(b) to the values given in Fig. 1•1•1(a). At present there is no statistically reliable data of the solar-calm period at the locations with geomagnetic cutoff rigidity lower than 4.5 Gv.

1•1•2. *Prince Albert Exposure*

In the Prince Albert Project, an exposure was carried out at geomagnetic latitude 61°N, Canada. The corresponding nominal geomagnetic cut-off energy as given by Webber[1103] is 0.1 Gev/nucleon for primary nuclei with $A=2Z$, where A and Z are the mass number and the nuclear charge, respectively.

As shown in Fig. 1•1•2, the stack consisted of 200 pellicles of Ilford G5 emulsions of dimensions 600 $\mu \times 15$ cm $\times 10$ cm and was exposed with the 10 cm side vertical at an altitude corresponding to the mean amount of residual air of 5.5 g/cm². The total amount of air plus packing material and horizontal plates above the vertical emulsion sheets was equivalent to 7.6 g/cm² of air with respect to nuclear collision losses and to 2.65 cm of Ilford G5 emulsion with respect to ionization losses, respectively. In order to see the detailed features of low energy side of the heavy primaries,

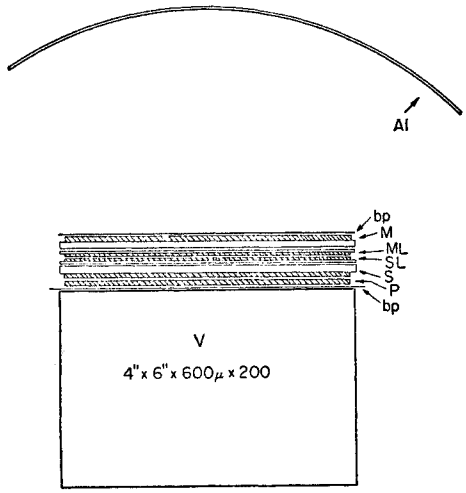

Fig. 1•1•2. Construction of the Prince Albert Stack.
Al: aluminum sphere of thickness (1/16)″
bp: black paper
M and S: glass-backed 600 μ emulsion sheets
ML and SL: lucite-backed 200 μ emulsion sheets
P : a 600 μ pellicle
V : vertical emulsion pellicles

careful corrections are necessary before analysing the data. These corrections are shown as follows.

1) *Ascent correction*

The flight curve of the Prince Albert Project is shown is Fig. 1•1•3. Balloons require a certain time to reach their ceiling altitude. Therefore the nuclei coming in the stack during the ascent should be corrected. The correction procedure in the case where ionization loss effect can be neglected is given in Appendix 2.

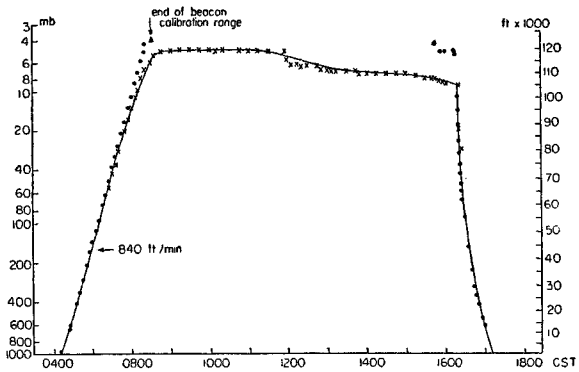

Fig. 1•1•3. The flight curve of the Prince Albert Exposure.
×: pressure determined from photographing Wallace-Tiernan gauge
•: pressure determined from radio-sonde

Ascent correction procedure used in the Prince Albert Project

For nuclei whose energy at the air-top is higher than 700 Mev/nucleon,

the ascent correction is carried out in the way explained in Appendix 2, because even an iron group nucleus of energy 800 Mev/nucleon goes through more than one absorption mean free path of air before being stopped by ionization losses.

For nuclei of lower energy the effect of ionization losses in the air has to be taken into account. Roughly speaking, the effect is not insignificant for H-nuclei of energy $<$800 Mev/nucleon, M-nuclei of energy $<$500 Mev/-nucleon, L-nuclei of energy $<$400 Mev/nucleon and for He nuclei of energy $<$300 Mev/nucleon. The ascent correction taking into account this effect is very complicated. However, at least the following is clear: the ascent correction taking into account the ionization loss effect is smaller than that which neglects this effect.

For this reason we give two sets of flux values in the case of the Prince Albert Project:

(i) the flux values without ascent correction,

(ii) the flux values with uniform ascent correction for the whole energy range.

2) *Geomagnetic cutoff correction*

A balloon does not always fly along the equi-cutoff-energy line, thus it is usually necessary to take into consideration the change in cutoff energy during a flight. In Prince Albert Exposure, however, this change is restricted only in the interval $<$120 Mev/nucleon. Therefore, except in the case of α-particles, this change turns out to be below the air cutoff energy and give no effect on the results.

3) *Air cutoff energy*

Fig. 1•1•4 gives the range-energy relations of various nuclei in the air.[1104] From this one will see the minimum energies for various nuclei to reach the vertical emulsion sheets in our stack. In order to make the ionization measurement, however, the track must have a length in the stack larger than a certain value, say about 1 cm. Minimum energies of the heavy primaries having potential range in the stack of at least 1 cm will be seen from Fig. 1•1•5 which gives the range-energy relations of various nuclei in Ilford G5 emulsion.[1105]

1•1•3. *Scanning*

The emulsion plates have to be systematically scanned for tracks of heavy primaries which are suitable for the measurements. In the scanning, the tracks are picked up under a certain criterion, restricting ionization, dip angle, and projected angle of the tracks.

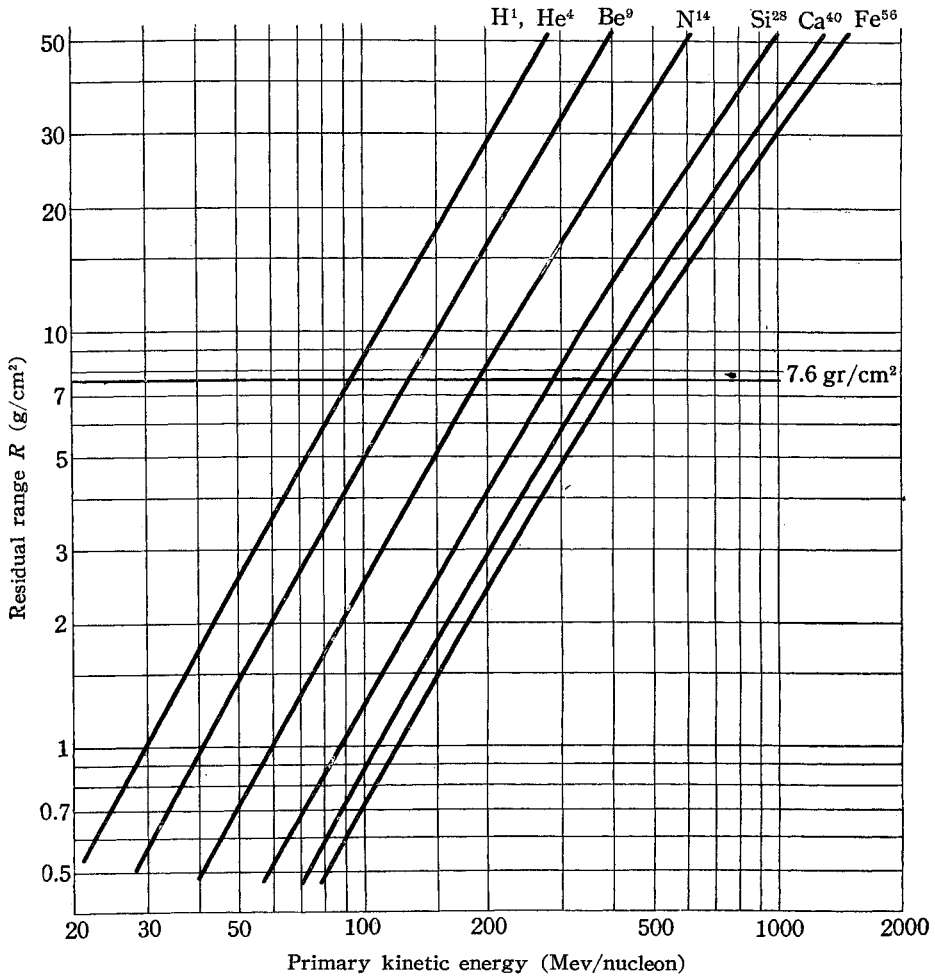

Fig. 1•1•4. Range-energy relations of various nuclei in the air. The curve for H^1 is that given in ref. 1104). The curves for other nuclei are obtained by means of the similarity law

$$R(E, A, Z) = \frac{A}{Z^2} R_p(E),$$

where A and Z are the charge and the mass number, respectively, of the nucleus in question, and $R_p(E)$ is the residual range of a proton of energy E.

1) *Dip angle criterion*

When the dip angle is larger than a certain value, say ~10°, grains of the track are closely pressed to each other due to the shrinkage of the emulsions, so that the ionization measurement becomes inaccurate.

2) *Projected angle criterion*

Acceptance of the tracks with large zenith angles gives us two com-

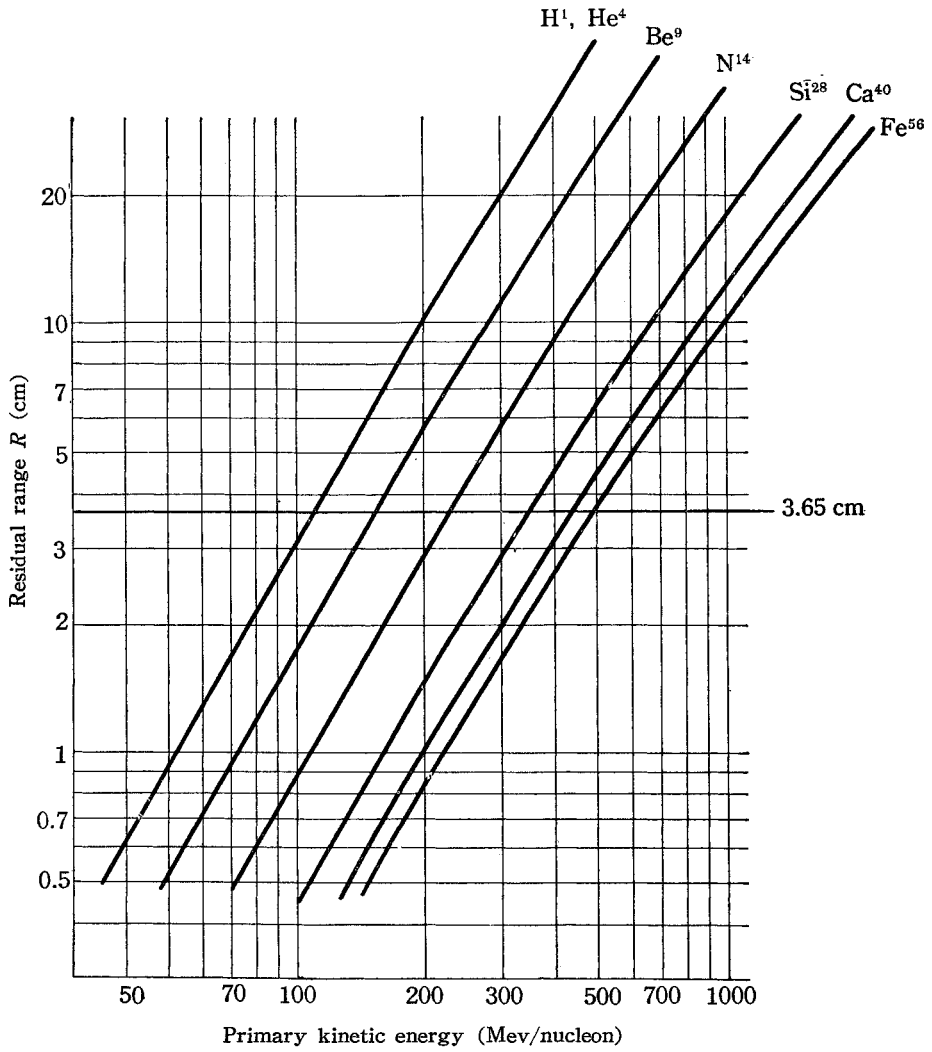

Fig. 1•1•5. Range-energy relations of various nuclei in Ilford G5 emulsion of density 3.815 gr/cm³. The curve for H^1 is given in ref. 1105). The same similarity law as in Fig. 1•1•4 is used for obtaining the curves of other nuclei.

plementary effects. It gives better statistics, but the particle with greater zenith angle must have traversed greater thickness of the atmosphere. In view of the fact that we do not have as yet the exact data on the fragmentation parameters in air, the smallest possible atmospheric depths are desirable, especially for very heavy nuclei and for Li, Be and B nuclei.

Scanning in Prince Albert Stack

In our Prince Albert Project, four independent scans, *A*, *B*, *C* and *D*, are made along the line near the top edge of every emulsion plate in the

middle part of the stack. Scan B is made to obtain better statistics and at the same time to check the scanning efficiency by comparing with scan A. This comparison showed that about 95 % of tracks satisfying the criteria were picked up without missing. Scan C is for light component and scan D is for He nuclei. Detailed criterions for scans, A, B, C and D, are given in Table 1•1•1.

Table 1•1•1. Applied scans.

Specifics \ Scan	A	B	C	D
Objective	M & H tracks	M & H tracks	L tracks	α tracks
Projected track length per plate, l	>3 mm	>3 mm	>3 mm	>6 mm
Projected zenith angle χ	<20°	<30°	<30°	<30°
Ionization	greater than that of ~2 Gev/nucleon boron nuclei	greater than that of ~2 Gev/nucleon boron nuclei	7 times greater than that of ~2 Gev protons*	2.5 times greater than that of ~2 Gev protons**
Position of scan line	at top edge	5mm below top edge	5mm below top edge	5mm below top edge
Magnification	10×1.5×10	10×1.5×10	10×1.5×10	10×1.5×10 20×1.5×10
Applied number of plates	120	160	92	7

* More specifically. the number of blobs in 260 μ of each track was counted and the tracks with less than 80 blobs were accepted.

** More specifically. the number of gaps longer than 1.8 μ was counted for a length of 270 μ of each track and the tracks with less than 20 gaps were accepted.

Conversion of the number of tracks into the flux value

Let the zenith direction be the polar axis, the zenith angle be θ, the azimuthal angle φ, the dip angle ψ, and the projected angle χ as shown in Fig. 1•1•6. Then

$$\sin\psi=\sin\theta\,\sin\varphi$$
$$\tan\chi=\tan\theta\,\cos\varphi, \qquad (1\cdot1\cdot1)$$

so that

$$\sin\theta d\theta d\varphi=\cos\psi d\psi d\chi. \qquad (1\cdot1\cdot2)$$

Therefore the solid angle Ω is given by

$$\Omega=4\chi_{max}\sin\psi_{max}, \qquad (1\cdot1\cdot3)$$

where ψ_{max} and χ_{max} are the maximum

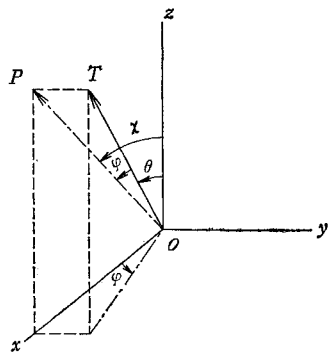

Fig. 1•1•6. Definition of angles. The plane of the emulsion surface is taken to be the x-z plane. The lines, OT and OP, represent the track and its projection into the x-z plane, respectively.

dip angle and the maximum projected angle, respectively, of acceptable tracks. The relation between the observed number of track N and the flux $\Phi(\theta)$ of the nuclei coming in a unit time within unit solid angle around the direction of zenith angle θ into a unit horizontal area is given by

$$N=4At\int_0^{\chi_{max}}\int_0^{\psi_{max}}\Phi(\theta)\cos\theta\cos\psi\,d\psi\,dx, \tag{1·1·4}$$

where A is the total horizontal area where the scanning is made and t the exposure time. (The time variation of the flux during the exposure time is neglected here.)

In usual cases the Liouville's theorem holds for the cosmic ray flux at the top of the atmosphere, which means, in particular, that $\Phi(\theta)$ is independent of θ at the top of the atmosphere. On this basis one can treat $\Phi(\theta)$ at the balloon altitude also as nearly independent of θ, if ψ_{max} and χ_{max} are so small that one can neglect the variation of path length in the air due to variation of θ. Therefore in usual cases (1·1·4) can be approximated by

$$N\approx At\Phi(0)\int_0^{\chi_{max}}\int_0^{\psi_{max}}\cos\theta\cos\psi\,d\psi\,dx. \tag{1·1·5}$$

As

$$\cos\theta=\cos\psi\cos\chi, \tag{1·1·6}$$

$$\Phi(0)\approx\frac{N}{At\sin\chi_{max}(2\psi_{max}+\sin2\psi_{max})}. \tag{1·1·7}$$

§1·2. Charge and energy determination of the heavy primaries

As mentioned at the beginning of this chapter, Prince Albert Stack was the first one that was analysed so widely to get the charge and energy distribution of heavy primaries at the low energy side.

The relative abundances of the elements in the cosmic rays directly reflect the features of the source of the cosmic rays and the mechanism of the acceleration, and also give information as to the synthesis of the elements at the source. Thus the charge and the energy must be measured as precisely as possible. As we are mainly concerned with the nonrelativistic tracks, we are faced with many difficulties in our charge and energy determination. For example, a relativistic C track shows the same ionization as that of a slow B track. As slow B is much less abundant compared with relativistic C, it is necessary to make quite precise measurements to separate slow B from the relativistic C tail. Similar situation, of course, exists for other nuclei.

The methods of the gap, blob and delta-ray countings usually adopted for measuring the ionization of the track are summarized and critically discussed, stressing the limitation of different methods. After some im-

Table 1•2•1(a). Quantities used in the ionization measurement in the Prince Albert Project.

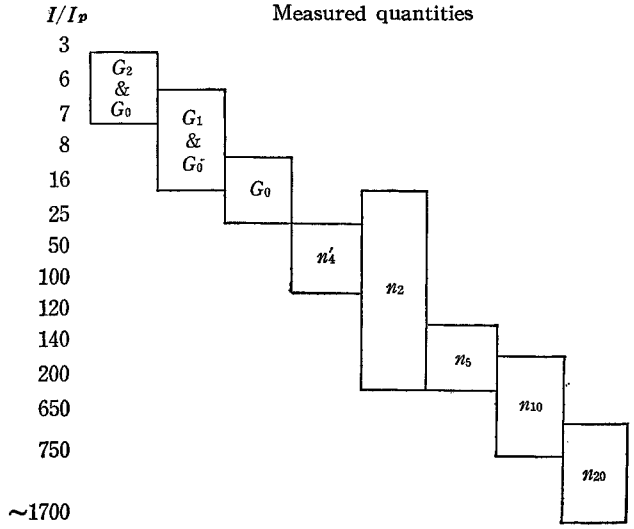

I_p : plateau ionization of protons
I : ionization to be measured
G_l : density of gaps longer than $l\,\mu$
n'_4 : 4-grain delta-ray density
n_l : density of delta rays which have their ends outside $l\,\mu$ from the primary track

Table 1•2•1(b). Methods adopted in the charge and energy determination in the Prince Albert Project.

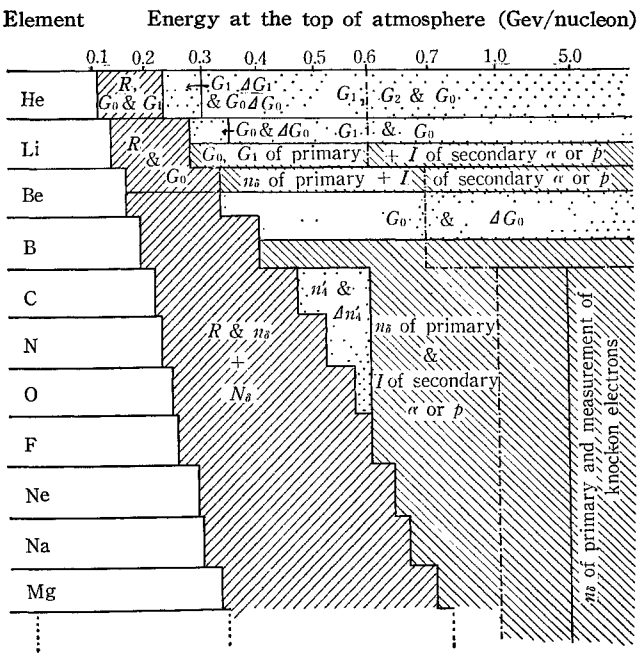

R : residual range
n_δ : delta-ray density of range convention
N_δ : total number of delta rays longer than certain values contained in a certain length of track-end
ΔG_1, ΔG_0, $\Delta n'_4$ & Δn_δ: change of respective quantities while the nucleus traverses a certain length of emulsion

ending tracks

"through" tracks

"interacting" tracks

upper limit of the energy region where detailed energy determinaton has been done

provements they are widely used in our experiment according to the strength of the ionization of the track, as summarized in Table 1·2·1.

The residual range, the variation of the ionization along the track and other quantities are measured to get the information on the energy, and by combining them with the above ionization measurements we get the final results on the charge and energy distribution of the primary particles.

Two independent methods are always applied to each track to ensure the precision of the measurements, and the results are quite satisfactory.

1·2·1. *Ionization loss*

When a charged particle passes through nuclear emulsions, it transfers energy to the electrons of atoms near the path of the particles.

If the impact parameter is large enough, it gives a small amount of energy to the electrons or only excites the atomic electrons. The small energy transfers are observed as silver grains along the track. This is the primary ionization. Secondary ionization comes from rather high energy transfer to the electrons, and they are observed as delta rays along the track.

The amount of energy loss by ionization of a nucleus with charge Z and velocity v in unit of c, the light velocity, is expressed by the following formula,[1201]

$$-\frac{dE}{dx}=\frac{2Cm}{v^2}Z^2\left[\ln\frac{4m^2v^4}{(1-v^2)^2I^2(Z')}-2v^2\right], \qquad (1\cdot2\cdot1)$$

where m is the electron mass, $I(Z')$ is the average ionization potential of the traversed matter. When the loss $-dE/dx$ is expressed per g/cm^2, the constant C is

$$C=0.150\ (Z'/A'), \qquad (1\cdot2\cdot2)$$

where Z' and A' are the atomic number and mass number of the traversed matter.

1·2·2. *Gap and blob method*

Let G_l be the density of gaps longer than l. According to O'Ceallaigh,[1202] G_l can be expressed as

$$G_l=ge^{-g(l+\alpha)}. \qquad (1\cdot2\cdot3)$$

Fowler and Perkins[1203] showed that g is proportional to the primary ionization loss in a good approximation up to about the ionization of relativistic Be nuclei. α is a constant related to the mean grain size and thus depends on the type of emulsions and the developing conditions.

The "signal" S_l associated with G_l is

$$S_l \equiv \left|\frac{\partial G_l L}{\partial g}\right| = \left|\frac{1}{g} - (l+\alpha)\right| G_l L = |1 - g(l+\alpha)| L e^{-g(l+\alpha)}, \quad (1\cdot2\cdot4)$$

while the "noise" N_l is

$$N_l \equiv (G_l L)^{1/2} = (gL)^{1/2} e^{-(1/2)g(l+\alpha)}, \quad (1\cdot2\cdot5)$$

where L is the total track length in which gaps are counted and is taken to be the maximum length for which the ionization does not change appreciably, or beyond which subjective errors begin to increase. The optimum gap length l^* in the gap counting is therefore given by the condition that

$$\frac{\partial}{\partial l}\left(\frac{S_l}{N_l}\right) = 0 \quad \text{for} \quad l = l^*, \quad (1\cdot2\cdot6)$$

i.e.,

$$l^* = \frac{3}{g} - \alpha. \quad (1\cdot2\cdot7)$$

For Fowler-Perkins coefficient g, the condition becomes, again using the relation (1·2·3),

$$l^* = \frac{2}{g} \quad (1\cdot2\cdot8)$$

in the case where $G_0 \gg G_l$, G_0 being the blob density, i.e., the density of all discernible gaps.

In the Prince Albert Stack, a minimum blob density is found to be 20~22 per 100μ. For a relativistic α-particle track which has four times minimum ionization, the blob density is 40~44 per 100μ and the optimum gap length l^* is expected to be ~2μ.

For a relativistic Li-nucleus track which has approximately the same ionization as a 200 Mev/nucleon α-particle track, blob density is ~25 and the optimum gap length is ~1μ. The method becomes impracticable for a track with ionization heavier than that of a relativistic Be, which is roughly equivalent to a ~100 Mev α-particle.

The limit of applicability of the blob-gap method is of course dependent on the types of emulsions and the developing conditions.

In the case of Ilford G5 emulsions whose degree of development is smaller than that of the Prince Albert Stack, the method will be applicable to tracks of heavier nuclei.[+]

1·2·3. *Blob counting*

The method of blob counting for ionization measurement is being widely used, because the elaborate work of gap counting can be avoided and,

[+] Although for these tracks g is no more proportional to ionization and an empirical relation between them should be established instead.

furthermore, for heavier ionizing tracks gap counting becomes practically impossible.

There are several points which must be particularly mentioned regarding the blob counting method. If one plots the relation between blob density and ionization of the particle, one has a series of curves of different forms for different emulsion stacks as shown in Fig. 1•2•1. This shows that the

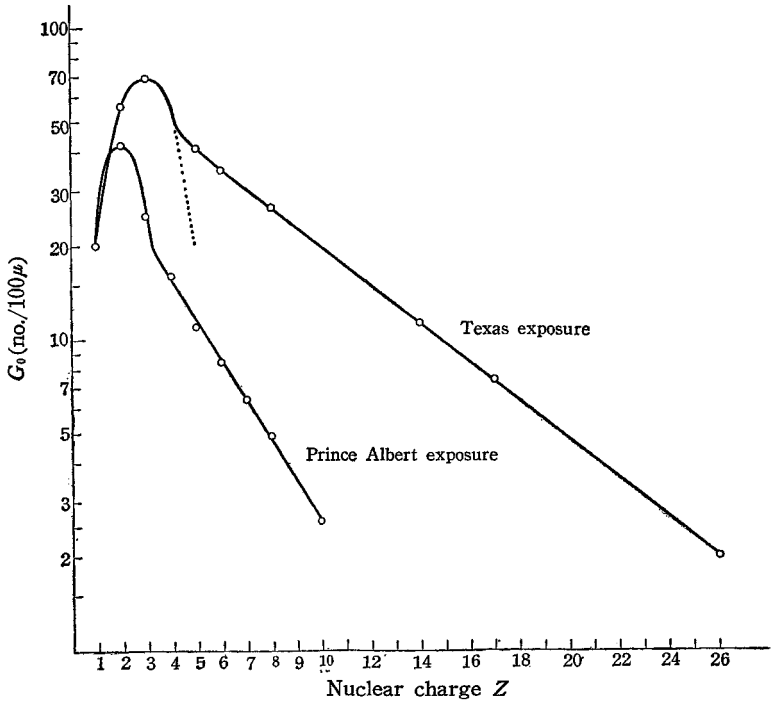

Fig. 1•2•1. Relation between blob density, G_0, and nuclear charge, Z.
∘ : Calibrated by delta-ray counting and/or examination of break-up.
···: Curves which would be expected if G_0 were proportional to $g\exp(-g\alpha)$, where $g \propto Z^2$ and α is a constant which depends only on the developing conditions.

relation is dependent strongly on the properties of emulsion and development. Therefore complete calibration is necessary to remove possible plate-to-plate variation in the same stack. Precaution should also be taken to avoid variation of degree of development due to the difference in position and depth in an emulsion sheet.

If one looks at the decrease of blob density with increasing ionization, one always find a kink. This seems to suggest that the mechanism responsible for producing a blob is different before and after the kink. One might be able to interpret that the kink shows a kind of saturation effect and beyond this kink the variation of g with ionization depends mainly on the sensitivity distribution of silver halide crystals. This tells

us that the fluctuation of blob density due to variation of emulsion sensitivity and degree of developing will be particularly large in the region beyond the kink, so a careful calibration is essential for the blob measurement of heavy primaries.

Blob measurement in Prince Albert Project

As shown in Fig. 1•2•1 the Prince Albert Stack was rather over-developed, so that the blob density is considerably less than other stacks. Still the blob method can be used for tracks with ionization equivalent to that of light and medium nuclei. The calibration of the blob density was carried out by using light or medium nucleus tracks which are identified as relativistic from their interaction.

1•2•4. *Delta-ray counting*

The delta-ray counting method is widely used for ionization measurement for ionizations greater than those of, say, relativistic boron nuclei.

The theoretical formula giving the variation of the delta-ray density with charge Z and velocity v of an ion is, as is well known, derived from the Rutherford scattering cross-section.

In view of the fact that the formula also applies to the case of high energy knock-on electrons which will be discussed in the following subsection, we shall give its detailed form here.

The differential scattering cross-section of an electron of velocity v by a bare point nucleus of charge Z at rest is given by

$$\frac{d\sigma}{d\Omega}=\frac{r_0^2Z^2}{4}\frac{1}{v^4\gamma^2\sin^4(\theta/2)}\left[1-v^2\sin^2\frac{\theta}{2}+\pi\alpha Zv\sin\frac{\theta}{2}\left(1-\sin\frac{\theta}{2}\right)\right] \tag{1•2•9}$$

in the second Born approximation, where

$r_0=2.818\times10^{-13}$cm (classical electron radius)

$\gamma\equiv(1-v^2)^{-1/2}$

$\alpha=1/137$

and θ is the scattering angle.[1204]

The delta-ray density n_δ along the track of a bare nucleus of charge Z and velocity v is then given by

$$n_\delta=\frac{2\pi r_0^2N_eZ^2}{v^2}\left[\left(\frac{m}{\eta}-\frac{1}{2\gamma^2v^2}\right)-\frac{1}{2\gamma^2}\ln\frac{2m\gamma^2v^2}{\eta}+\frac{\pi\alpha Z}{\gamma^2v}\left\{\left(\frac{2m\gamma^2v^2}{\eta}\right)^{1/2}-\frac{1}{2}\ln\frac{2m\gamma^2v^2}{\eta}-1\right\}\right]. \tag{1•2•10}$$

where N_e is the number of electrons per unit volume of the medium, m is the rest mass of an electron and η is the minimum energy of a knocked-on electron which can give rise to a delta ray satisfying the counting convention.*

Fig. 1•2•2 shows a series of curves for delta-ray density *vs.* Z and E. For comparison, the total and the primary ionizations are also plotted by a dotted and a broken lines, respectively, in the same figure. One sees that beyond 5 Gev/nucleon n_δ is practically independent of energy, and that at 1.5 Gev/nucleon it is about 15% higher than this value. Relativistic O nuclei have the same delta-ray density as 1.2 Gev/nucleon N or 0.7 Gev/nucleon C.

In actual delta-ray counting, the effect of background grains must be taken into account. For smaller values of η the background fogs are inevitably counted in, and for larger values of η, the Compton electron tracks.

These contribute an ionization-independent part in addition to the net delta-ray density. The background effects, of course, depend on the conditions of exposure and development.

Counting convention

In counting delta rays it is necessary to set some criterion defining the lower limit of their energy. Usually two conventions are adopted; the grain convention and the range convention. The former is to count the delta rays which contain at least a certain number of grains. Usually this number is four. The latter is to count the delta rays having at least a certain length of range.

The present authors prefer the range convention because the grain convention has the following two shortcomings:

(i) Large subjective errors in determining the number of grains, especially because the grains often stick with each other for small

---

* Some heavy primary research workers cite the formula given in differential form by Bradt and Peters,[1205] which is based upon the incorrect Rutherford scattering formula given by Mott:[1206]

$$\frac{d\sigma}{d\Omega}=\frac{r_0^2Z^2}{4}\frac{1}{v^4\gamma^2\sin^4(\theta/2)}\left[1-v^2\sin^2\frac{\theta}{2}+\pi\alpha Zv\sin\frac{\theta}{2}\left(1-\sin^2\frac{\theta}{2}\right)\right]. \qquad (1\cdot2\cdot9')$$

If we had adopted this, the terms in the { } of (1•2•10) would have been

$$\left(\frac{2m\gamma^2v^2}{\eta}\right)^{1/2}+\left(\frac{\eta}{2m\gamma^2v^2}\right)^{1/2}-2. \qquad (1\cdot2\cdot10')$$

Although the discrepancy is negligible for the usual purpose of delta-ray counting, it becomes important when the frequency of high energy knock-on electrons is in question.

The correction arising from the fact that the nucleus has a finite size is negligible for nuclei of $Z\leqq13$. For example, even for electrons of energy 15.7 Mev incident upon an Al nucleus at rest, which is equivalent to an Al nucleus of energy ~29 Gev/nucleon incident upon electrons in the medium, the deviation from the point nucleus approximation is $<10\%$ for all scattering angles.[1207]

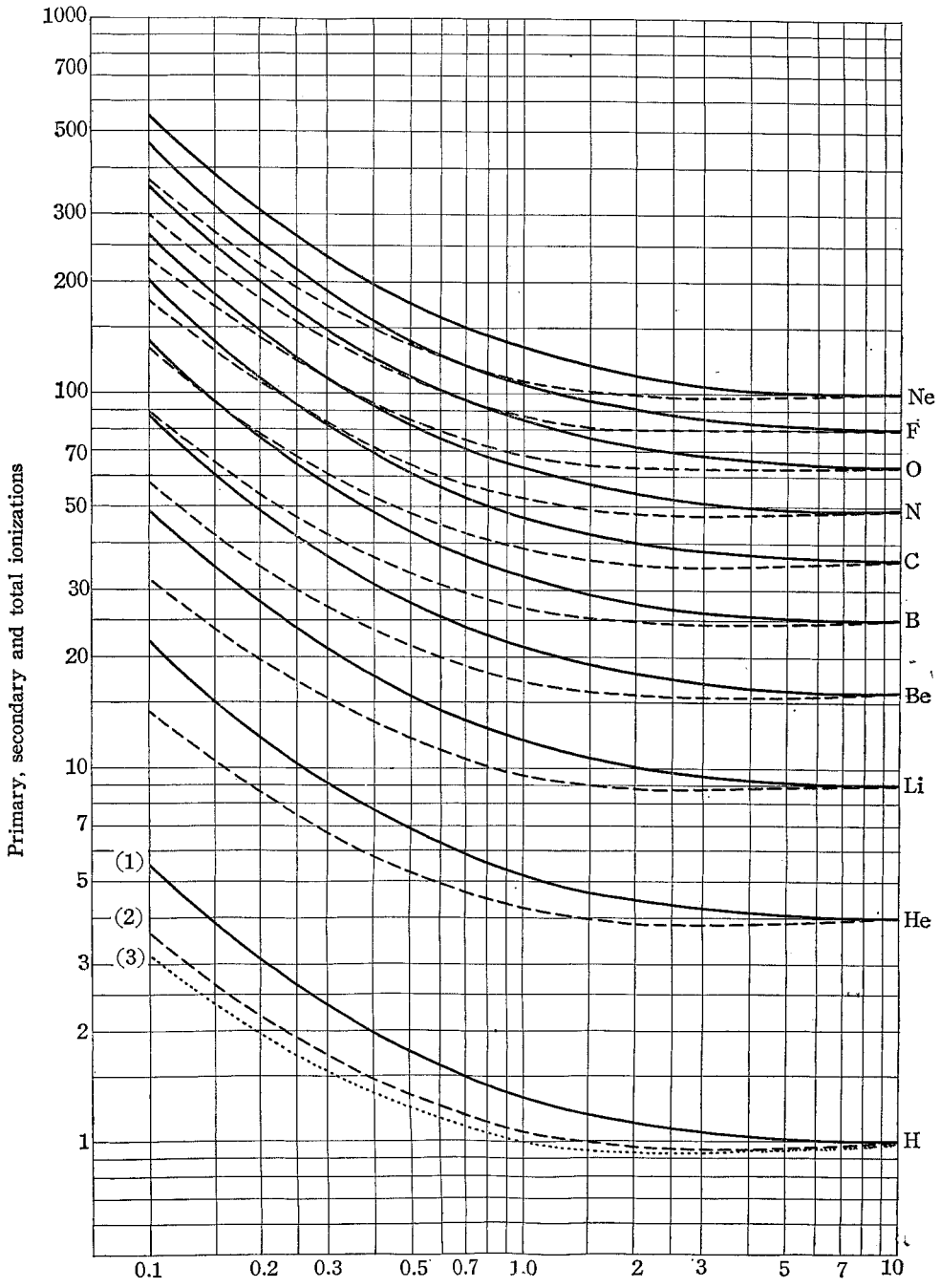

Fig. 1•2•2. Energy dependence of net delta-ray density. total ionization and primary ionization.
(1) —— net delta-ray density (2) - - - primary ionization (restricted energy loss rate)
(3) ····· total ionization (total energy loss rate)
To make the comparison in practical cases convenient, all the three quantities are normalized to 1 for 10 Gev protons. It is only (1) and (2) which are used in practical ionization measurement in emulsion work.

electron energies.

(ii) Systematic shift in the lower limit of energy as the ionization gets greater. As ionization increases the track width becomes larger by the effect of very low energy delta rays, and so the delta rays which have four grains outside the track width have, in reality, more grains outside the track which is formed by the primary ionization only.

In spite of these shortcomings, however, the grain convention has its merit in that;

(a) it needs no special apparatus in counting procedure,

(b) skillful observers can attain to very high speed of measurement.

Therefore, if one sees to that stable counting level should be maintained on the one hand and that the measurement should be checked by sufficient number of charge-indicating interactions on the other, this convention will provide a quite efficient tool in the measurement. For this reason this convention was adopted at the earliest stage of analysis in the Prince Albert Project, and applied to a limited ionization range where sufficient number of charge-indicating and quasi-charge-indicating interactions were available. In Fig. 1•2•3, are shown, in the form of a histogram, the results of the 4-grain delta-ray countings on the tracks of the nuclei which are known to be relativistic from the observed nuclear interactions they produced. The counting has been performed by three different observers and the countings on the same track by different observers are counted as different cases. In each case a total of at least 400 delta rays have been counted. Some of the tracks have been counted by all three observers and the average taken over the countings of the three observers has been used for each track. This is shown in Fig. 1•2•3 in the shaded histogram. The cases shown include the fragmentation of one C→3α and one O→4α, both at relativistic energies. A clear-cut separation of C, N, O tracks at relativistic energies is observed in Fig. 1•2•3.

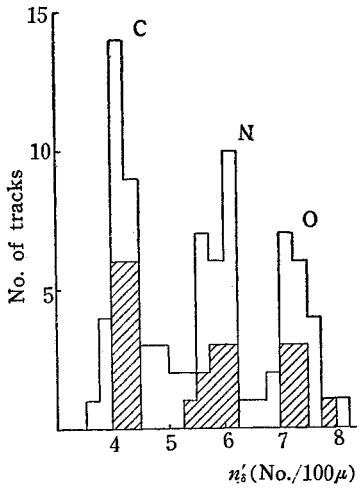

Fig. 1•2•3. Distribution of 4-grain delta-ray densities, n_8', of high-energy tracks. n_8' is expressed in unit of no./100μ. For details, see text.

In the greater part of the analysis, the present authors adopted the range convention. The present authors counted the delta-ray tracks which end outside a certain distance from the center-line of the heavy primary

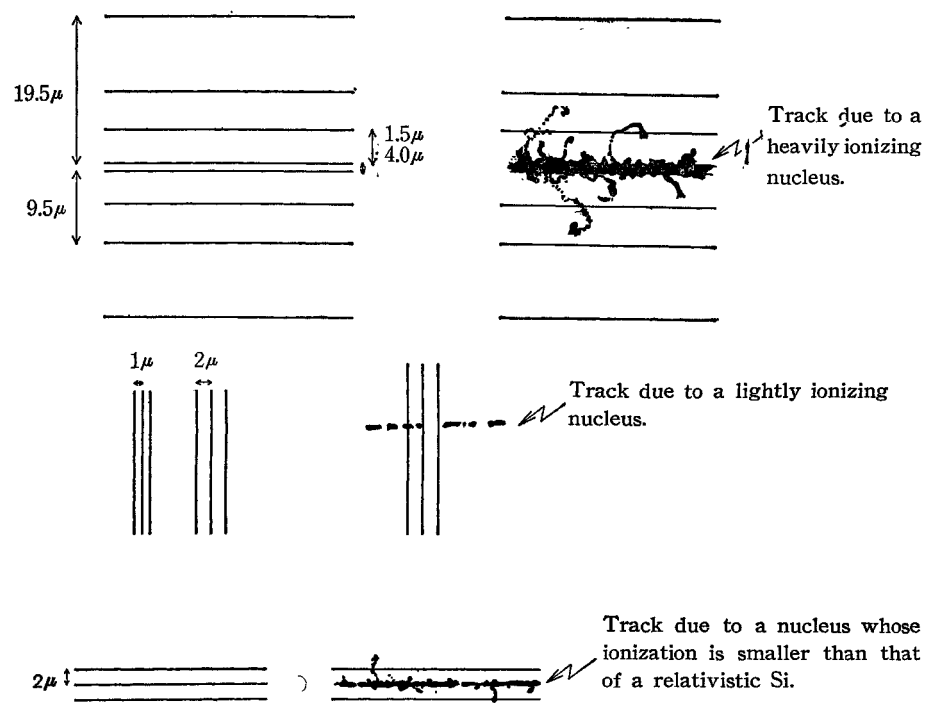

Fig. 1•2•4. Views of the eye-piece scales used in gap countings and restricted delta-ray countings in the Prince Albert Project. Sketches illustrate the view in the practical cases, i.e., the views when a 100× objective is used. Incidentally, the total magnification was 1000×.

track. The eye-piece micrometers used for this purpose are shown in Fig. 1•2•4. This distance D_δ was taken to be 2.0μ, 5.0μ, 10μ and 20μ.

The reproducibility of this range convention is quite satisfactory for $D_\delta = 2.0\ \mu$; The difference in the measurements by different observers and in the repeated measurements by the same observer does not exceed 5% after a short period of training.

Calibration

Tracks of relativistic nuclei are important to get the standards of delta-ray density. For the calibration of delta-ray density using relativistic tracks, it is necessary to pick up tracks of energy higher than 3 Gev/nucleon. Even a particle of 1.5 Gev/nucleon has a delta-ray density about 15% higher than the relativistic value. This remark is necessary for measurements on stacks exposed at high geomagnetic latitude. In the Prince Albert Project, we checked the energy of the tracks used for calibration by using the knock-on electron[120S] method. The methods of energy determination will be discussed in detail later in §1•2•5.

For the selected relativistic tracks the delta-ray measurement is made in the following way. In the ionization range from that of relativistic Li up to that of relativistic Si, the minimum distance for delta rays, D_δ, is chosen to be 2.0 μ. 200 and 400 delta rays were counted for $n_\delta < 3.3$ and for $n_\delta > 6.7$, respectively, where n_δ denotes the delta-ray density per 100 μ. For intermediate delta-ray densities the track-length of 6 mm was used in counting.

Fig. 1•2•5 shows the diagram of energy versus delta-ray density thus obtained. One sees that each charge is well separated in this delta-ray diagram in the L- and M-nuclei region. There is no difficulty in identifying

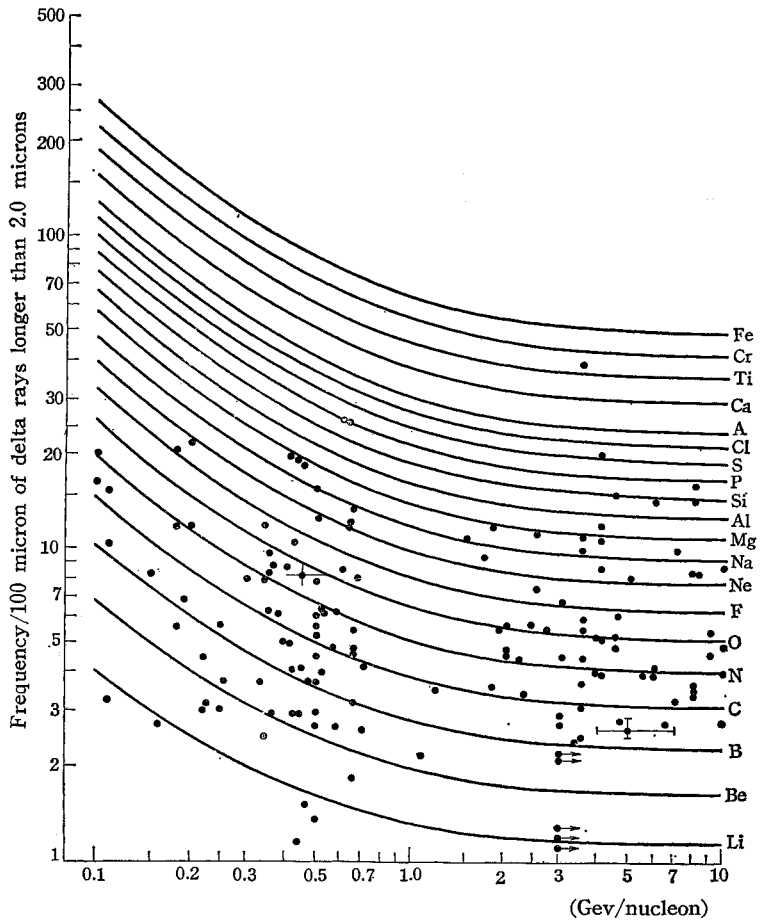

Fig. 1•2•5. Semi-empirical relation between kinetic energy vs. delta-ray density with $D_\delta = 2\mu$. The dots are the experimental points. The horizontal bars represent the precision in energy determination, while the vertical bars represent the statistical errors in delta-ray countings. The points accompanied by an arrow mean lower limits of energy. For further details, see text.

the abundance peaks as Li, Be, B and on up to Ne.* The relation of delta-ray density n_δ with particle charge is then obtained as

$$n_\delta = aZ^2 + b, \qquad (1\cdot2\cdot11.)$$

where $a=0.072$, $b=0.50$ for $D_\delta=2\mu$ when n_δ is expressed in number per 100 μ.

Theoretically the expected error in the charge determination by counting delta rays is given as

$$\Delta Z = \frac{Z}{2}\frac{\Delta n_\delta}{n_\delta} \sim \frac{1}{2\sqrt{aL}}, \qquad (1\cdot2\cdot12)$$

where L is the distance over which the delta rays are counted. Errors in the actual charge measurement do not appreciably differ from the above expected values which are illustrated in Fig. 1·2·6.

The charge calibration of delta-ray density can be supplemented by measurements on tracks of charge-indicating interactions. One can unambiguously identify the charge of a track showing a clean break-up interaction

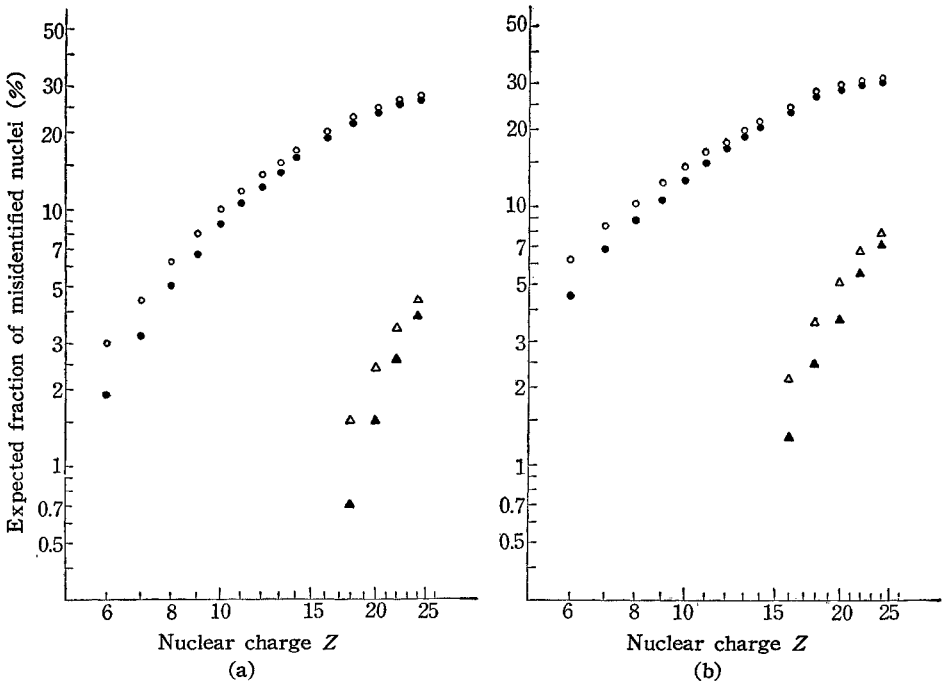

* For Li, Be and B tracks the method of knock-on electrons is hard to apply. Therefore in obtaining relativistic Li, Be or B nuclei those which made multiple pion production were selected out. In the Prince Albert Stack a glance of the track sufficed in discriminating relativistic Li from relativistic He. and uncalibrated blob counting for a short track length sufficed in discriminating relativistic Li from relativistic Be.

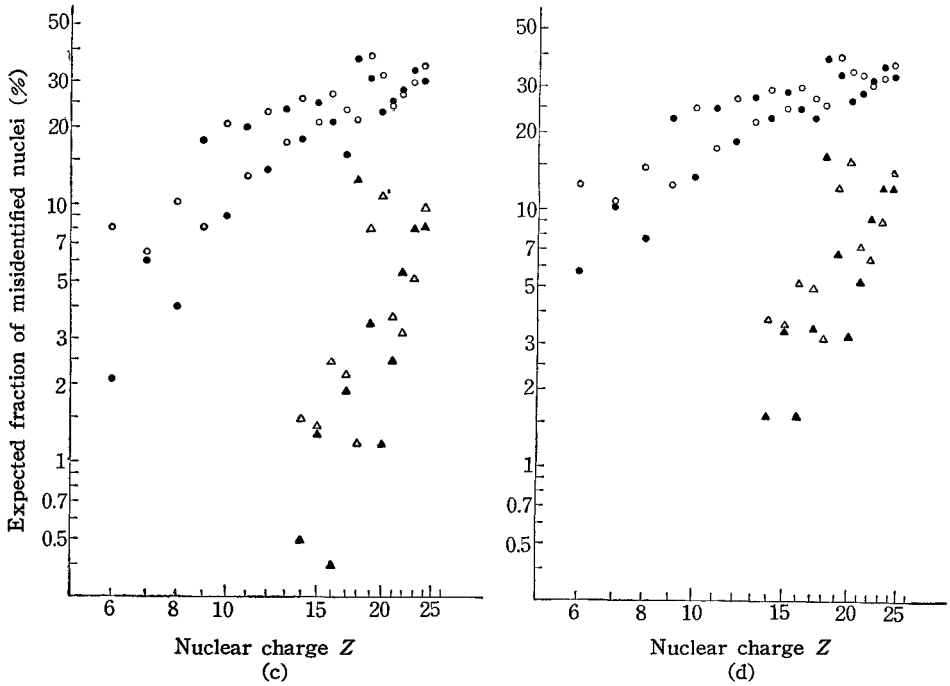

Fig. 1•2•6. Expected errors in charge determination by means of delta-ray counting. The errors are expressed in the form of the percentages of misidentified nuclei. The points in the figures represent the expected percentages of the nuclei whose actual charge number is Z and whose measured charge number is Z':

○: $Z' \leqq Z-1$, △: $Z' \leqq Z-2$, ●: $Z' \geqq Z+1$, ▲: $Z' \geqq +2$.

Subjective error of 5% is taken into account in all cases.

Fig. 1•2•6(a). The case of relativistic nuclei ($E>3$ Gev/nucleon) where 400 delta-rays are counted for each track.

Fig. 1•2•6(b). The case of relativistic nuclei where 200 delta rays are counted for each track.

Fig. 1•2•6(c). The case of stopped nuclei where 400 delta rays are counted for each track at 1.57 cm from its end.

Fig. 1•2•6(d). The case of stopped nuclei where 200 delta rays are counted for each track at 1.57 cm from its end.

which has only secondary fragments of charge $\geqq 2$. If the interaction has a minimum secondary track, one is not sure whether the minimum track is a proton or a meson so that one can not be free from ambiguity.

In the Prince Albert Stack, we found thirteen charge-indicating and quasi-charge-indicating interactions of this kind. Table 1•2•2 shows a list of such events together with measured delta-ray density and velocity of the particle.

Charge determination of stopped particles

Energy and charge measurements can be made quite accurately for particles which are stopped in nuclear emulsion by measuring both the ionization and the range of the particle.

Table 1•2•2. List of charge-indicating and quasi-charge-indicating break-up events in the Prince Albert Stack.

Type of break-up	N_g	N_b	Energy at interaction point (Gev/nucleon)	n_2 of primary track (No./100 μ)	Method of energy determination
C $\rightarrow 3\alpha$	0	0	1.2	3.56 ± 0.15	Knock-on electrons
C $\rightarrow 3\alpha$	0	0	0.5	5.00 ± 0.25	Ionization and multiple scattering of secondary α's
O $\rightarrow 4\alpha$	0	0	>3	4.90 ± 0.25	Opening angles of secondary α's
O $\rightarrow 4\alpha$	0	0	0.3	11.0 ± 0.6	Ionization and multiple scattering of secondary α's
O $\rightarrow 4\alpha$	1	0	0.26	11.9 ± 0.6	〃
Mg$\rightarrow 5\alpha pd$	0	0	0.0925	$n_5=30\pm2$	Residual ranges of all secondaries
C $\rightarrow 2\alpha 2p$	0	0	1.2	3.60 ± 0.18	Knock-on electrons
C $\rightarrow 2\alpha 2p$	0	0	1.2	3.62 ± 0.18	〃
C $\rightarrow 2\alpha 2p$	0	0	1.2	3.64 ± 0.26	〃
C $\rightarrow \alpha 4p$	1	0	2.3	3.41 ± 0.24	〃
N $\rightarrow 2\alpha 3p$	0	0	1.2	4.96 ± 0.25	〃
O $\rightarrow 3\alpha 2p 2\pi$	1	0	4	5.42 ± 0.27	〃
Mg$\rightarrow 5\alpha 2p 2\pi$	0	3	1.0	$n_2=14.2\pm0.7$ $n_5=7.32\pm0.37$	〃

From the previous formula for the energy loss by ionization and for the delta-ray density, one can find a relation between the delta-ray density n_δ and residual range R as follows:*

$$n_\delta = Z^2 f\left(\frac{Z^2R}{A}\right) \equiv Z f^2\left(\frac{ZR}{2}\right). \qquad (1\cdot2\cdot13)$$

It should be noted that range R appears in the formula only through the factor Z^2R/A. The function $f(ZR/2)$ has a complicated form, and it is

* As the ionization loss is given by the formula

$$-\frac{dE}{dx} = Z^2 F_0(v),$$

the range of the particle with energy E is given by

$$\frac{Z^2R}{A} = F_1(E/A),$$

delta-ray density is also given by the formula

$$n_\delta \sim Z^2 g(v).$$

Then this can also be written by

$$n_\delta \sim Z^2 f(Z^2R/A),$$

as, for the heavy primary, we can usually put $Z/A \sim 1/2$ except for Li, Be and B.

difficult to obtain its explicit form from a theoretical study alone. Once one experimentally obtains $f(ZR/2)$ from measurement on some long ending tracks, then one is able to draw a diagram of delta-ray density n_δ for the different Z and R.

Fig. 1•2•7 shows an example of such curves and several experimental points which gave this curve.

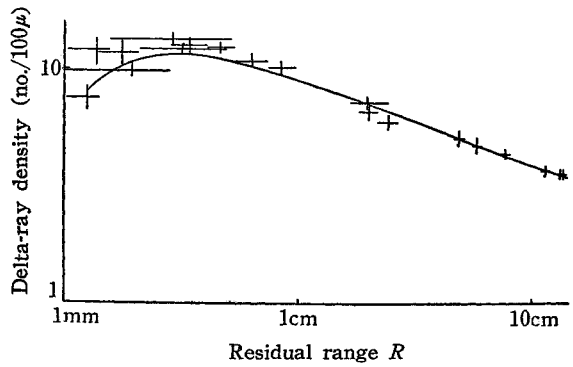

Fig. 1•2•7. The calibration curve of the delta-ray density, n_δ, with $D_\delta=5.0\mu$. All results have been converted into those of C according to the similarity law (1•2•13). The solid curve is the the theoretically expected variation of n_δ (1•2•10) with the residual range,[1105] corresponding to the case $m/\eta=10$.

The function $f(ZR/2)$ which describes the variation of delta-ray density with range has a maximum at $ZR=(ZR)_{max}$, which corresponds to the velocity of the nucleus

$$v_{max}\fallingdotseq(\eta/\mathrm{m})^{1/2}, \qquad (1\cdot2\cdot14)$$

with the maximum value of $f_{max}=n_\delta^{max}/Z^2$. This can be shown from the formula (1•2•10). The cross-section for knocking out delta-rays becomes smaller beyond this maximum, while below the maximum, the emission of delta rays satisfying the range criterion becomes difficult from kinematical restriction. Naturally, the position of the maximum is a function of the distance D_δ used for range convention of delta rays. One has an approximate relation,

$$(ZR)_{max}\sim 2000D_\delta\,. \qquad (1\cdot2\cdot15)$$

In charge determination for ending tracks, one usually compares delta-ray density n_δ at a fixed range. One can easily see that delta-ray density nearer to the end of the track gives greater information. At larger residual range beyond the position of maximum, n_δ follows the law

$$n_\delta \propto Z^{1.5}, \qquad (1\cdot2\cdot16)$$

assuming an approximate energy-range relations. At around the maximum of delta-ray density, one finds $n_\delta\propto Z^2$.

At shorter residual range, Z-dependence of delta-ray density still be-

comes larger. The fact that only small statistics of delta rays is available at such small residual range makes the idea impractical. Thus the method which was adopted in the Prince Albert Project is the integral delta-ray counting method. One counts the number of delta rays satisfying a certain range-convention along the track, starting from the end of the track. Then the number of delta-rays thus counted, N_δ, varies with the distance from the end of the track in the following way:

$$N_\delta(R)=\int_0^R drn_\delta(r)=Z\cdot F(ZR), \qquad (1\cdot2\cdot17)$$

where $F(ZR)$ is a certain function of the product ZR only.*

One plots the number of delta rays N_δ versus range R, both in a logarithmic scale. Then the data of every track, irrespective of the charge, should fall on the same curve expressing $F(ZR)$ after applying a translation along a $-45°$ line, i.e., $N_\delta \to N_\delta/Z$ and $R\to RZ$. The charge of the particle is now obtained from the magnitude of the translation along the $-45°$ line. Fig. 1·2·8 demonstrates several examples of the data for medium components.

A particular remark should be made for very heavy tracks. A similarity law (1·2·17) of N_δ and R for tracks of various charges is experimentally confirmed by our measurements up to nuclei as heavy as Si or so. But at the same time one finds experimentally a certain deviation from the similarity law in cases of very heavy nuclei. As will be discussed in detail in Appendix 3, there is enough reason to suspect from the data that a very heavy nucleus captures electrons before coming to the end of its range. Therefore a very heavy particle suffers ionization loss of less

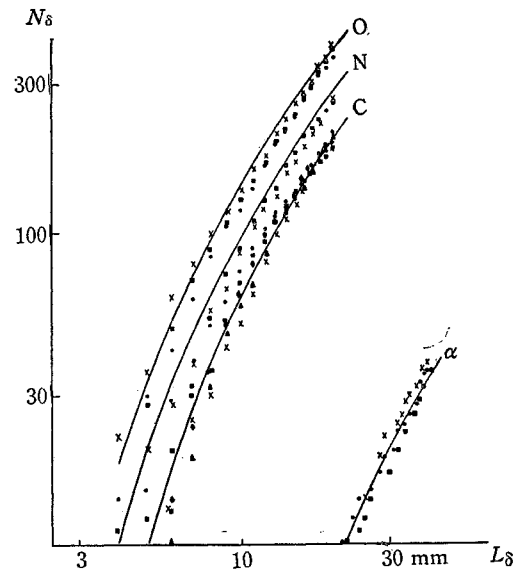

Fig. 1·2·8. The calibration of the integrated number of delta rays, N_δ. of stopped He and C, N, O nuclei. D_δ has been chosen to be 4.38μ. The four different symbols used in the figure refer to individual delta-ray countings of four different observers.

* Here, too, we assume the relation

$$Z/A\sim 1/2.$$

If this relation does not hold, we must have

$$N_\delta(R)\sim AF(2Z^2R/A).$$

magnitude when it becomes slow, so that its range becomes longer by a certain amount than the value predicted from the similarity argument. This effect of increasing range is found to be about 200μ for Fe group nuclei, and 100μ for Ca, and the results seem to agree with accelerator work.[1209] This effect is of course negligible for lighter nuclei.

1·2·5. *Other methods*

Method of high energy knock-on electrons[1208]

The method using high energy knock-on electrons is very useful for energy determination of nuclei heavier than C with energies between ~2 Gev/nucleon and ~10 Gev/nucleon.

Let the electron mass be m, the emission angle of the knocked-out electron θ, kinetic energy of the electron η, the velocity and the Lorentz factor of the incident nucleus $c\beta$ and γ, respectively. Then the relation

$$\frac{1}{\gamma^2\beta^2}=\frac{2mc^2}{\eta}\cos^2\theta-\sin^2\theta \qquad (1\cdot2\cdot18)$$

holds in the approximation neglecting the effect of recoil of the incident nucleus. Therefore, the measurement of θ and η will enable us to determine γ.

The relation (1·2·18) is derived only from kinematical considerations, so that if the method should involve any ambiguity it is merely of technical, not of theoretical nature. η is determined by multiple Coulomb scattering measurement and we measure both multiple scattering and $\tan\theta$ by means of the sagitta method.

If one denotes the mean deviation by $\overline{D}$, its error $\Delta\overline{D}$, and the error in $X\equiv\tan\theta$ by ΔX, then the relative error in $\gamma\beta$ is given by

$$\left|\frac{\Delta\gamma\beta}{\gamma\beta}\right|=\frac{1}{2}\gamma^2\beta^2\left[\left(\frac{2mc^2}{\eta}\frac{1}{1+X^2}\frac{\Delta\overline{D}}{\overline{D}}\right)^2+\left\{\frac{\eta+2mc^2}{\eta}\frac{2X\Delta X}{(1+X)^2}\right\}^2\right]^{1/2}. \qquad (1\cdot2\cdot19)$$

For small η, $\overline{D}$ is large and the accuracy in X is poor and, moreover, the tracing of the electron track is difficult. Therefore some lower bound of η is desirable if we want to determine X and $\overline{D}$ with sufficient accuracy. If we put, for example, the condition that $\overline{D}$ should not be greater than the scale-reading error in the measurement of X, then this lower bound will be 5 Mev.

For details of scattering measurement the reader is referred, for example, to the review article by Voyvodic.[1210]

The diagram showing the relation between η and X for several values of energies of primary nuclei is given in Fig. 1·2·9. As can be seen in

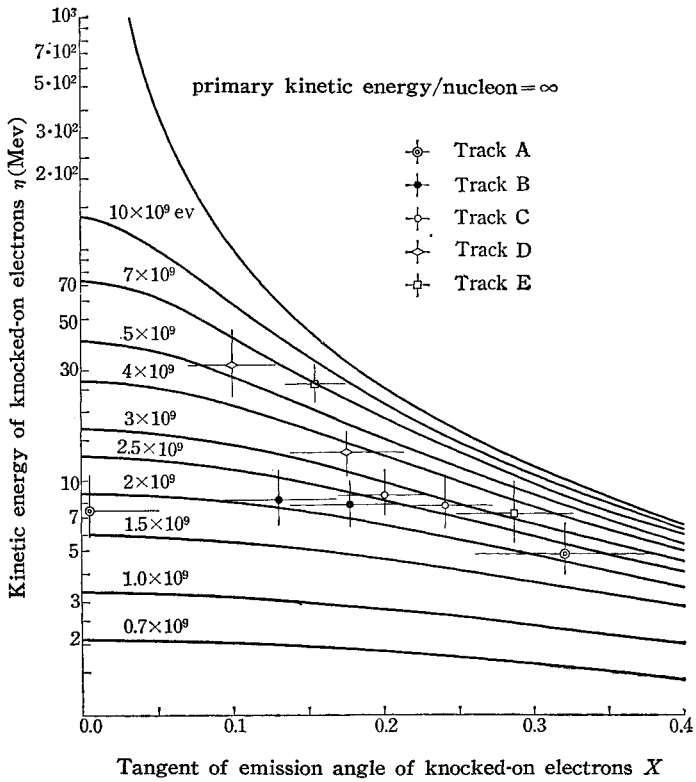

Fig. 1•2•9. Diagram showing the kinematical relation between the energy and the emission angle of high energy knock-on electrons for various kinetic energies of the primary nucleus. Several examples of energy determination by means of the knock-on electron method are also shown in the figure.

the figure, large values of X give quite poor precision in primary energy determination if the primary energy is high.

The precision in the determination of the emission angle θ has an upper bound. The reason is as follows: while the component of θ which is projected in the plane of emulsion surface can be measured quite accurately, the component which is projected in the plane perpendicular to the emulsion surface is hard to be measured accurately because of the shrinkage after development of the emulsions.

While the frequency per unit track length for accompanying knock-on electrons of energy greater than η is given by the formula (1•2•10), we now introduce here another more practical quantity. Let ν_X represent the frequency per 1 cm length of a heavy primary track accompanying an electron, which is knocked-out with an emission angle smaller than arctan X by the incident nucleus of charge Z and velocity $c\beta$. Then in the Ilford G5 emulsions, ν_X is given by

$$\nu_X = 0.268\frac{Z^2}{\beta^4}\left[X^2 - \frac{\beta^2}{r^2}\ln(r^2X^2+1) + \frac{2\pi Z\beta}{137r^2}\left\{(r^2X^2+1)^{1/2} - \frac{1}{2}\ln(r^2X^2-1) - 1\right\}\right]. \qquad (1\cdot2\cdot20)$$

The values of ν_X in the case of neon nuclei are given in Fig. 1·2·10 for several values of X.

Multiple scattering measurement was done by means of Olympus DF Bi-III microscopes. From the measurement of the secondary particles of a high energy jet, the noise level of the scattering measurement was determined to be 0.20 μ for cell-lengths between 20 μ and 200 μ. This means that the upper limits of measurable η are 35 Mev and 115 Mev for cell-length 50 μ and 100 μ, respectively, which corresponds to a signal-to-noise ratio of 2 : 1. In actual energy determination the cell-lengths were chosen so that the S-N ratio should not be smaller than 5.

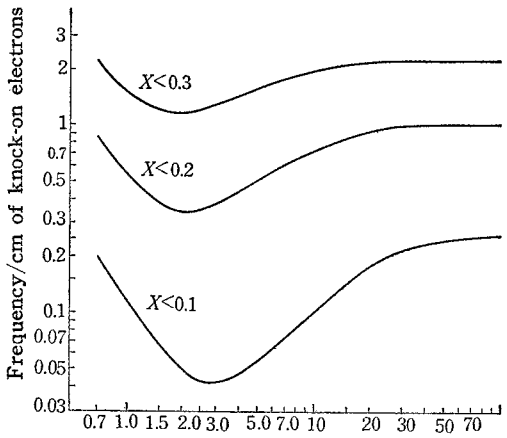

Fig. 1·2·10. Frequency per 100μ, ν_X, of knock-on electrons whose emission angles are smaller than $\tan^{-1}X$ as a function of the charge Z and the energy E of the primary nuclei. The case of $Z=10$ is taken as an example.

Several examples of energy determination are also plotted in Fig. 1·2·9. A consistency between the results obtained from the measurements of two or more electrons knocked-out by the same incident nucleus is satisfactory and it may well be said that the incident energy of 5 Gev/nucleon is determined with an error of $^{+2}_{-1}$ Gev/nucleon.

Energy determination by means of the mean opening angle of the secondary He nuclei

An estimate of the primary energy can often be obtained by observing characteristics of nuclear interaction of heavy primaries.

Now, in view of the fact that we are dealing with heavy primaries of energy from ~0.1 Gev/nucleon up to ~10 Gev/nucleon, we shall restrict ourselves to the method of energy determination by the measurement of secondary He nuclei.

An energy estimation by means of measurement of the mean opening angle of secondary He nuclei is applied by several authors, and Kaplon et al.[1211] have made an excellent critical analysis and application of the method.

An idea of the method is as follows: When an incident nucleus collides with a target nucleus, the former is excited and light nuclear fragments —protons, neutrons, alphas and others—evaporate out of it. Mean energy in the rest system of the incident nucleus $\langle T \rangle$ of the evaporating He nuclei can be estimated from other experiments.* Then, we get the following relation between the momentum/nucleon of the primary nucleus P and the root-mean-square opening angle $\langle \theta^2 \rangle^{1/2}$ of the He nuclei:

$$\langle \theta^2 \rangle^{1/2} = 0.056/P, \qquad (1\cdot2\cdot21)$$

where P is expressed in units of Gev/c and the primary nucleus is assumed to belong to the Mg-Si group.

Several ambiguities are inherent in the method. They arise from the following reasons:

(i) We do not know exactly the values of $\langle T \rangle$ for various nuclei.

(ii) The mean energy $\langle T \rangle$ will fluctuate from one collision to another.

(iii) The number of He nuclei is rather few and statistical error in "mean opening angle" is not small.

The last two factors will make the energy determination ambiguous by a factor ~ 2, even if we neglect the effect of the first one.

To see the precision of energy estimations by means of the mean opening angle method the present authors compared the results with those obtained, in some cases, by the method of high energy knock-on electrons and in the other, by means of the ionization of the secondary helium nuclei. The correlation diagram is given in Fig. 1•2•11, where ε' is the energy value obtained by the former method and ε is the one obtained by either of the other two methods. Though the statistics is not good, the diagram shows that;

(i) average values of ε and ε' almost coincide,

(ii) values of $\log(\varepsilon'/\varepsilon)$ distribute approximately symmetrically around the value 0,

(iii) in about half of the cases, ε'/ε falls between 0.5 and 2.

These conclusions are in agreement with the result of the criticism which

* For an example, from the data of nuclear disintegrations of C, O or Ag, Br nuclei of emulsion bombarded by incident protons we get an estimate of $\langle T \rangle$:[1212]

$\langle T \rangle \approx 2$ Mev/nucleon for C and O.
≈ 3.5 Mev/nucleon for Ag and Br.

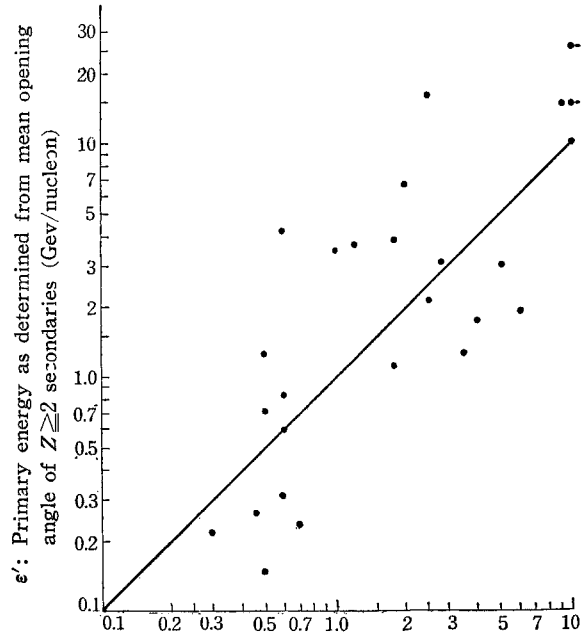

Fig. 1•2•11. Correlation diagram between the estimate ε' and the estimate ε of the energy of heavy primaries.

The estimate ε' is obtained from the mean opening angle of the secondary He nuclei, and the estimate ε is obtained:

(i) from the measurement of high energy knock-on electrons (for primary energy $\gtrsim$2 Gev/nucleon),

(ii) from the ionization measurement of the secondary He tracks combined with that of the primary track (for primary energy $<$0.7 Gev/nucleon).

Points with an arrow mean lower limits of ε.

Kaplon et al. made on their own "opening angle method".

Since we are concerned in rather low energy region, (say, several hundred Mev/nucleon to several Gev/nucleon) where the energy spectrum cannot be well approximated by a single power law, this method is not so powerful as in the case of Kaplon's work.

Energy determination by velocity measurement on the secondary He nuclei

When an incident nucleus breaks up into He nuclei or evaporates He nuclei, these He nuclei have approximately the same velocity as the primary

nucleus. Therefore energy determination of the secondary He nuclei will give us an estimate of the primary energy.

For very high energies the relative scattering measurement of the secondary He tracks is adequate,* while for energies lower than ~0.7 Gev/nucleon the ionization measurement will give energies of the secondary He nuclei.

Let the kinetic energy/nucleon, the primary velocity and the primary Lorentz factor of the primary be E, $c\beta$ and γ, respectively, q be the momentum/nucleon corresponding to the motion of a He nucleus in the rest system of the excited incident nucleus, and ε be the kinetic energy per nucleon of the concerned secondary He nucleus in the laboratory system. Then ε falls in the following energy range:

$$E-\gamma\beta q\leq\varepsilon\leq E+\gamma\beta q. \tag{1·2·22}$$

Therefore, if we estimate E by ε, the relative uncertainty $|\Delta E/E|$ of this estimate is

$$\left|\frac{\Delta E}{E}\right|=\beta\left(1+\frac{Mc^2}{E}\right)\frac{q}{Mc^2}, \tag{1·2·23}$$

which shows that an uncertainty increases for sub-relativistic energies.

Therefore in the measurement of primary energy of several hundred Mev/nucleon, this method of energy determination alone will not give enough accuracy and the measurement should be made in either of the following two ways:

(i) The ionization measurement and the measurement of the deviation angle from the incident direction should be made on two or more secondary He tracks.

(ii) The ionization measurement should be made on both the primary track and the secondary He nuclei.

1·2·6. *Charge and energy determination in the Prince Albert Project*

Now we explain how the charge and energy determination were made in the Prince Albert Project by the various methods discussed in the preceding five sections.

He measurement

A scanning —the scan D of Table 1·1·1— was carried out particularly for alpha particles in a small portion of the stack.

Among the selected tracks we had to discriminate between alpha-particle tracks and tracks of low-energy singly charged nuclei, viz., protons, deuterons

* Usually all the secondary He nuclei are assumed to be alpha particles.

and tritons. A relativistic alpha track has approximately the same ionization as that of a proton of 2 cm residual range in emulsions, a deuteron of 4 cm, and a triton of 6 cm. We rejected tracks of low energy singly charged particles without any ambiguity by tracing them in the stack until they either stop, suffer a large-angle scattering or show large change in their ionization.

The discrimination between alpha tracks and Li tracks involves greater technical difficulty, but this presents no serious problem because the latter are expected to have far lower abundance than the former in the energy range where both have similar degree of ionization.

After selecting the alpha-particle tracks as above, the gap and blob measurement were made near the bottom edge of the stack for each alpha track which traversed more than 8 cm of emulsion.

Conversion of ionization value g, gap density or blob density, into particle energy E is made as follows. We made measurements of G_1 and G_0 for several stopped alpha particles of long residual ranges and also for several slow alpha tracks which passed through the stack with short residual ranges. From these measurements, an empirical relation between G_1 and

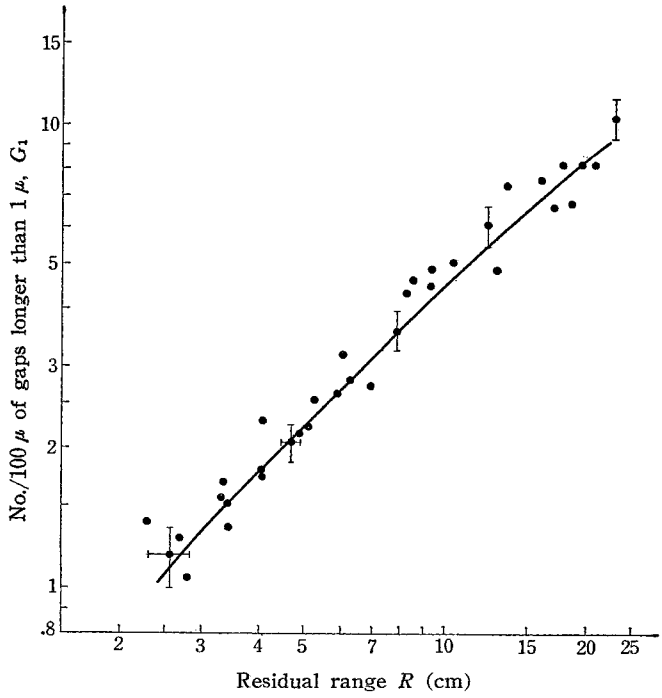

Fig. 1•2•12. Empirical G_1-R relation for alpha particles which were stopped in emulsion or passed through the stack with short residual ranges. Statistical errors in G_1 are illustrated in the figure.

G_0 and range R can be constructed up to a range of about 20 cm of emulsions. Fig. 1·2·12 shows the empirical G_1-R relation obtained. With the help of the energy-range relation, Fig. 1·1·5, one can construct g-E, G_1-E or G_0-E relation up to ~300 Mev/nucleon. Around this energy the values of g derived from G_1 and G_0 were found to agree with those given by theoretical calculation of ionization loss.[1105] An extrapolation of the g-E relation to higher energy region is made according to the aforementioned calculated results.

For the stopped alpha particles, we are able to measure the energy directly from the range.

In the measurement, 100 gaps of suitable lengths and 400 blobs are counted so that the relative error in g is given by

$$\left|\frac{\Delta g}{g}\right| = \frac{1}{gl}\left[\left(\frac{\Delta G}{G}\right)^2+\left(\frac{\Delta B}{B}\right)^2\right]^{1/2}, \qquad (1\cdot2\cdot24)$$

where

$$G \equiv G_1, \qquad B \equiv G_0,$$
$$(\Delta G)^2 = (\Delta G_N)^2+(\Delta G_D)^2+(\Delta G_S)^2,$$
$$(\Delta B)^2 = (\Delta B_N)^2+(\Delta B_D)^2+(\Delta B_S)^2, \qquad (1\cdot2\cdot25)$$

suffix N denoting the statistical errors, D the fluctuation due to non-uniform development and S the subjective errors. For the Prince Albert Stack,

$$|\Delta G_N/G| = |\Delta G_D/G| = |\Delta G_S/G| \approx 10\%,$$
$$|\Delta B_N/B| = |\Delta B_D/B| = |\Delta B_S/B| \approx 5\%, \qquad (1\cdot2\cdot26)$$

so that

$$|\Delta g/g| \lesssim 0.2/gl. \qquad (1\cdot2\cdot27)$$

These gap and blob measurements were made with the following precaution:

(i) They should be made at a location separated from any emulsion edge by more than 1 cm.

(ii) They should be made in the middle 2/3 of the emulsion depth.

Fig. 1·2·13 shows the distribution of measured values of ionization g. The width of the peak at g of relativistic alpha particles is about ~10 %, showing the consistency of the method. Thus we may conclude that the energy spectrum can be obtained from the observed g-distribution above 4.6 times minimum g, without suffering from the tail effect of the peak of relativistic alpha particles. The errors of energy determination in our measurement are given in Fig. 1·2·14.

Measurement of light nuclei

A difficulty in light component measurement lies in separating light

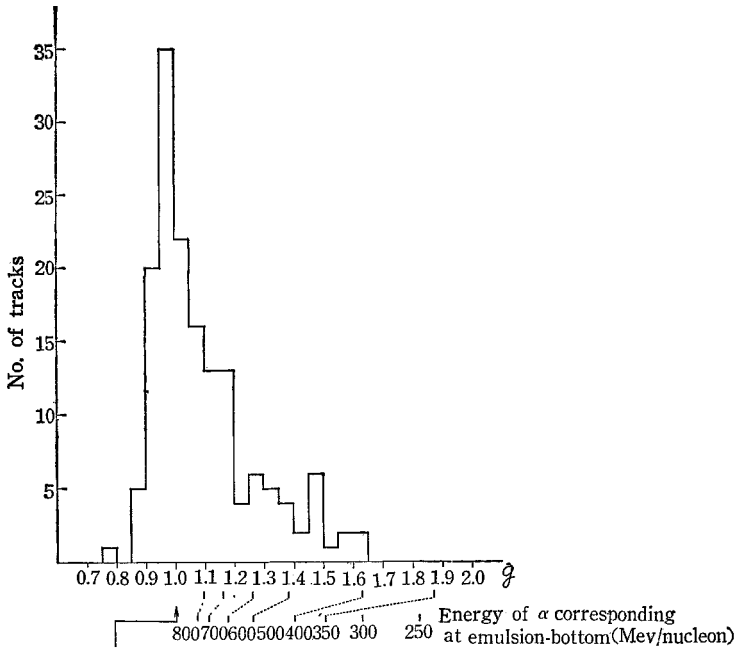

Fig. 1•2•13. Distribution of measured values of ionization g of alpha particles at the bottom of the stack. g of high energy alpha particles is taken as the unit.

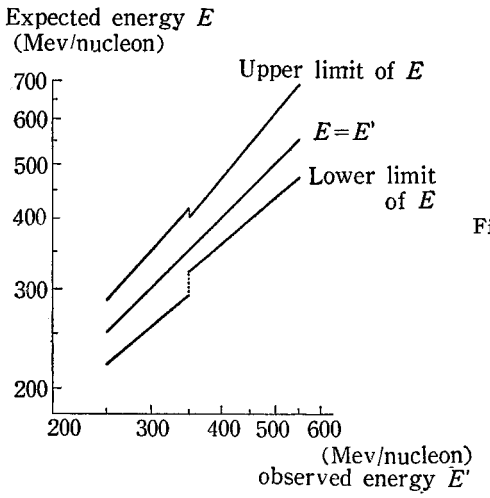

Fig. 1•2•14. Errors of energy determination of alpha particles. Errors for $E \gtrsim 350$ Mev/nucleon correspond to the error in g of 10%, while those in the lower energy region correspond to the error in G_1 of 20%.

nuclei from alpha particles and carbon nuclei. Even for the case of relativistic tracks, the difficulty is not trivial. One remembers that until recently various authors claimed mutually contradictory results on the relative flux

values of light and medium components. In the case of measurement in the low energy region as in Prince Albert Project, the difficulty is still greater.

A relativistic Li nucleus has the same ionization as a ~200 Mev/nucleon alpha particle with residual range of ~10 cm, while ionization of a relativistic C track is about the same as that of a 450 Mev/nucleon B track. A careful ionization measurement is necessary in order to separate light nuclei from alpha particles or medium nuclei. Fig. 1•2•15 and Fig. 1•2•16 show residual range dependences in Ilford G5 emulsion of the primary ionization and the delta-ray density with $D_\delta = 2\mu$, respectively, for various lighter nuclei. The corresponding energy values are also marked on every curve.

Identification of Li nuclei among slow alpha particles is made in the following way. When a heavy primary collides with an emulsion nucleus, the identification is rather straightforward. An inspection of the interaction will suffice to separate a particle of incident energy of ~200 Mev/nucleon from that of energy $\gtrsim$1 Gev/nucleon, while a simple blob counting can separate a Li nucleus from an alpha particle of about the same energy. Unfortunately the collision mean free path of a Li nucleus is ~17.5 cm.

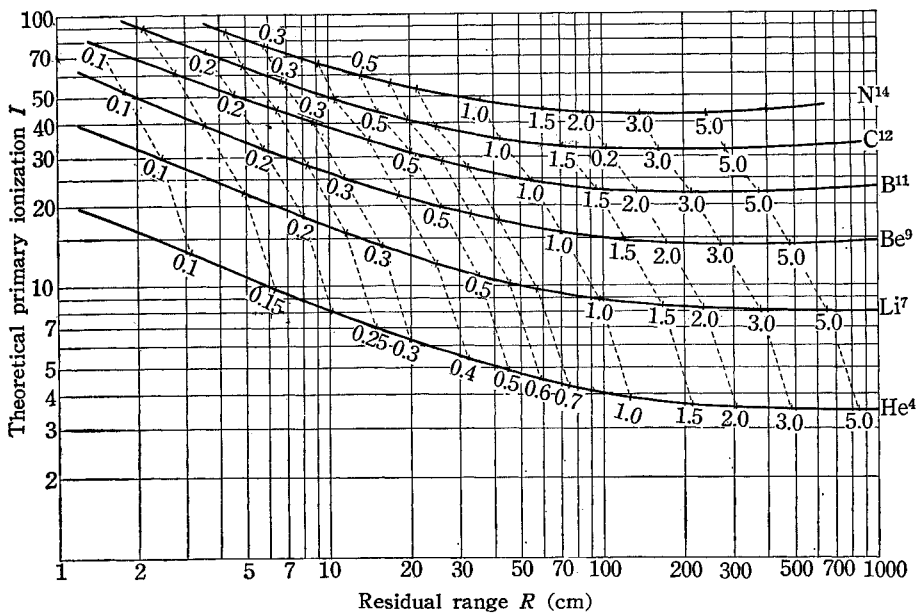

Fig. 1•2•15. Diagram showing the theoretical relation between the primary ionization I and the residual range R of several lighter nuclei in Ilford G5 emulsion.[1105] Plateau ionization of high energy electrons is taken as the unit. Energy values, expressed in Gev/nucleon, are marked on each curve.

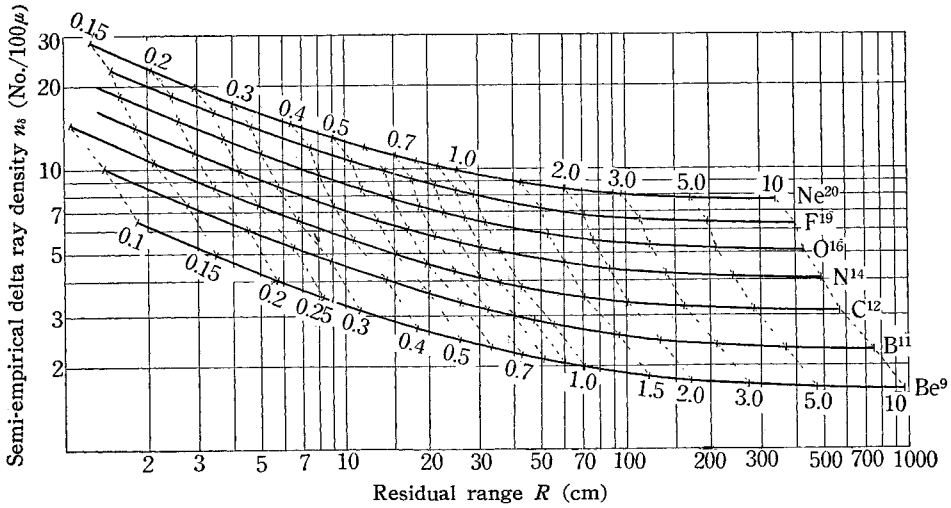

Fig. 1•2•16. Diagram showing the empirical relation in the Prince Albert Stack between the delta ray density n_δ with $D_\delta=2.0\mu$, and the residual range R of several lighter nuclei in Ilford G5 emulsion. Energy values are marked on each curve.

Therefore only ~40 % of Li nuclei make a nuclear collision in the Prince Albert Stack whose vertical depth is 10 cm, so that our statistics had to rely mainly upon the Li tracks which passed through all 10 cm of the emulsion and left the stack. On these tracks the identification was made by observing the change of their ionization while travelling through the stack. Ionization measurement was made by gap and blob countings on the track at two positions, one near the top and the other near the bottom edge of the emulsions. Let the measured values of ionization near the top and the bottom be g_{in} and g_{out}, respectively. Then one obtains the corresponding residual ranges R_{in} and R_{out} assuming that the track were due to an alpha particle. Then one makes a diagram of R_{in} and $R_{out}+L$ for each measured track, L being the distance between the position of measurement of g_{in} and g_{out}. If the selected track is really the one due to a slow alpha particle, then naturally R_{in} and $R_{out}+L$ should coincide within an expected error. Fig. 1•2•17 shows an example of the R_{in} *vs* $(R_{out}+L)$ diagram obtained by one observer. A separation between He and Li appears to be as good as expected.

The measurement for ionizations greater than that of relativistic Be were made by means of blob and delta-ray countings. The blob counting was applied to the tracks of light nuclei which passed through all 10 cm of emulsion, while for light nuclei which made nuclear collisions the delta-ray density of the primary track and the ionization of doubly or singly charged secondary tracks were measured. The opening angles of secondary particles also gave a rough estimate of primary energy.

Separation of slow B nuclei among C nuclei of higher energies is an important problem. The blobs are counted at two different positions of the tracks, one near the top and the other near the bottom of the stack. These positions will be called the entrance and the exit, respectively.

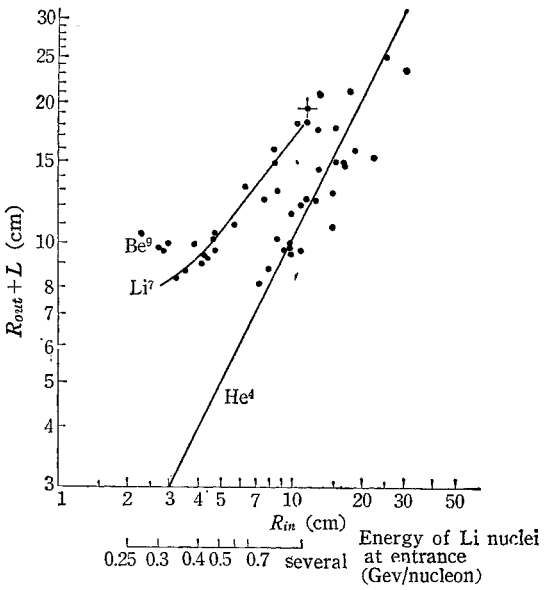

Fig. 1•2•17. Separation of Li nuclei from slow He nuclei. In the measurement L was usually taken to be 6 to 8 cm. Bars correspond to the statistical errors in G_1. For details see text, §1•2•6.

Let the ionization at entrance and at exit be I_{ent} and I_{ex}, respectively, the plateau ionization of high energy electrons being taken as the unit. About 400 blobs were counted at each measuring position. Allowing for possible ambiguities involved in the calibration of the blob densities, the total relative error in ionization I should be taken to be 8 to 10 %.

A track with I_{ent} ~30 can either be a track due to a B nucleus of energy 520 Mev/nucleon or the one due to a C nucleus of energy $\gtrsim$2 Gev/nucleon. In the former case I_{ex} will be ~35 after traversing ~8 cm of emulsion, while in the latter case no change will be observed. B nuclei of lower energies show greater differences between I_{ent} and I_{ex}, making it easier to separate them from the C nuclei with the same I. Thus B nuclei of energy $\lesssim$520 Mev/nucleon can be separated from C nuclei safely.

We can say quite safely that the probability of a C nucleus having I smallar than 27 is very small. This means that we can separate B nuclei of energy $\gtrsim$700 Mev/nucleon from C nuclei on the basis of their absolute ionization values.

For $27\lesssim I_{ent}\lesssim 30$, we should admit that the discrimination between a B track and a C track cannot attain to the same degree of certainty as the above two cases. This means that there remains some uncertainty in the separation of B nuclei of energy between ~520 Mev/nucleon and ~720 Mev/nucleon from C nuclei of the same ionization range, when we make the ionization measurement on the "through" tracks, i. e., the tracks which

pass through all 10 cm of emulsion without making nuclear collisions. As will be seen in Fig. 1•2•16, delta-ray counting, even if applied on the "through" tracks, will give no better result in this energy range, either.

Next, we shall consider the case of the delta-ray counting made on the tracks of the nuclei making nuclear interactions. The counting was made near the position of the interaction.

For example, a track with $n_\delta \approx 3.35$ can be either the track due to a 600 Mev/nucleon B nucleus or be due to a ~2 Gev/nucleon C nucleus. The discrimination between the two can be made by measuring the ionization of the doubly or singly charged secondaries. In the cases of larger n_δ, the discrimination on the basis of the secondary track measurements becomes easier, while in the cases of smaller n_δ the frequency of high energy knock-on electrons emitted within a certain angle of the primary tracks will enable us to make the discrimination.

Thus the separation of B nuclei from C nuclei can be made in all the energy ranges in this case, with the exception of the case where no doubly or singly charged secondaries are emitted.*

There is less trouble in discriminating slow Li from relativistic Be, and slow Be from relativistic B, because the competing components have about the same order of frequency and so that there is no trouble of large contaminating component as in the above two cases. The charge and energy determination of the light nuclei proceeded in a similar manner as the discrimination between B and C nuclei.

The results of measurement of L-component is presented in Fig. 1•2•18

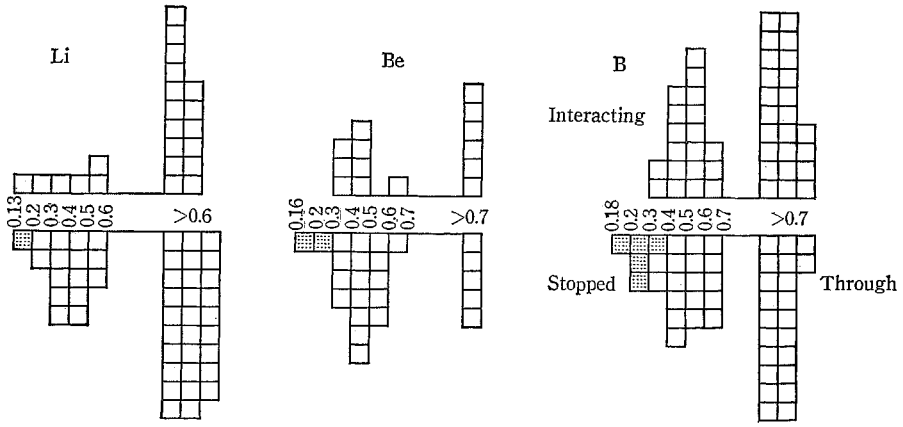

Fig. 1•2•18. Observed energy distribution of Li, Be and B nuclei. Energy values refer to the air top. The upper histograms are the ones obtained from interacting tracks and the lower the ones obtained from the rest of the tracks.

* Ambiguity also remains in the cases where no doubly charged secondaries occur (cf. the discussion concerning the charge-indicating interactions, § 1•2•4).

in the form of energy spectrum. Similarity between the shapes of the spectra suggests that there seems to exist no serious systematic error. Furthermore, the collision mean free path derived from comparison of numbers of leaving and interacting tracks turns out to be 18.8 ± 4.4 cm, in agreement with the expected value of 15.2 cm, so that a consistency of both measurements seems to be established.

Measurement of M- and H-components in the Prince Albert Project

Every track satisfying the scanning criteria was picked up and followed until it either ended in emulsion, suffered a nuclear interaction, or went through out of the stack. For tracks ending in emulsions, one is able to measure their energy and charge quite accurately from the range and the delta-ray density or the total number of delta rays as is already explained in the previous subsection.

In the practical application of the delta-ray measurement on the ending tracks, the following three different range conventions were used depending on the charge of the tracks: $D_\delta = 5\mu$ up to Mg, 10μ between Ne and S, and 20μ beyond Si. The D_δ-dependence of n_δ is illustrated in Fig. 1•2•19. At least two hundred delta rays are counted on each track, thus ensuring experimental resolution to be approximately $\Delta Z \sim 0.07Z$. The measurement was usually made at the residual range of 1.76 or 1.57 cm. In case the position was not suited for these measurements, another suitable position was chosen for the measurement and the value of n_δ at $R = 1.76$ cm or 1.57 cm was calculated by means of the theoretical formula confirmed by the calibration measurements.

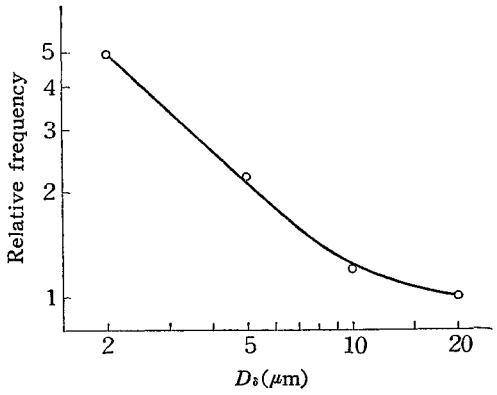

Fig. 1•2•19. Dependence of delta-ray density n_δ on the cutoff range D_δ.

The integrated delta-ray measurement was also applied for the ending tracks with the following conventions. Let the total track length counted be L_δ. For nuclei up to F, $D_\delta = 4.38\mu$ and $L_\delta = 2.6$ mm; for nuclei from O up to Al, $D_\delta = 8.76\mu$ and $L_\delta = 2.6$ mm; and for nuclei heavier than Mg, $D_\delta = 13.3\mu$ and $L_\delta = 2.8$ mm.

Every ending track was measured twice by the above two methods, if possible. A correlation diagram between the results of the two methods is shown in Fig. 1•2•20, showing an excellent consistency. We have presented

in Fig. 1•2•21 the charge spectrum thus obtained. In this way the energy and charge spectrum is obtained up to energy at air top of ~500 Mev/nucleon for M-nuclei, to ~650 Mev/nucleon for Ne, to ~740 Mev/nucleon for Mg, and so on, as will be seen from Fig. 1•1•5.

Tracks passing through the stack or interacting in emulsion give us informations of the higher energy part of the spectrum. Unfortunately, however, as the primary energy increases, measurements become more difficult. Therefore we have to exploit every possible use of parameters which can give us an information on charge and velocity for the concerned cases. The accuracy of the measurements in the case of these interacting or passing-through tracks is inferior to that in the case of ending tracks, so that one has to examine a consistency among

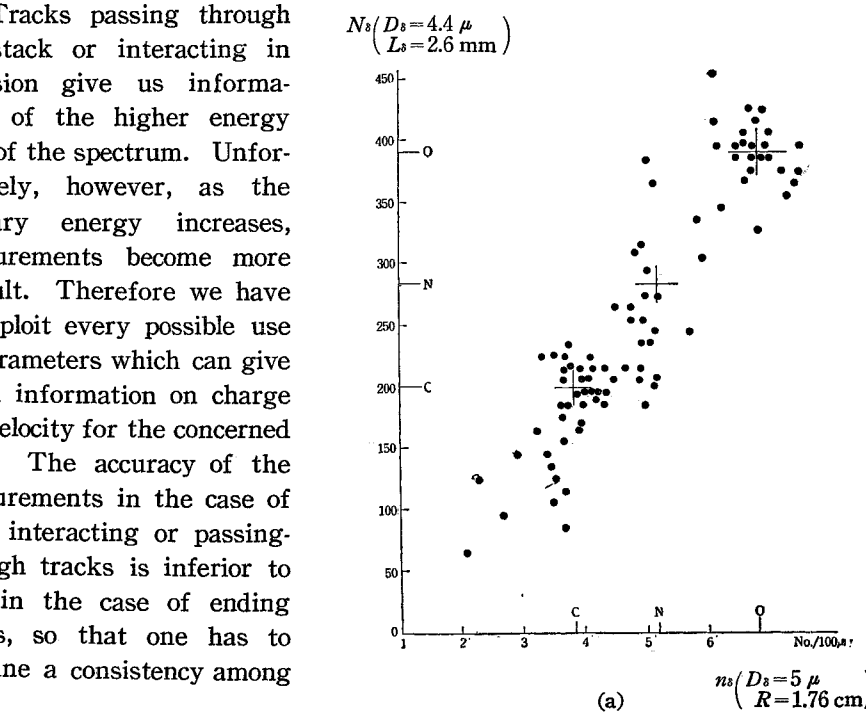

Fig. 1•2•20. Correlation diagram between n_s and N_s of stopped medium and heavy nuclei.

the results of several different kinds of measurements of mutually independent parameters, in order to ensure the reliability of the data.

We made use of the following four quantities:

(i) delta-ray density for a primary track,

(ii) change in delta-ray density while traversing through emulsion with a sufficient track length,

(iii) ionization of doubly or singly charged secondary particles for nuclei which made nuclear collisions,

(iv) energy and emission angle of high energy knock-on electrons.

Note that the last three quantities are completely independent of each other, and that therefore they can be used to check the consistency as mentioned above.

Now we shall consider the relative change of ionization $(dI/dR)/I$ while a primary nucleus traverses a medium. The ionization formula,

$$I=Z^2F_0(v) \tag{1·2·28}$$

can be expressed in terms of residual range R as,

$$I=Z^2h\left(\frac{Z^2}{A}R\right), \tag{1·2·29}$$

so that we have

$$\frac{dI}{dR}\Big/I=\frac{Z^4}{A}h'\left(\frac{Z^2}{A}R\right)\Big/Z^2h\left(\frac{Z^2}{A}R\right)=\frac{Z^2}{A}\varphi(E). \tag{1·2·30}$$

For the same value of E at the top of the emulsion the ionization difference between the top and the bottom of emulsion for a "through" track increases with increasing Z. Therefore the measurement of ionization change for "through" tracks can be applied in higher energy region at air top for nuclei with larger Z.

Now we shall explain how the actual charge-energy determination was made. Firstly we shall treat the case of M-nuclei. A track with $n_\delta=6.1$ can be either due to a 115 Mev/nucleon Be, a 200 Mev/nucleon B, a 340 Mev/nucleon C, a 600 Mev/nucleon N, a 1.2 Gev/nucleon O or a >5 Gev/nucleon F nucleus. This situation can be seen in Fig. 1·2·16. Note that a given value of n_δ corresponds to several *discrete* alternatives in energy, and therefore in the measurement of other parameters for energy determination, it is sufficient to have an accuracy that will enable us to distinguish between these various alternatives. If the nucleus does not make a nuclear collision, the identification of C and lighter nuclei is easy, because the track will end in the emulsions. In the case of a N nucleus it will pass through the stack and its n_δ will increase to ≈ 7.3 at the exit, so that the identification is not difficult by observing the change in n_δ. If, on the

other hand, the nucleus makes a nuclear collision, the ionization measurement of the secondary tracks will enable us to identify the nuclei up to, again, N. In case n_δ shows no significant variation between the entrance and exit, or in case the secondary tracks show no appreciable deviation from relativistic ionizations, there remain two alternative possibilities: a 1.2 Gev/nucleon O or a >5 Gev/nucleon F. The measurement of high energy knock-on electrons will enable us to make the discrimination between the two cases.

For heavy group, however, the situation is more complicated. The separation $\Delta Z/Z$ is smaller than that in the case of M-nuclei. When the variation in n_δ or the ionization of secondary tracks shows no significant deviation from those in the case of relativistic nuclei, there remain greater number of alternative possibilities. For example, if $n_\delta=15$ and the track shows no sign indicating that the nucleus is of energy <600 Mev/nucleon, the nucleus can be either a 800 Mev/nucleon Mg, a 1.4 Gev/nucleon Al or a >3 Gev/nucleon Si. We have, however, a fortunate compensation: the frequency of accompanying high energy knock-on

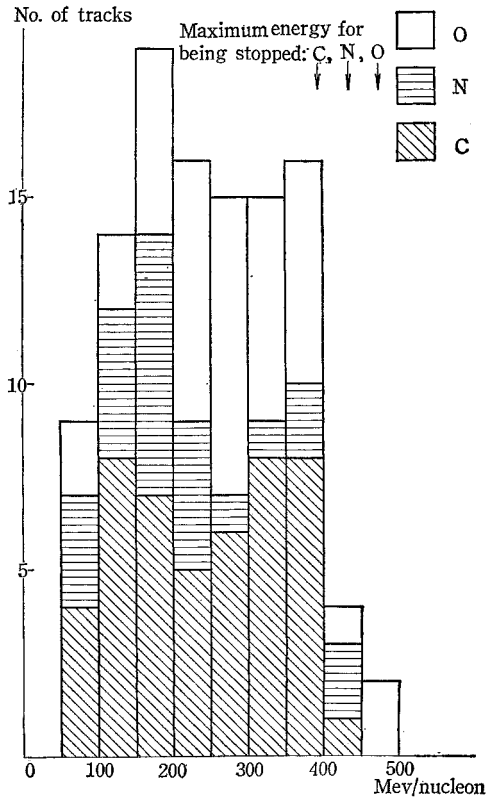

Energy at the top of the stack

(a)

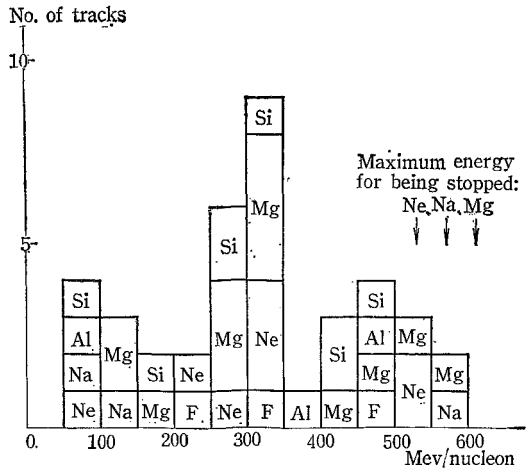

Energy at the top of the stack

(b)

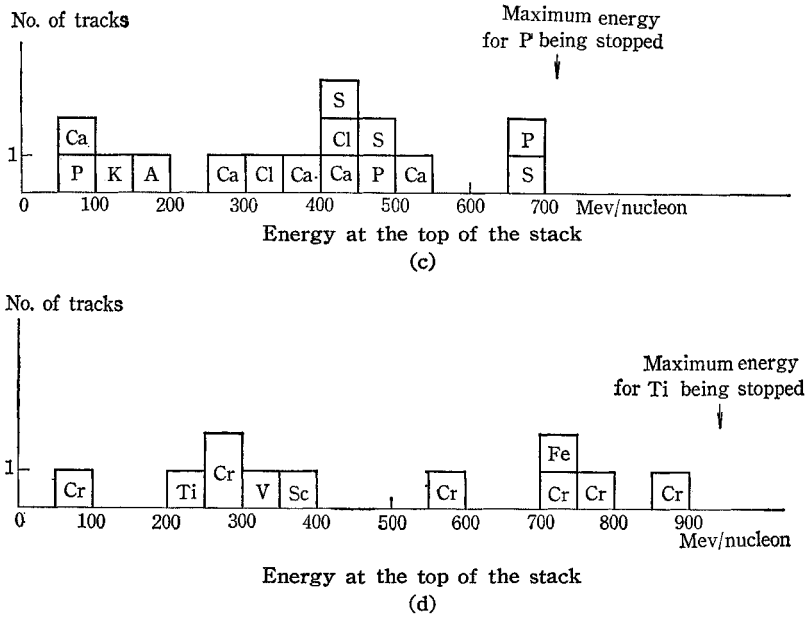

Fig. 1•2•21. Observed charge and energy distribution of stopped medium and heavy nuclei. Energy values refer to the top of vertical emulsion sheets.

electrons increases with increasing Z and the probability of their absence for an energetic nucleus becomes negligible. Thus we can proceed as follows: If high energy knock-on electrons are absent the nucleus can be assigned as Mg, while if we can find them they will enable us to discriminate between Al and Si.

In the actual measurement "through" tracks were used only for the following purposes:

(i) To determine that portion of the energy spectrum of M-nuclei which lies between 500 Mev/nucleon and 600 Mev/nucleon at air top.

(ii) To know the total number of "through" tracks of M-nuclei in order to make a cross-check on the total flux value of M-nuclei with energy greater than 500 Mev/nucleon at the air top which was determined from an analysis of interacting tracks only. The consistency was satisfactory: They agreed within 5% of each other assuming the collision mean free path in G5 emulsion as 13.0 cm.

(iii) To know the total number of "through" tracks of H-nuclei in order to make a similar cross-check as above about the total flux value of H-nuclei with energy greater than 700 Mev/nucleon at air top. The agreement in the case of H-nuclei was not so satisfactory with the assumption of the average collision mean free

path of 9.6 cm for G5 emulsion, so that in obtaining the flux value of H-nuclei of energy >0.7 Gev/nucleon both the interacting and the "through" tracks were used. The ratio of this flux value to the one obtained by means of the interacting tracks only, was adopted as a correction factor and applied to the flux values of H-nuclei of other energies, assuming that its energy dependence is weak.

In performing the measurement needed for (i) and (ii) mentioned above, 4-grain delta-ray counting, as well as blob counting, was used. At first the calibration curve was constructed as follows: We already had a number of ending tracks of identified charges, two C$\rightarrow 3\alpha$'s and an O$\rightarrow 4\alpha$ of known energies, and a relativistic O$\rightarrow 4\alpha$. Then the construction of the calibration curve was straightforward. It is, however, to be noted that the similarity law, as represented in Fig. 1•2•7, cannot be used here, because we have to expect some saturation effect of the delta-ray density to occur as well as some background contribution. The calibration curves for the 4-grain delta-ray countings are shown in Fig. 1•2•22.

Examples of the 4-grain delta-ray countings on the "through" tracks are shown in Fig. 1•2•23, where each mark represents a track specified by the delta-ray densities at entrance and at exit, both measured 1cm inside the stack in order to avoid edge effects. Different marks correspond to different observers. The expected variation of the delta-ray densities at exit as a function of the one at entrance has been obtained for each charge from the results plotted in Fig. 1•2•22. They are shown by the solid lines in Fig. 1•2•23. In order to demonstrate the existence of slow particles among the "through" tracks more clearly, in Fig. 1•2•24 a histogram is shown with respect to the ratio, r, of the delta-ray densities at each end.

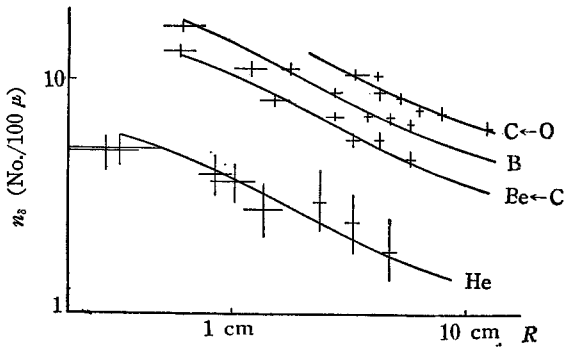

Fig. 1•2•22. Calibration curves of the 4-grain delta-ray density versus residual range.

Out of 118 "through" tracks of C, N and O nuclei which were found in the scan A, 28 was found out to have energies lower than 600 Mev/nucleon at emulsion top.

The measurement needed for (iii) was done by means of the delta-ray counting with range convention.

The rest of the measurement was done by the use of interacting tracks under the following criteria:

Firstly, tracks of primary nuclei which traversed less than 1cm of emulsion before their interaction were omitted in the measurement in order to secure sufficient number of delta rays and at the same time to eliminate possible edge effect on the delta-ray density.

Secondly, interactions whose secondary tracks lay entirely within 1.5cm from the emulsion edges were omitted, for blob and gap densities may suffer considerable influences from non-uniform developing conditions near the edge.

Finally, interactions with $N_h \geqq 8$ were omitted, N_h being the number of grey and black prongs. This is because measurement of these interactions are not free from the ambiguity in energy determination of the incident nuclei when their energy is sub-relativistic.*

The correction factor

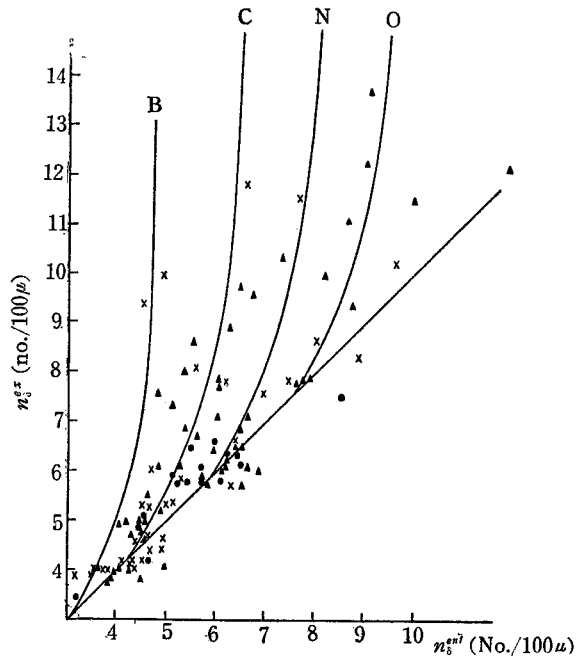

Fig. 1•2•23. The results of the 4-grain delta-ray countings on "through" tracks. n_δ^{ent} and n_δ^{ex} mean the 4-grain delta-ray densities of the nuclei near the top and near the bottom, respectively, of the stack. Also illustrated in the figure is the energy dependence of the relation between n_δ^{ent} and n_δ^{ex} for several nuclear charge numbers.

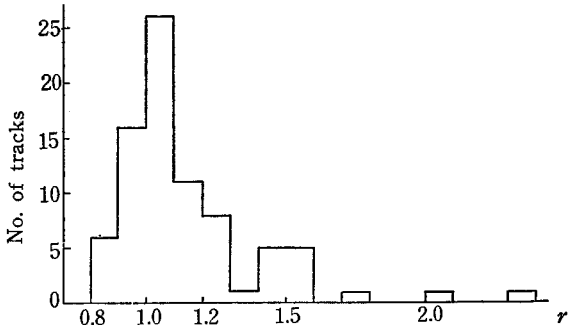

Fig. 1•2•24. r-distribution of the "through" C, N and O nuclei, where r is the ratio of n_δ^{ex} to n_δ^{ent}. r is, in the lowest order approximation, a function of the velocity of the primary nuclei only. The figure shows clearly the existence of slow nuclei among the "through" nuclei.

* In the case of L-nuclei this condition was not applied. This was because:
(i) We wanted as good statistics as possible of the L-nuclei whose tracks are harder to scan than those of heavier nuclei and whose flux is small compared with that of M-nuclei.
(ii) The number of nucleons in the primary L-nuclei is rather small and consequently the ambiguity is much less serious.

for putting the third criterion on N_h is obtained as follows. Among primary nuclei which made interactions, those satisfying the first and the second criteria were picked up and their numbers were counted for the M-nuclei and H-nuclei groups. Out of these the number of interactions with $N_h \leqq 7$, i.e., those satisfying the third criterion were counted. The energy measurement was made only on the latter group of interactions. The ratio of the former group of interactions to the latter was assumed to be not sensitive to the energy of the incident nuclei and was used as the correction factor in calculating the flux value, common for all energy intervals. The ratios were

$$\frac{135}{82} = 1.65 \pm 0.23 \quad \text{for M-nuclei,}$$

and

$$\frac{84}{49} = 1.71 \pm 0.31 \quad \text{for H-nuclei.}$$

These values can be compared with those obtained by Rajopadhye and Waddington[12,13] at different energy intervals,

$$\frac{398}{254} = 1.57 \pm 0.13 \quad \text{for M-nuclei,}$$

and

$$\frac{196}{114} = 1.72 \pm 0.20 \quad \text{for H-nuclei.}$$

In this way the differential energy spectra of M- and H-nuclei were determined up to 1 Gev/nucleon at air top, together with the integrated flux values of nuclei with energy >1 Gev/nucleon. The charge and energy distribution is given in Fig. 1·2·25.

A tentative determination of the flux values of M- and H-nuclei of energy greater than 5 Gev/nucleon

The energy spectra in the region above 1 Gev/nucleon was investigated by the knock-on electron method.

The energy determination was made for medium nuclei which interacted after traversing more than 2 cm of emulsions and for heavy nuclei which interacted after traversing more than 1 cm of emulsions, irrespective of N_h.

Out of 300 interactions of $Z \geqq 6$ primaries satisfying the afore mentioned criterion 200 were excluded by the opening angle measurement or the ionization measurement of the doubly or singly charged secondaries. Knock-on electrons were scanned in the primary tracks of the remaining 100, and two or more electrons suitable for measurement were found and

measured in 62 tracks. 13 M-nuclei and 8 H-nuclei were found to have energies >5 Gev/nucleon.

There may be some nuclei of energy >5 Gev/nucleon among the nuclei which were excluded because of large opening angle of the interaction. The number, however, will not exceed 30 % of the actually measured ones of energy >5 Gev/nucleon in the light of the correlation of the opening angle of secondaries and the energy in the actually measured cases.

Again, there may be nuclei of energy >5 Gev/nucleon which have no knock-on electrons suitable for measurement in the whole scanned length of the track. To estimate the number of such cases, the total number of knock-on electrons suitable for measurement was counted for some nuclei with energy >5 Gev/nucleon which had traversed more than 5 cm of emulsions before they interacted. It was found out that magnesium nuclei with energy >5 Gev/nucleon knocked out one electron with $X<0.25$ per 1 cm of track and that the frequency depended on the charge of the nuclei approximately according to the Z^2-law (cf. §1•2•5).

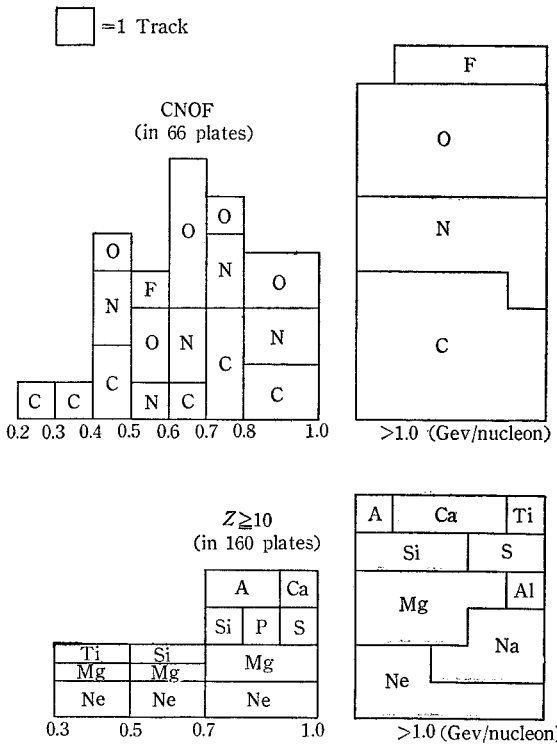

Fig. 1•2•25. Charge and energy distribution of interacting medium and heavy nuclei. Energy values refer to the energy at air-top.

This means that, if we take the nuclei which both have energy >5 Gev/nucleon and satisfy the selection criterion of the knock-on electron scanning, the ratio of the total number to the number of the nuclei which knocked out at least one electron which is suitable for measurement is

$$\frac{\int_{2.1}^{10.5} \frac{1}{13.0} e^{-\frac{x}{13.0}} dx}{\int_{2.1}^{10.5} \frac{1}{13.0} \left(1-e^{-\frac{x}{4}}\right) e^{-\frac{x}{13.0}} dx} \fallingdotseq 1.38 \quad \text{for M-nuclei, and}$$

$$\frac{\int_{1.05}^{1.05}\frac{1}{9.6}e^{-\frac{x}{9.6}}dx}{\int_{1.05}^{10.5}\frac{1}{9.6}\left(1-e^{-x}\right)e^{-\frac{x}{9.6}}dx}\fallingdotseq 1.06 \quad \text{for H-nuclei,}$$

where 13.0 cm and 9.6 cm are the collision mean free paths in emulsion of M-nuclei and H-nuclei, respectively. Combining the two corrections, i. e., the one which takes into account the possible over-exclusion of tracks and the other which takes into account the accidental nonexistence of knock-on electrons in the scanned track-length, the upper bounds of the observed interactions of the nuclei with energy >5 Gev/nucleon are obtained by increasing the actually observed cases of M- and H-nuclei by 80 % and 40%, respectively.

Chapter 2. Experimental Results

§ 2•1. Extrapolation to the top of atmosphere

For obtaining the flux value of heavy primaries at the top of atmosphere from the observational data at the stratosphere, one must apply corrections for their interactions with atoms of air. One is the correction for break-up of heavy primary due to its nuclear collision, and the other is that for ionization loss of its energy.

2•1•1. *Break-up of heavy primaries*

There are two different ways of making this correction for break-up of heavy primaries. One is first to measure the altitude variation of various component of heavy primaries in a direct way or making use of zenith angle distribution, and then extrapolate the obtained relation to the top of atmosphere. The difficulty in this method lies in measuring the altitude variation with sufficient statistical accuracy to obtain a reliable extrapolation.

The other way is to solve the equation of diffusion of heavy primaries in the atmosphere. Let $N_j(x)$ be the flux value of j-component at the atmospheric depth x. Then the equation is expressed as,

$$\frac{d}{dx}N_j(x)=-\frac{1}{\Lambda_j}N_j(x)+S_j(x). \qquad (2\cdot1\cdot1)$$

Λ_j is the absorption mean free path, which is related with the collision mean free path λ_j by the following equation,

$$\Lambda_j=\frac{1}{1-P_{jj}}\lambda_j. \qquad (2\cdot1\cdot2)$$

$S_j(x)$ in (2·1·1) is the source function. Noting that j-component is produced by the break-up of heavier component, one has

$$S_j(x)=\Sigma_{i\leq j}\frac{P_{ij}}{\lambda_i}N_i(x). \tag{2·1·3}$$

P_{ij} is called as the fragmentation probability and expresses the expected number of j-component nuclei in a nuclear break-up of i-nuclei.*

Once one knows the values of parameters, Λ_j and P_{ij} in (2·1·1), the equation (2·1·1) gives a correction for the break-up. Here, we shall write down a solution of (2·1·1) in an explicit form. When the depth x is not large compared with the absorption mean free path Λ_j, the solution can be obtained by a successive approximation. The zeroth approximation is, of course,

$$N_j^{(0)}(x)=N_j(0)\exp(-x/\Lambda_j). \tag{2·1·4}$$

The first approximation is, taking a one-step break-up ($i\to j$) into account,

$$N_j^{(1)}(x)=\Sigma_{i<j}P_{ij}N_i(0)\frac{\Lambda_j}{\Lambda_j-\Lambda_i}\frac{\Lambda_i}{\lambda_i}[\exp(-x/\Lambda_j)-\exp(-x/\Lambda_i)]. \tag{2·1·5}$$

The second approximation covers a two-step break-up ($h\to i\to j$).

$$\begin{aligned}N_j^{(2)}(x)=&\Sigma_{h<i}\Sigma_{i<j}P_{hi}P_{ij}N_h(0)\frac{\Lambda_i}{\Lambda_j-\Lambda_h}\frac{\Lambda_h}{\lambda_h}\\&\times\left[\frac{\Lambda_j}{\Lambda_j-\Lambda_i}\frac{\Lambda_i}{\lambda_i}(\exp(-x/\Lambda_j)-\exp(-x/\Lambda_i))\right.\\&\left.-\frac{\Lambda_j}{\Lambda_j-\Lambda_h}\frac{\Lambda_h}{\lambda_i}(\exp(-x/\Lambda_j)-\exp(-x/\Lambda_h))\right].\end{aligned} \tag{2·1·6}$$

2·1·2. *Fragmentation parameters*

It is difficult to obtain directly the fragmentation parameters in air. Instead, the break-up of heavy primaries by lighter nuclei such as carbon, nitrogen or oxygen can be studied, and their data can be used for the diffusion problem of heavy primaries in the atmosphere.

Among the nuclear interactions produced in nuclear emulsions, one can set a certain criterion and try to select the events which are plausibly produced by the nuclei C, N, or O. The method adopted currently is to pick up the events with the number of evaporation prongs N in a certain region; $1\leq N\leq 7$. This method has, of course, a defect, because a certain fraction of events produced by heavy nuclei will have the prong number

* $i<j$ if i-nuclei are heavier than j-nuclei.

in this region. But it can be expected that the majority of events thus selected do belong to the C, N and O events and that the fragmentation parameters of Ag and Br events with few evaporation prongs will not be largely different from those of C, N and O events.

In Table 2•1•1, the values of fragmentation parameters are presented together with the results of other authors. In the fourth row of the Table we quote the values published in Waddington's review article.[2101] This value is an average of experimental results by various authors, and in most of the works mean energy of primaries are 3 Gev per nucleon. In our experiment, the cutoff energy of primaries is very low and the fragmentation parameters are obtained in the lower energy region in comparison to the above cases.

It is seen from the table that no significant difference exists beyond the statistical errors for the values of fragmentation parameters in the different energy regions. This is consistent with our knowledge of the high energy nuclear reactions, according to which some change in the fragmentation parameters below a few hundred Mev per nucleon is expected. To detect such a change at the low energy region, we need a few times better statistics than the present work.

In the fifth row of the Table 2•1•1, the results of the measurements by Hirashima[2102] are quoted. He used an emulsion chamber, which is a pile of carbon plates and nuclear emulsion plates put alternately, and observed break-ups of heavy primaries in carbon plates. By this method he was able to pick up the break-up events by lighter nuclei in an unambiguous way. But the vertical incidence of the track in the emulsion plates makes the measurement on charge of particles rather inaccurate.

Comparing all of the results, we arrive at the so-called best values which are presented in the last row of the table. We shall use these values throughout this paper, and assume these to be constant in the energy region concerned.

Table 2•1•1. Fragmentation parameters in air.

	P_{LL}	P_{MM}	P_{ML}	P_{HH}	P_{HM}	P_{HL}
Ours ($E_0 \geq 1$Gev)		0.14±0.06	0.19±0.07	0.23±0.13	0.38±0.13	0.09±0.06
($E_0 < 1$Gev)		0.16±0.07	0.19±0.08	0.31±0.14	0.31±0.14	0.19±0.11
Average	0.08±0.05	0.15±0.05	0.19±0.05	0.29±0.10	0.34±0.10	0.13±0.06
Waddington ($E \sim 3$Gev)	0.13±0.03	0.16±0.02	0.21±0.02	0.31±0.04	0.33±0.04	0.14±0.03
Hirashima ($E \sim 7$Gev)	0.17±0.12	0.08±0.04	0.35±0.08	0.18±0.06	0.28±0.07	0.35±0.08
Best value	0.15	0.15	0.25	0.30	0.33	0.15

2•1•3. *Collision mean free path*

Another important quantity in the diffusion equation is the collision mean free path. In Table 2•1•2, the observed collision mean free paths in emulsion are shown together with the values compiled by Waddington[2101] from various experiments for primaries with average energy ~3 Gev/nucleon.

Table 2•1•2. Collision mean free path in emulsion.

	L	M	H
Ours (≳0.5 Bev)	18.7±2.1	16.2±1.3	12.1±1.4
Av. for low energy data*	18.7±2.1	16.1±1.2	12.2±1.0
Av. for high energy** (~3 Gev)	14.4±1.1	13.3±0.6	10.9±1.2

* Noon and Kaplon, Freier et al., and ours.
** Rajopadhye and Waddington, and Cester et al.

It appears that our values at low energy region are higher by ~20% than those obtained at high energy region. Other experiments at lower energy region, such as those of Freier et al.[2103] and Kaplon and Noon,[2104] both with geomagnetic cutoff energy of ~400 Mev/nucleon, showed essentially the same results as ours. In the second row of the Table 2•1•2, an average of the three experiments made at lower energy region is given.

A semi-empirical expression for the cross-section of beak-up can be constructed from the numerical data in Table 2•1•2. Let A_t and A_t be the mass numbers of incoming and target nucleus, respectively, we have

$$\sigma=\pi r_0^2(A_t^{1/3}+A_t^{1/3}-b)^2, \qquad (2\cdot1\cdot7)$$

where

	r_0	b
high energy (~3 Gev)	1.1±0.2	−0.5±1.1
low energy (~0.5 Gev)	1.0±0.3	−0.7±1.6.

This relation can be used for obtaining the collision mean free paths in air, which are given in Table 2•1•3.

Table 2•1•3. Collision mean free path in air in g/cm².

	L	M	H	VH	error
Low energy	40.0	28.6	22.4	14.4	±10%
High energy	38.2	27.6	21.6	13.9	± 5%

2·1·4. *Correction procedures used in the Prince Albert Project*

Corrections in the emulsion

In the Prince Albert Project the measurement was made on both the "interacting" tracks and the "non-interacting" tracks. The interactions which occurred outside the measurement area were corrected for. In Ilford G5 emulsion of density 3.9 g/cm^3, the averaged values of $A_t^{2/3}$ and $A_t^{1/3}$ are

$$\overline{A_t^{2/3}}=7.60 \quad \text{and} \quad \overline{A_t^{1/3}}=2.37,$$

respectively.

For the average mass numbers of the heavy primaries we adopted the values 13.5 and 28.0 for M- and H-nuclei, respectively.* As pointed out in §2·1·3, it is likely that the collision mean free paths have some energy dependence. In the above correction procedure, however, this energy dependence has not been taken into account, because, as mentioned above, the correction was only for the small number of nuclei which made nuclear collisions near the emulsion edges.

Extrapolation to the top of atmosphere

The extrapolation of the balloon height flux values to the top of atmosphere is carried out by means of the "best set of fragmentation parameters in the air" given in §2·1·2 of this chapter according to the prescription explained there or in Appendix 1.

In the case of the Prince Albert Project, however, we deal with the primary nuclei of energy several hundred Mev/nucleon and for these nuclei the ionization loss in the air is not negligible.

The extrapolation procedure which takes into account this effect as well as the fragmentation in the air is given in Appendix 5. As will be seen there, the evaluation can be carried out only by means of numerical integrations.

For this reason we made an approximation which amounts to neglecting the difference in ionization of incident nuclei before and after their fragmentations. The effective mean atmospheric depth of the Prince Albert Exposure was 8.0 g/cm^2. We adopted an approximate model in which all the fragmentations corresponding to the 8.0 g/cm^2 of air occurred at the top of the atmosphere. For example, if a primary Si nucleus passes through 5 g/cm^2 of air, makes a nuclear collision there, turns into a secondary O nucleus and then passes through the remaining 3 g/cm^2 of air, the ionization

* In the case of H-nuclei of energy <700 Mev/nucleon at air top, we did not use the above average mass number but made the correction separately for each nucleus.

loss is approximated by that of a primary O nucleus which passes through 8 g/cm^2 of air. Therefore we underestimate the ionization loss effect in adopting this approximation. The error arising from this is estimated in Appendix 5. The result is as follows:

It is the case of L-nuclei where the effect of the above-mentioned "ionization difference" can be really significant. However, in the case of the fragmentation M→L which contributes the main part to the secondary production of L-nuclei, the effect is significant only in the energy region lower than 200 Mev/nucleon at air top. It is true that in the case of the fragmentation H→L the effect is not negligible even for higher energies. But both P_{HL} and the flux of H-nuclei is small compared with P_{ML} and the flux of M-nuclei. Therefore we can see that the error under consideration is not significant even for L-nuclei.

The extrapolation was carried out in the following manner. We divided the whole energy interval into two regions—the lower energy part covering the interval from 200 up to 700 Mev/nucleon and the higher energy part covering the interval higher than 700 Mev/nucleon at air top. The flux value of each charge component corresponding to each energy region was treated as a single set and no further division of energy intervals was made. As the lowest order approximation the same set of fragmentation parameters were assumed in both energy intervals, although it is more natural that fragmentation parameters are energy-dependent.

For heavier nuclei we failed to observe the whole energy interval down to 200 Mev/nucleon because of the air cutoffs. For these nuclei the small portions of differential energy spectra which lay in the immediate vicinity of 200 Mev/nucleon were extrapolated assuming the similarity of these parts to the corresponding part of the spectrum of M-nuclei.

§ 2·2. Experimental results

2·2·1. *Differential energy and rigidity spectra*

The differential energy spectra of α-, L-, M- and H-components at the air top are shown in Table 2·2·1 and in Fig. 2·2·1.* In Fig. 2·2·1, the differential energy spectrum of α component observed by Minnesota Group[2201] on 18 June, 1954 at Saskatoon is also shown for comparison. It is seen that all components have spectra of similar shape, all having very broad maxima at ~500 Mev/nucleon with half widths of ~300 Mev/nucleon and low energy ends of a "fade-out" shape.

The behavior at the low energy ends gives another support to the view that there is no rigid barrier against primary cosmic ray particles of energy lower than a certain threshold value.

* See also ref. 2202).

Table 2•2•1. Differential energy spectra.
(Figures in the parentheses are the flux values after ascent correction (see text, §2•2•1.).)

E at air top (Gev/nucleon)	Differential flux at top of atmosphere (particles/m²•sec•sterad•0.1 Gev/nucleon)			
	He	LiBeB	CNOF	$Z \geqq 10$
0.135				
	7.3±1.1 (6.6±1.0)			
0.2				
	9.1±2.6 (8.2±2.4)	0.12±0.05 (0.10±0.04)	0.51±0.08 (0.47±0.07)	
0.3				
	5.3±2.0 (4.8±1.8)	0.31±0.07 (0.25±0.06)	0.71±0.11 (0.65±0.10)	0.27±0.06 (0.25±0.06)
0.4				
		0.52±0.10 (0.43±0.08)	0.91±0.14 (0.84±0.13)	0.34±0.08 (0.31±0.07)
0.5	11.8±2.1 (10.2±1.9)			
		0.41±0.08 (0.34±0.07)	0.96±0.18 (0.88±0.17)	0.30±0.08 (0.28±0.08)
0.6				
		0.23±0.07 (0.19±0.06)		0.29±0.08 (0.27±0.07)
0.7			0.71±0.20 (0.65±0.18)	
	6.7±0.6*			
0.8				
	(6.0±0.5)			0.19±0.06 (0.18±0.05)
0.9			0.49±0.16 (0.45±0.15)	
1.0				

* Obtained by extrapolation using the measured integral flux value above 0.6 Gev/nucleon and assuming the integral energy spectrum of the form $\propto (1+E)^{-1.4}$.

The coincidence in the position of maxima rejects the "ionization loss theory", according to which the aforementioned maxima are formed as a result of the equilibrium between the energy gain by means of, e. g., statistical acceleration and the energy loss by way of ionization in, e. g., the interstellar space, of cosmic ray particles.[2203] If this theory were true, the maximum at 500 Mev/nucleon for He nuclei would mean the maximum at 2.7 Gev/nucleon for N nuclei and at 5.6 Gev/nucleon for Mg nuclei, or the maximum at 500 Mev/nucleon for N nuclei would mean the maximum around 1 Gev/nucleon for Mg nuclei, in obvious disagreement with the observed results.

On this basis it is highly probable that features of the energy spectra of these heavy primary components have to be explained by a magnetic effect of some kind. If this picture is true, it will be more natural to take magnetic rigidity as the parameter in place of energy per nucleon.*

The relation between energy E and magnetic rigidity R is illustrated

* This discussion does not directly hold in the case of L-nuclei. See §2•2•2.

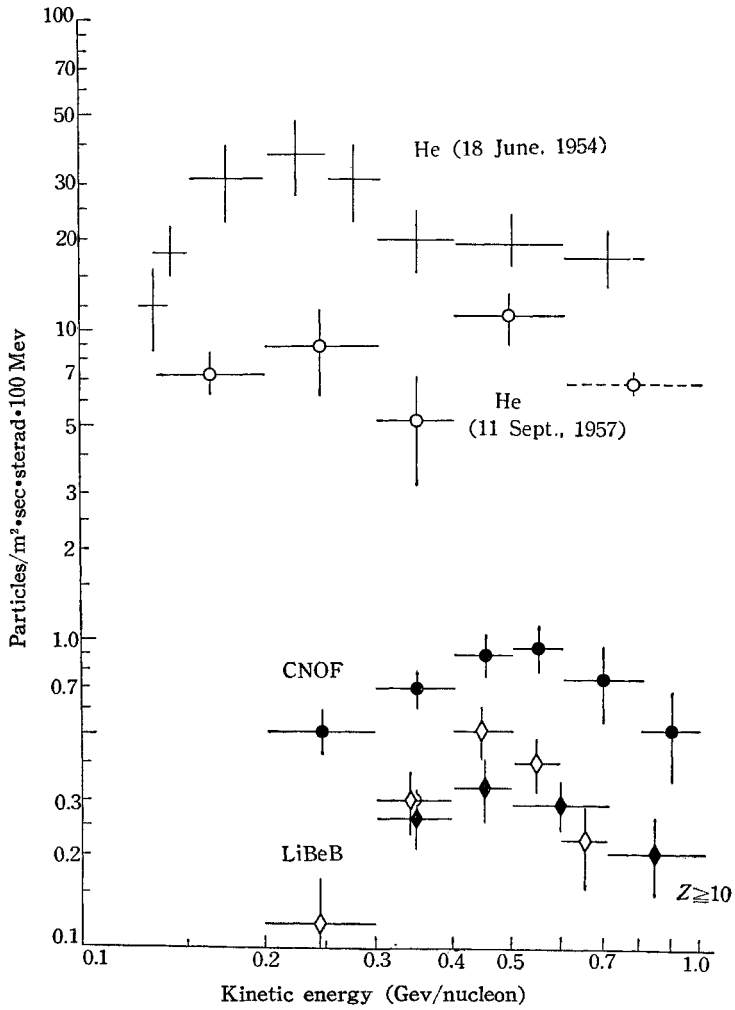

Fig. 2•2•1. Differential energy spectra of α-, L-, M- and H-components. For comparison, the α spectrum observed on 18 June, 1954, at Saskatoon is also shown in the figure.

in Fig. 2•2•2 for various values of A/Z and, using this relation, we can draw the differential rigidity spectra of the various heavy primary components.

The differential rigidity spectra of α-, L-, M- and H-components are shown in Table 2•2•2 and Fig. 2•2•3. It is seen that the maxima of all the spectra fall at $R \sim 2.2$ to 2.3 Gv.

The comparison of the 1957 Prince Albert α spectrum with the 1954 Saskatoon α spectrum shows:

(i) a displacement of the maximum position to a higher rigidity,

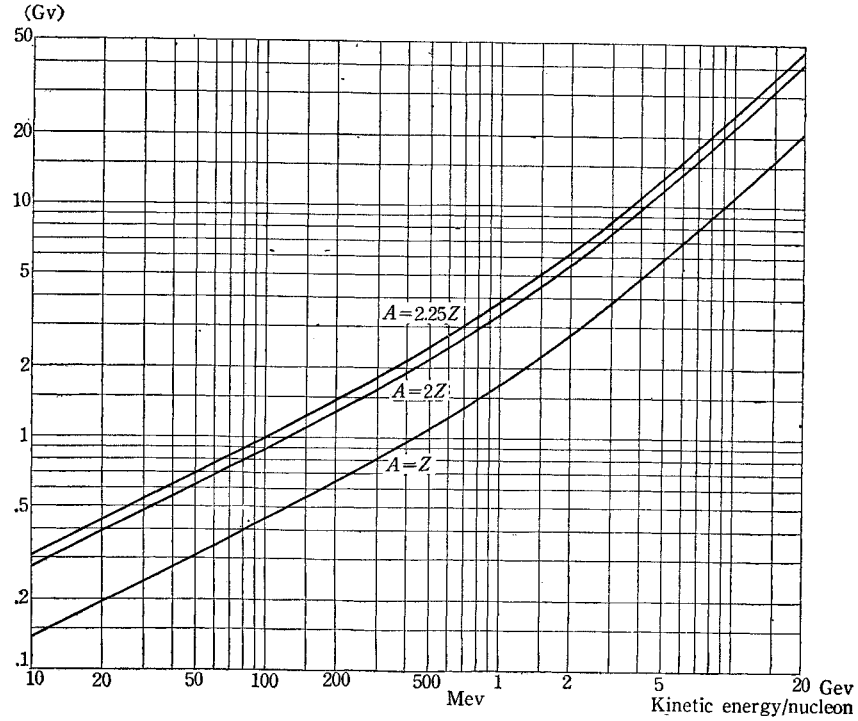

Fig. 2•2•2. Relation between kinetic energy/nucleon E and magnetic rigidity R for various values of A/Z.

(ii) a decrease in absolute flux value at the maximum.

Discussions about these features are given in § 3•3.

2•2•2. *Chemical composition*

The Prince Albert Project has given an information for the first time about the chemical composition of heavy primary cosmic rays of very low energy——several hundred Mev/nucleon.

Table 2•2•3 and Table 2•2•4 give the flux values and charge ratios without and with ascent correction, respectively, of various charge components at air top in the lower and the higher rigidity regions.

No substantial difference is observed between the charge ratios in the two rigidity regions——1.3 Gv$<R<$2.7 Gv and $R>$2.7 Gv.

In Table 2•2•3, the individual flux values of Li, Be and B are given together with their ratios to the M-component, in order to see whether there is any difference in their rigidity dependences. It will be seen that there is no substantial difference except for the case of Be, which is the least abundant and for which, therefore, the statistical error and the contamination arising from the adjacent B and Li may have large effect.

Table 2•2•2. Differential rigidity spectra.
(Figures in the parentheses are the flux values after ascent correction (see text §2•2•1.).)

R at air top (Gv)	Differential flux at top of atmosphere (particles/m²•sec•sterad•Gv)			
	He	LiBeB	CNOF	$Z \geqq 10$
1.04				
	19.3±2.8			
	(17.4±2.5)			
1.29				
	27.4±7.9		1.55±0.24	
1.45				
	(24.7±7.1)	0.32±0.14	(1.42±0.22)	
1.62				
	18.3±6.9	(0.26±0.12)	2.45±0.38	0.93±0.21
1.82				
	(16.5±6.2)	0.95±0.21	(2.25±0.35)	(0.86±0.19)
1.91				
		(0.78±0.17)	3.37±0.52	1.26±0.30
2.15				
	42.8±7.8		(3.09±0.48)	(1.16±0.28)
2.18				
	(38.5±7.0)	1.70±0.33	3.69±0.69	1.15±0.32
		(1.40±0.27)	(3.38±0.63)	(1.06±0.30)
2.44				
				1.16±0.34
2.46				
		1.40±0.27	2.88±0.80	(1.07±0.31)
2.69				
		(1.15±0.22)	(2.64±0.73)	
2.75				
	27.7±2.4*	0.83±0.25		
2.93				
	(25.0±2.2)	(0.68±0.21)		0.82±0.24
3.03				
			2.00±0.68	(0.76±0.22)
3.17				
			(1.89±0.62)	
3.40				

* Obtained by extrapolation. See Table 2•2•1.

A special remark will be made about L-component. L-component can have a rigidity spectrum which is different from the rigidity spectra of M- and H- component. This arises from the fact that L-component is absent at the cosmic ray source, while M- and H-components already exist there. For example, if the main part of L-component is produced after the main features of M- and H-rigidity spectrum have already been formed, it is the *energy* spectra, not the *rigidity* spectra, of L-, M- and H-component that are to be compared with each other. For L-component, therefore, it is interesting to investigate which gives more reasonable result, the description in terms of R, magnetic rigidity, or the description in terms of E, kinetic energy per nucleon.

Table 2•2•5(a) gives the flux values in the lower and the higher energy regions—0.2 Gev/nucleon$\leq E \leq$0.7 Gev/nucleon and $E \geq$0.7 Gev/nucleon.

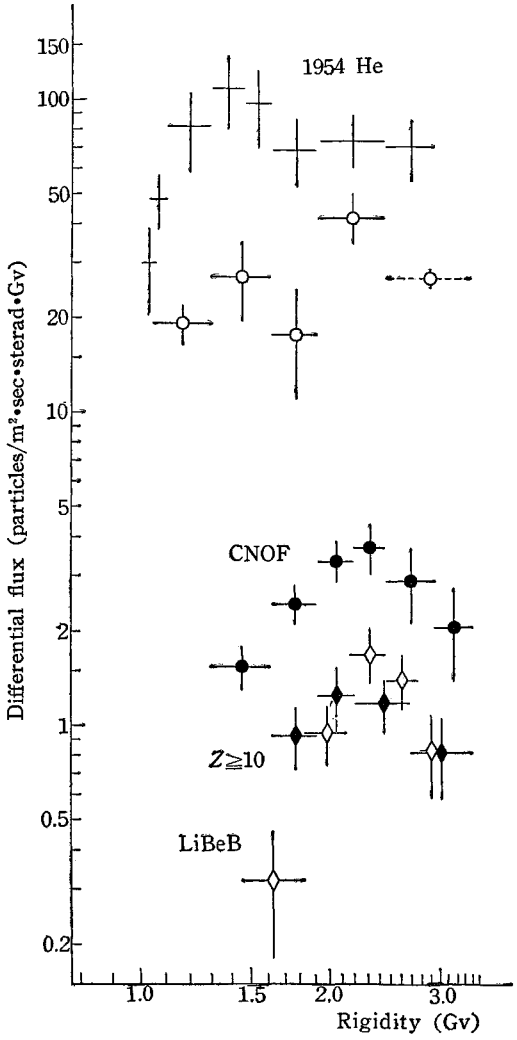

Fig. 2•2•3. Differential rigidity spectra of α-, L-, M- and H-components.

Uniform (i.e., energy independent) ascent corrections have been made on the flux values. Table 2•2•5(b) gives the charge ratios in the two energy regions. Table 2•2•5(c) gives the charge ratios given by the authors quoted in § 2•2•3.[2204] These authors have observed the flux values in the period of minimum solar activity at the places of cutoff rigidity 4.5 Gv, which corresponds to cutoff energy 1.5 Gev/nucleon for M- and H-components. Cutoff energy 1.5 Gev/nucleon for L-component in turn corresponds to cutoff rigidity 5.1 Gv. The L-flux of this cutoff rigidity has been obtained by an extrapolation assuming the integral rigidity spectrum of the form $\propto R^{-1.5}$.

Inspection of Table 2•2•5(b) and Table 2•2•5(c) suggests a higher L/M ratio in the lower energy region. The H/M ratio, on the other hand, shows no significant energy dependence. Therefore the energy dependence of L/M ratio can originate from several possible reasons such as:

(i) the fragmentation parameters for hydrogen target may have significant energy dependence,

(ii) the path length in the interstellar matter may increase with decreasing energy,

(iii) the representation in terms of E may be inadequate and we have to adopt the representation in terms of R.

An extensive study at the period of minimum solar activity is important to settle the question.

Table 2•2•6 gives the flux values at air top of individual element of

Table 2•2•3. Integral flux values and charge ratios in the Prince Albert Project (without ascent correction).

Flux values (particles/m²•sec•sterad)				
	$1.3<R<2.7$ Gv	$R>2.7$ Gv	$R>3.4$ Gv	$R>11.7$ Gv
He	45.0 ±5.8	90.0 ±7.9		
L (LiBeB)	1.40±0.16	1.82±0.17		
M(CNOF)	3.97±0.35	6.96±0.87	5.35±0.76	0.65±0.18
H ($Z\geqq10$)	1.34±0.18	2.02±0.19	1.44±0.26	0.25±0.09
Li	0.31±0.06	0.73±0.10		
Be	0.45±0.09	0.09±0.02		
B	0.64±0.11	1.00±0.13		
Charge ratios				
L/M	0.35±0.05	0.26±0.04		
H/M	0.34±0.05	0.29±0.05	0.27±0.06	0.38±0.17
L/H	1.05±0.18	0.95±0.13		
He/M	11.3 ±1.8	12.7 ±2.0		
Li/M	0.08±0.02	0.10±0.02		
Be/M	0.11±0.02	0.013±0.004		
B/M	0.16±0.03	0.14±0.03		

Table 2•2•4. Integral flux values and charge ratios in the Prince Albert Project (with rigidity-independent ascent correction).

Flux values (particles/m²•sec•sterad)				
	$1.3<R<2.7$ Gv	$R>2.7$ Gv	$R>3.4$ Gv	$R>11.7$ Gv
He	40.6 ±5.2	81.1 ±7.2		
L (LiBeB)	1.15±0.13	1.61±0.15		
M(CNOF)	3.64±0.32	6.37±0.80	4.90±0.70	0.60±0.17
H ($Z\geqq10$)	1.24±0.16	1.87±0.18	1.33±0.24	0.22±0.08
Charge ratios				
L/M	0.32±0.05	0.25±0.04		
H/M	0.34±0.05	0.29±0.05	0.27±0.06	0.37±0.17
L/H	0.93±0.16	0.86±0.11		
He/M	11.2 ±1.8	12.7 ±2.0		

$Z\geqq2$ in the rigidity region of $1.3\,\text{Gv}<R<2.7\,\text{Gv}$.

Table 2•2•7 gives the relative abundances among the elements of $Z\geqq3$ in the region $1.3\,\text{Gv}<R<2.7\,\text{Gv}$. The relative abundances in the latter rigidity region are the values given in the review article by Waddington,[2205] based on the results obtained by the Chicago Group, the Torino Group

Table 2•2•5. Integral flux values and charge ratios expressed in terms of kinetic energy per nucleon E, (with energy-independent ascent correction). E is expressed in Gev/nucleon.

Table 2•2•5(a). Integral flux values in the Prince Albert Project. (particles/m²•sec•sterad)

	$0.2<E<0.7$	$E>0.7$
L (LiBeB)	1.35±0.14	1.34±0.13
M(CNOF)	3.64±0.32	6.37±0.80
H($Z\geqq 10$)	1.24±0.16	1.87±0.18

Table 2•2•5(b). Charge ratios in the Prince Albert Project.

	$0.2<E<0.7$	$E>0.7$
L/M	0.37±0.05	0.21±0.03
H/M	0.34±0.05	0.29±0.05
L/H	1.09±0.18	0.72±0.10

Table 2•2•5(c). Charge ratios given by the three authors quoted in § 2•2•3. ($E>1.5$ Gev/nucleon)

	Waddington	Cester et al.	Koshiba et al.
L/M	0.21±0.03	0.21±0.02	0.25±0.03
H/M	0.36±0.05	0.51±0.07	0.41±0.06
L/H	0.58±0.10	0.40±0.06	0.61±0.10

and the Bristol Group. It is seen that, again, there is no substantial difference between the two rigidity regions.

The discussions about the chemical composition of the heavy primaries are given in Chap. 3, § 1 and § 2.

2•2•3. *Integral flux values in the higher rigidity region*

Now there are several observations of heavy primaries of $Z\geqq 3$ at places corresponding to the geomagnetic cutoff rigidity of 4.5 Gv, and it will be interesting to compare the higher rigidity portion of the Prince Albert flux values with the results of these observations.

We have chosen four observations. Three of them, i.e., the observation by Waddington, that by Cester et al., and that by Koshiba et al.,[2204] are the ones carried out during the period of minimum solar activity—1954 to 1955. The remaining one, i.e., the observation by Freier et al.,[2206] is the one carried out about a month after the Prince Albert Exposure, so that it gives another data obtained during the period of maximum solar activity.

Table 2•2•6. Integrated fluxes of elements at the top atmosphere ($1.3 \leq R \leq 2.7$ Gv), in unit of particles/m²•sec•steradian (without ascent correction).

He	44.7±5.8	
Li	0.29±0.06	1.40±0.15
Be	0.44±0.09	
B	0.62±0.11	
C	1.70±0.25	3.97±0.35
N	0.85±0.18	
O	1.33±0.22	
F	0.08±0.05	
Ne	0.16±0.06	0.74±0.12
Na	0.03±0.03	
Mg	0.32±0.09	
Al	0.08±0.05	
Si	0.16±0.06	
P	0.05±0.03	0.33±0.09
S	0.07±0.04	
Cl	0.05±0.03	
A	0.02±0.02	
K	0.02±0.02	
Ca	0.12±0.05	
Sc	0.04±0.04	0.27±0.09
Ti	0.04±0.04	
V	0.04±0.04	
Cr	0.15±0.08	
Mn	—	
Fe	—	

The reason why we have chosen the above four is that these authors have given their direct observational results and have clearly specified the correction procedures they have applied so that their data allow us to make a re-calculation by means of the "best set of fragmentation parameters" given in § 2•1•2.

Waddington and Freier et al. accepted tracks with projected zenith angle $\chi \leqq 60°$, while the other authors, including the present authors, accept only those tracks with $\chi \leqq 30°$. Therefore to make the comparison more convenient, we re-calculated the data of the above two groups of authors in the following manner;

We assumed isotropy at air top of the primary incident direction and estimated the fraction of tracks with $\chi \leqq 30°$ out of those with $\chi \leqq 60°$ at the atmospheric depths where these authors made their observations. The result is given in Table 2•2•8. We adopted the number of tracks

Table 2•2•7. Relative abundance of elements of $Z \geq 3$ at top of atmosphere.

Element \ Rigidity region	Relative abundance (%)	
	1.3 Gv$<R<$2.7 Gv	$R>$4.5 Gv
Li	4.4	5.2
Be	6.6	4.3
B	9.3	11.9
C	25.5	25.1
N	12.8	14.9
O	20.0	14.5
F	1.2	4.0
Ne	2.4	4.3
Na	0.5	2.7
Mg	4.8	4.7
Al	1.2	0.9
Si	2.4	1.6
P	0.8	0.2
S	1.1	0.0
Cl	0.8	0.1
A	0.3	0.5
K	0.3	0.0
Ca	1.8	0.9
$Z \geq 21$	4.1	3.9

Table 2•2•8. Re-calculation of Bristol and Minneapolis data.

Author		Waddington	Freier et al.
Mean amount of material above the stack (air-equivalent)		12.0 g/cm²	4.1 g/cm²
Amount of Ilford G 5 emulsion above the scan line		4.8 g/cm²	5.5 g/cm²
Angle criteria of scanning	Projected zenith angle χ	$\leqq 60°$	$\leqq 60°$
	Track length per plate l	$\geqq 6$ mm	$\geqq 8$ mm
Scanned area		54.4 cm²	33.8 cm² (94 plates)
No. of accepted tracks	H	49.7	32
	M	172.7	103
	L	84.2	41
Expected fraction of the tracks with $\chi \leqq 30°$ among the accepted ones	H	56%	53%
	M	54%	52%
	L	48%	51%
No. of tracks used in the present re-calculation	H	27.6	17
	M	92.7	53.5
	L	40.7	21

thus re-calculated as the basic data, adopting the original number of tracks when statistical errors were in question.

In the Prince Albert Project we have only the flux values of L-component of $R>3.0$ Gv, M- and H-components of $R>3.4$ Gv, no rigidity separation being made in the rigidity region above these values. Therefore we have to make an extrapolation to get the flux values of $R>4.5$ Gv. On the basis of the various measurements which are cited in Waddington's review article, it will be almost safe to assume that the flux values of heavy primaries with rigidity greater than R depend on R as R^{-n}, n being not very different from 1.5. In the rigidity region where we make our extrapolation, the value of n might well become as low as 1.0, because the region is in the vicinity of the position of the knee in the integral rigidity spectra. We give two sets of extrapolated flux values of $R>4.5$ Gv, one corresponding to $n=1.0$ and the other corresponding to $n=1.5$.

The re-calculated flux values of the five observations together with the specific numerical figures characterizing them are given in Table 2·2·9.

The comparison between the data of minimum solar activity shows that the three are consistent with each other on the assumption of the fragmentation parameters we adopted, in spite of the fact that the methods of measurement adopted by the three groups of authors are entirely different from each other.

The comparison between the fluxes of minimum and maximum solar activities shows that the latter is significantly lower—by about 30%—than the former. As to the comparison between the charge ratios of minimum and maximum solar activities, it will be safe to say that no significant difference exists, in view of the fluctuations among the solar minimum data themselves.

The integral rigidity spectra of L-, M- and H-components are illustrated in Fig. 2·2·4 together with the flux values given by the four groups of authors mentioned above. Also the flux values near equator obtained by Waddington and by Jain et al.[2207] are given in the same figure. These observations were carried out during Jan. to Feb., 1957, but unfortunately there are no observational data near the equator during the period of minimum solar activity. Therefore we cannot talk about the solar effect on heavy primaries of $R\geq 10$ Gv. However, as seen in Fig. 3·3·2(b), the solar activity during Jan. to Feb., 1957 is significantly lower than that during the period around the Prince Albert Exposure and we see in Fig. 2·2·4 that the Prince Albert flux values of $R>12$ Gv are somewhat below the line connecting the solar minimum flux values and the equator flux values. Therefore it might well be that the decrease in flux values during the period of high solar activity occurs also for heavy primaries of $R\sim 10$ Gv.

Table 2•2•9. Flux value of heavy primaries with magnetic rigidity greater than 4.5 Gv observed by various authors during solar-calm and solar-active periods.

Author	Waddington	Cester	Koshiba	Freier	Present* Authors
Date of flight	14 Sept. '54	'54 to '55	24 June '55	19 Oct. '57	11 Sept. '57
Rising velocity of balloon (m/min)	305	(275)	(275)	360	256
Floating time (hr)	5.75	(7.0)	7.9	8.5	8.0
Atmospheric depth corresponding to flight altitude (g/cm^2)	8.3	14.4	9.0	3.8	5.5
Amount of packing materials, etc., above emulsion stack (g/cm^2)	3.7	2.3	1.0	0.3	2.1
Total amount of material above emulsion stack (g/cm^2)	12.0	16.7	10.0	4.1	7.6
$\overline{\sec\theta}$	1.05	1.06	1.06	1.05	1.06
Effective total amount of material above emulsion stack x (g/cm^2)	12.6	17.7	10.6	4.3	8.0
Ascent corrections $\frac{\Delta\Phi_i}{\Phi_i'}$ (%) H	7.2	4.8	5.5	6.0	7.6
M	8.4	5.7	6.6	6.8	8.6
L	12.2	9.1	9.8	9.9	13.1
Flux values under $x\,g/cm^2$ of air plus packing material (particles/m^2•sec•sterad) $\Phi_H(x)$	1.28 ± 0.15	1.42 ± 0.16	1.43 ± 0.18	1.23 ± 0.22	0.83 ± 0.08 (0.64 ± 0.06)
$\Phi_M(x)$	4.12 ± 0.32	3.51 ± 0.24	3.96 ± 0.30	3.66 ± 0.36	3.07 ± 0.38 (2.37 ± 0.30)
$\Phi_L(x)$	1.64 ± 0.20	1.56 ± 0.14	1.65 ± 0.18	1.36 ± 0.21	1.05 ± 0.10 (0.81 ± 0.08)
$T\Phi_H(x)$	1.28 ± 0.15	1.42 ± 0.16	1.43 ± 0.18	1.23 ± 0.22	0.83 ± 0.08 (0.64 ± 0.06)
$T\Phi_M(x)$	8.14 ± 0.57	7.94 ± 0.57	8.44 ± 0.63	7.49 ± 0.77	5.68 ± 0.46 (4.39 ± 0.35)
$T\Phi_L(x)$	15.80 ± 0.94	15.04 ± 0.90	16.13 ± 1.01	14.30 ± 1.23	11.07 ± 0.92 (8.55 ± 0.71)
Flux value at top of atmosphere (particles/m^2•sec•sterad) $\Phi_H(0)$	2.04 ± 0.24	2.72 ± 0.32	2.11 ± 0.26	1.44 ± 0.25	1.12 ± 0.11 (0.86 ± 0.08)
$\Phi_M(0)$	5.68 ± 0.44	5.31 ± 0.37	5.15 ± 0.38	4.08 ± 0.40	3.82 ± 0.48 (2.95 ± 0.37)
$\Phi_L(0)$	1.42 ± 0.18	1.31 ± 0.12	1.53 ± 0.17	1.32 ± 0.21	0.96 ± 0.09 (0.74 ± 0.07)
Charge ratio at top of atmosphere $\frac{\Phi_H(0)}{\Phi_M(0)}$	0.36 ± 0.05	0.51 ± 0.07	0.41 ± 0.06	0.35 ± 0.07	0.29 ± 0.05
$\frac{\Phi_L(0)}{\Phi_M(0)}$	0.25 ± 0.04	0.25 ± 0.03	0.30 ± 0.04	0.32 ± 0.06	0.25 ± 0.04
$\frac{\Phi_L(0)}{\Phi_H(0)}$	0.70 ± 0.12	0.48 ± 0.07	0.73 ± 0.12	0.92 ± 0.22	0.86 ± 0.11
Method of charge determination	Delta-ray counting and blob-gap counting	Photometric opacity measurement	Blob counting	Delta-ray counting and blob-gap counting	Delta-ray counting gap counting and blob counting

*Flux values are the ones obtained by extrapolation assuming the integral rigidity spectra of the form $\propto R^{-\gamma}$, where $\gamma=1.0$. If $\gamma=1.5$ is assumed, the values in the parentheses are obtained.

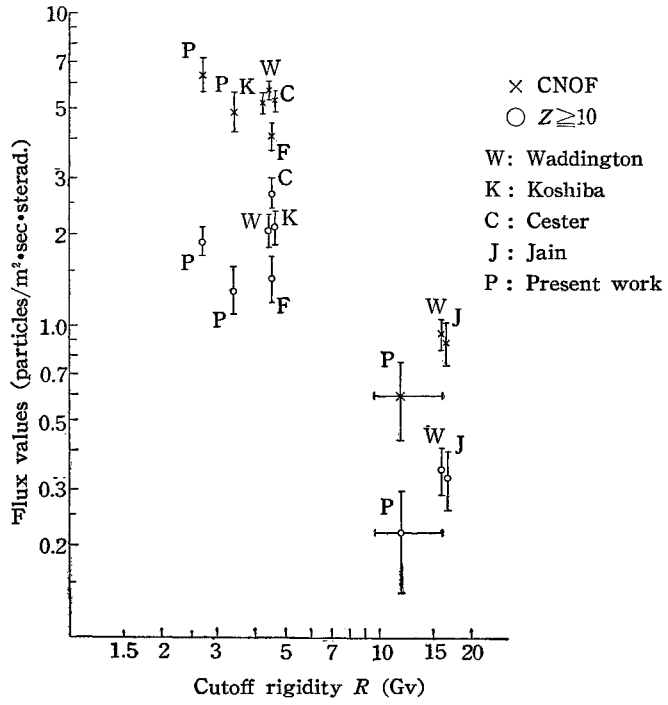

Fig. 2•2•4. Integral rigidity spectra of M- and H-components. The flux values obtained by the four observations in the solar-calm period and those obtained by the two equator observations during Jan. to Feb., 1957 are also plotted in the figure.

Chapter 3. Interpretation of the Experimental Results of Heavy Primaries

§3•1. Propagation in the interstellar space

Heavy primaries are believed to be produced at some remote celestial bodies in our galaxy. Before coming to our earth, they must have travelled a long distance in the interstellar space and have received some electromagnetic as well as nuclear interaction during their travelling.

Although one may not be able to define unambiguously the traversed path length of primaries from their source to our earth, yet one can ask the question how much the thickness of matter is traversed in an average by heavy primaries and what the chemical composition of primaries at their source is.

As was pointed out by the review article by Hayakawa, Ito and Terashima,[3101] the above question can be answered by the analysis on the light nuclei component. The light nuclei, Li, Be and B, are, as is known, easily destroyed by nuclear reactions at relatively low temperature, so that they

can not exist in the hot matter like stellar interior and their cosmic abundance is really small. Thus, almost all the light nuclei component in cosmic rays must be produced through the break-up of heavier component during the period through which they are being accelerated and are travelling the space.

Therefore, one can trace back the propagation of heavy primaries in the interstellar space by solving the diffusion equation, and ask the place where the flux of light component becomes zero. This place will be called as the "*source*" of cosmic ray.

3·1·1. *Break-up in hydrogen gas*

The major component of the interstellar space is the hydrogen gas. The break-up of heavy primaries by a collision with a hydrogen nuclei can be studied from the investigation on the reverse process, i. e., the nuclear disintegration by proton bombardment. The collision cross section has been studied well, and from their data one can obtain the collision mean free path in hydrogen gas as shown in Table 3·1·1. These values are known to be little energy-dependent in the energy range concerned.

Table 3·1·1. Collision mean free path in hydrogen.

L	M	H	VH
9.8	6.65	4.15	2.64 g/cm^2

An observation on hydrogen-target break-up has been attempted by looking for the so-called "clean" break-up events in the nuclear emulsion, that is, the nuclear interaction without any black evaporation prong. Nearly half of the clean events are real hydrogen collisions but the remaining half are due to peripheral collisions with heavier nuclei. One may try to reject the peripheral neutron collisions by examining the charge conservation in the events, but the charge measurement can not be made as accurate as required, particularly beyond neon nuclei or so. Table 3·1·2 shows a summary of investigations on clean break-up processes, including our 41 events together with the published data by Waddington et al.[3102] and Cester et al.[3103]

The above results on hydrogen fragmentation parameters should be looked at with large reservation. Not negligible errors may arise from poor statistics, contamination of peripheral collisions and scanning difficulty. One can expect that a certain fraction of hydrogen collisions are of the type where a heavy primary does not lose its charge or loses its charge only by one unit. This type of events are easily missed in scanning. For

Table 3•1•2. Fragmentation of heavy primaries for collisions on nucleon target in the emulsion (stars with $N_h \leq 1$).

(a) $N_h=0$ and $r=$odd, or $N_h=1$ and $r=$even ($r \equiv n_s -$ [total charge of fragments of $Z \geqq 2$]).

(b) Total stars with $N_h \leq 1$.

Primary particle		No. of collisions		No. of α-fragment		No. of L-fragment		No. of M-fragment		No. of H-fragment	
		(a)	(b)	(a)	(b)	(a)	(b)	(a)	(b)	(a)	(b)
L	Present work	6	17	3	17	3	6				
	Bristol	14	33	14	34	1	3				
	Torino	12	23	14	27	2	3				
	Koshiba et al.	/	8	/	10	/	0				
	Lohrman-Teucher	/	/	/	/	/	/				
	Total	32	81	31	88	6	12				
M	Present work	24	49	35	65	7	17	3	4		
	Bristol	25	53	27	78	6	15	2	3		
	Torino	14	56	14	53	2	12	3	9		
	Koshiba et al.	/	27	/	45	/	7	/	2		
	Lohrman-Teucher	/	51	/	46	/	15	/	8		
	Total	63	236	76	287	15	66	8	26		
H	Present work	/	17	/	20	/	1	/	7	/	5
	Bristol	11	31	16	51	1	5	4	7	1	8
	Torino	10	24	11	33	0	2	2	8	5	8
	Koshiba et al.	/	8	/	9	/	3	/	3	/	2
	Lohrman-Teucher	/	23	/	26	/	1	/	12	/	9
	Total	21	103	27	139	1	12	6	37	6	32
Total		116	420								

	P_{LL}	P_{ML}	P_{MM}	P_{HL}	P_{HM}	P_{HH}	$P_{L\alpha}$	$P_{M\alpha}$	$P_{H\alpha}$
(a) Proton target	0.19 ±0.08	0.24 ±0.07	0.13 ±0.05	0.05 ±0.05	0.29 ±0.13	0.29 ±0.13	0.97 ±0.24	1.20 ±0.21	1.29 ±0.40
(b) All $N_h \leq 1$ stars	0.15 ±0.05	0.28 ±0.04	0.11 ±0.02	0.12 ±0.04	0.36 ±0.07	0.31 ±0.07	1.09 ±0.17	1.22 ±0.11	1.35 ±0.18

example, the fragmentation parameter P_{CB} is expected to be larger than 0.1 from the observed cross section for $C^{12}(p, pn)C^{11}$ reaction,[3104] while none of such is found in 28 events of clean C break-up.

The fragmentation parameters can be obtained also from an investigation on the reverse process, that is, the spallation of a nucleus by proton bombardment. Unfortunately, so much experiments have not been made so far on the spallation, so that we have to rely on the theoretical guess. A

Table 3•1•2′ Fragmentation of heavy primaries for collision on nucleon target in the emulsion (stars with $N_h \leq 1$).

Primary particle	Author	No. of collisions	Li	Be	B	C	N	O
Be	Present	6	0	0				
	Bristol	5	1	0				
	Torino	6	1	0				
	Total	17	2	0				
B	Present	11	6	8	0			
	Bristol	15	2	0	0			
	Torino	14	0	1	1			
	Total	40	8	9	1			
C	Present	23	1	1	4	1		
	Bristol	26	4	4	0	0		
	Torino	25	3	2	1	1		
	Total	74	8	7	5	2		
N	Present	14	5	1	2	0	0	
	Bristol	17	2	0	3	2	0	
	Torino	9	0	2	3	0	0	
	Total	40	7	3	8	2	0	
O	Present	11	0	2	0	3	0	1
	Bristol	12	0	0	2	1	0	0
	Torino	9	0	0	0	2	3	0
	Total	32	0	2	2	6	3	1

Table 3•1•3. Fragmentation parameter in hydrogen.

	VH	H	M	L
VH	0.40	0.55	0.05	0
H		0.50	0.30	0.15
M			0.15	0.40
				0.15

summary of the informations on the spallation is given in Appendix 6.

From the above two sources of informations, the numerical value for the fragmentation parameters can be given as in Table 3•1•3. It is hoped that the improvement will be made in near future by the spallation experiment and the observation of hydrogen break-up with subtraction method of paraffin and carbon difference or with some other methods.

3·1·2. *Thickness of matter traversed by cosmic rays*

In evaluating the thickness of matter traversed by primaries from the measured flux value of L-group, one assumes, as the first approximation, that the thickness of matter is not large and effect of secondary or higher order collisions can be neglected. Then the solution for diffusion equation simply becomes,

$$N_L(t)=\left\{\frac{P_{ML}}{\lambda_M}N_M(t)+\frac{P_{HL}}{\lambda_H}N_H(t)\right\}t, \qquad (3\cdot1\cdot1)$$

where t is the thickness of matter. $N_L : N_M : N_H$ is 2.0 : 5.6 : 1.9 at the top of atmosphere.

If one uses the value of fragmentation parameters obtained in the previous subsection,

$$P_{ML}=0.40, \quad P_{HL}=0.15,$$

then the thickness t is obtained as

$$t=5\text{g/cm}^2.$$

This value is apparently higher than that obtained previously by Hayakawa, Ito and Terashima, 3g/cm².[3101] The main reason for the difference is P_{HL}, 0.15 in our calculation and 0.30–0.40 in theirs.

It should be remarked that our P_{HL} is obtained taking a simple average nuclei in the H-region. If the original charge distribution in H-region is not flat but the lighter nuclei, such as Ne, Mg and Si, occupy the majority of the H-nuclei, P_{HL} will become as large as 0.30. In this case the thickness of matter turns out to be $t=4$ g/cm². Later discussion shows that the above consideration is more plausible.

In conclusion, the thickness of matter is estimated to lie between 3∼6 g/cm², most probably 4 g/cm².

3·1·3. *Original charge distribution at source*

Now let us first examine the diffusion of VH-group through hydrogen gas of several grammes. Assuming a VH-component of unit flux at $t=0$, one can calculate flux values for various components at a given thickness. The results are shown in Fig. 3·1·1.

In Table 3·1·4 a comparison was made between the flux values of various components observed at the top of atmosphere and the calculated ones.

It is seen from the Table that the contribution to L- and M-components from VH-nuclei is negligible. This shows a consistency of the assumption made in the previous subsection for the production of L-component.

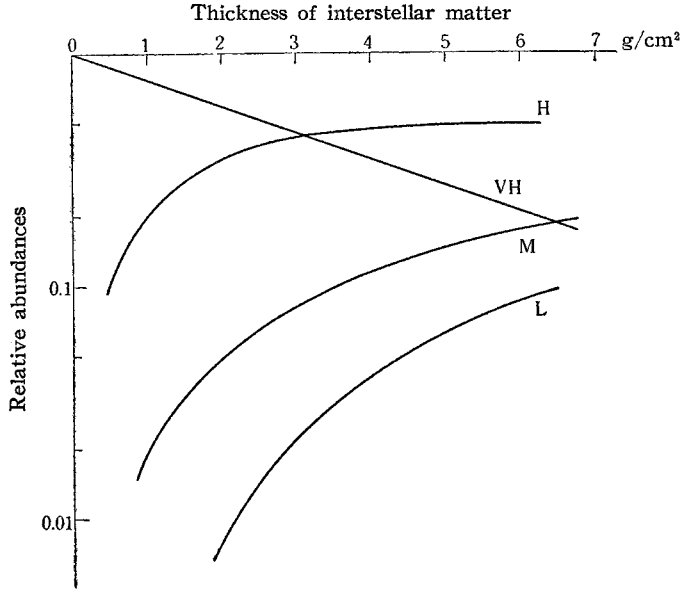

Fig. 3•1•1. Calculated flux value for various component at a given thickness, assuming a VH-component of unit flux at the source.

Table 3•1•4. Relative values of flux of various components.

Component	VH	H	M	L
Observed at the top of atmosphere	1	2.7	8.0	2.9
Calculated $t=3$	1	0.9	0.18	0.05
4	1	1.3	0.34	0.12
5	1	1.5	0.57	0.25

For the H-component, it appears that about half of them are the fragmentation product of VH-nuclei and the rest are H-nuclei from the beginning. When one looks at the charge spectrum of H-nuclei, one finds that the lighter nuclei Ne, Mg and possibly Si are more abundant than the rest and constitute nearly half of all. Such a tendency cannot be expected from the fragmentation of VH-nuclei, which will result in a charge distribution nearly constant but slightly more abundant at heavier side after smoothing out the even-odd variation. The observed charge distribution is now explained in the following way. Original H-component at the source will consist mainly of the abundant Ne, Mg and Si nuclei. The rest of H-nuclei found at the top of atmosphere will be the fragmentation product of VH-nuclei.

Now we are at the position of tracing back the various components to

their origin. The calculated flux values at the source are shown in Table 3•1•5 together with the values at the top of atmosphere. In this calculation, we assumed as above that the H-component at the source consist mainly of Ne, Mg and Si, so that we adopted the following values for the parameters in the diffusion equation:

$$t=4.0\ \mathrm{g/cm^2},\quad P_{HH}=0.20,\quad P_{HM}=0.30$$

Table 3•1•5. Flux value of various components at the source.

	VH	H	M	L
At the top of atmosphere	0.7	1.9	5.6	2.0
At the source	2.0	2.0	8.9	0

3•1•4. *Detailed charge spectrum in M-region*

The detailed charge spectrum in the region between C and Mg is interesting because of the astrophysical significance. The fragmentation parameters connecting these elements are unfortunately not known accurately enough. We assign tentatively the following values for them as in Table 3•1•6, and solve the diffusion problem. The result is given in Table 3•1•7.

Table 3•1•6. Tentative values of fragmentation parameters.

Parent \ Daughter	Mg	Ne	O	N	C
Mg		0.3	0.2	0.05	0.05
Ne			0.4	0.05	0.10
O				0.2	0.3
N					0.2
C					

Table 3•1•7. Charge spectrum (relative value).

	Mg	Ne	O	N	C
At the top of atmosphere	0.32	0.30	1.00	1.03	1.74
At the source	0.46	0.24	1.00	0.97	1.45

As is seen from Table 3•1•7, general shape of the spectrum is not altered by the correction of fragmentation. This conclusion does not change even if the assumed value for fragmentation varies considerably. Apparent carbon overabundance and neon underabundance in the cosmic

ray spectrum is not due to the fragmentation but must be attributed to the element abundance at the source itself.

§3·2. Astrophysical discussions of origin of cosmic rays

The very existence of heavy primary itself, particularly its chemical composition and the shape of its energy spectrum, has great significance in investigating the problem of how and where the cosmic ray particles are produced. Before starting the discussions on the origin of cosmic rays, we shall make a brief review of two important astrophysical phenomena which have close relations to the cosmic rays. These are the element synthesis in a star and the matter ejection from a star.

Recent development in nuclear astrophysics reveals that nuclear synthesis of elements is going on all the time in the interior of stars and sometimes in their atmospheres. These stellar nuclear reactions provide the energy source of stars, and at the same time build up heavier nuclei from lighter ones. Taketani, Hatanaka and Obi[3201] have made clear the relation between the nuclear synthesis and the evolutionary process of stars. After the birth of a star, the gravitational contraction makes the temperature of the interior region of the star gradually higher until the nuclear reaction of hydrogen burning into helium sets in at the inner core. After most part of the hydrogen content is converted into helium in the central part, the inner temperature increases by a further contraction and helium nuclei start to burn to form heavier alpha-nuclei, C, O and Ne. Exhaustion of helium content again induces a contraction and produces still higher temperature in the core of the star. At the last stage of the highest inner temperature, the most stable nuclei, i.e., the nuclei of iron group, are believed to be synthesized. Nuclei heavier than iron up to uranium are considered to be produced by the successive neutron capture by the iron group nuclei.

From this theory of nuclear synthesis, it is expected that the chemical abundances of elements should considerably differ among stars at different stages of evolution. Astronomical observations are well in accord with this expectation, and shows that stars advanced in the evolutionary process are rich in heavier elements and deficient in light elements. Element abundances of cosmic rays should be looked at from this view of element synthesis.

Various observations have confirmed the existence of continuous matter ejection as well as sudden explosions from a star. Supernova explosion is, of course, the most vigorous phenomenon of matter ejection known to us. The sun, which is believed to be a typical example of stars in a quiet stage, sometimes emits corpuscular clouds in her active period. The solar flare is one of such phenomena. Red giants and supergiants are known

to be in far more active states than the sun. Various astronomical observations provide direct evidence for existence of continuous ejection of matter[3202),3203)] of huge quantity from red giants and supergiants. This matter ejection from a giant star seems to play an important role in the evolution process of a star.

Matter ejection and cosmic ray production seem to have a close connection with each other. We have at least two good examples to show this relation. One is the solar flare phenomenon, and the other is the supernova explosion. A strong radio wave emission from the Crab Nebula, a remnant of the supernova of 1054, is interpreted as evidence of electrons of cosmic ray energy. A detailed analysis of the above two examples was carried out by Hayakawa, Ito and Terashima.[3204)] Although one is, at present, not able to understand the dynamics of matter ejection and the production of cosmic rays, it is quite plausible that the relation found in the above two examples is common for all stars. Matter ejected from a star will be a high temperature plasma. One can expect the existence of a moving electromagnetic field accompanying the moving ionized matter, and this field will be effective in accelerating ionized particles up to cosmic ray energies.

Table 3•2•1 shows various pieces of information about matter ejection and production of cosmic rays, mostly quoted from the review article of Hayakawa, Ito and Terashima.* Q_{matter} is the estimated quantity of ejected matter expressed in number of nucleons per sec. Q_{CR} is the estimated number of produced cosmic rays. The ratio Q_{CR}/Q_{matter} is called the production efficiency of cosmic rays.

Table 3•2•1

	Matter ejected Q_{matter}/sec	Cosmic rays produced Q_{CR}/sec	Production efficiency Q_{CR}/Q_{matter}	Number of stars of similar type	Estimated total production of cosmic rays in Galaxy
Sun	$10^{33\sim34}$	$3\cdot10^{24\sim25}$	$3\cdot10^{-9}$	10^{11}	$\sim10^{36}$ ($10^{37\sim38}$)
Magnetic variable star		10^{31}	large	10^{6}	$\sim10^{37}$
Supergiant and red giant	$\sim10^{43}$	$\sim3\cdot10^{35}$	$3\cdot10^{-9}$	$10^{7\sim8}$	$\sim10^{42}$ ($10^{33\sim35}$)
Novae and supernovae (Crab Nebula)	$10^{46\sim47}$	10^{40}	$10^{-6\sim-7}$	$\sim10^{2}$	$\sim10^{42}$ ($10^{36\sim37}$)

* Data of the unusual cosmic ray increase have been used to determine Q_{CR} for the sun, and, assuming the same production efficiency, Q_{CR}. for the supergiants and red giants has been determined. For the values of the supernovae, analysis of the synchrotron radiation from high energy electrons in Crab Nebula has been made, and, from the energy spectrum of these electrons, Q_{CR} in the supernovae has been estimated.

These estimates are made for the particle acceleration by some electromagnetic effects inside the hot plasma surrounding the stars. For instance, in the sun, the estimate is based on the data of unusual increase of cosmic rays associated with solar flares.

Another type of the acceleration is also possible as explained in Appendix 7. Outward sweeping plasma ejected from the stars accelerates the cosmic rays by the Fermi process. In this case, acceleration efficiency can be calculated, if one knows the velocity and the area of the surface of such an expanding plasma.

In the bracket of the last column in Table 3•2•1, figures of the cosmic ray acceleration by this process are listed for the comparison. For the stars similar to the sun, this process is one or two order more efficient than that of the direct production of high energy particles.

3•2•1. *Element abundances*

One often compares the chemical abundances of cosmic ray heavy primaries with the abundances of elements averaged over our cosmos. A remarkable conclusion from this comparison is that nuclei heavier than He are more abundant in cosmic rays than the universal average. Or it might be better to express that cosmic rays contain hydrogen and helium far less than the average. Table 3•2•2 demonstrates this situation. According to the theory of nuclear synthesis, the abundance of heavier elements becomes richer, as a star approaches the final stage of its evolution. Therefore, one comes to the conclusion that in the production of cosmic rays a main contribution comes from stars advanced in the evolutionary process.

To see a more detailed comparison, Fig. 3•2•1 presents the overall relative abundances of the elements of cosmic rays heavier than $Z=6$ and those of the observations on the various astronomical objects.[3205] The abundance of Si nuclei is taken as unit. Unfortunately the figures have large uncertainty, because they are mainly based on the spectroscopic observations of the atmospheres of stars and the abundance values are obtained from the observations only after crude averaging over the star.

Table 3•2•2. Comparison of cosmic ray nuclei with cosmical abundance.

Element	Suess-Urey	Cosmic ray	
		at the earth	at the source
H	100	110	100
He	7	10	12
Li, Be, B	3.56×10^{-7}	0.18	0
C, N, O, Ne	0.1	0.64	0.83
Mg, Si, S, A	6.3×10^{-3}	0.10	0.15
Fe	1.5×10^{-3}	0.04	0.11

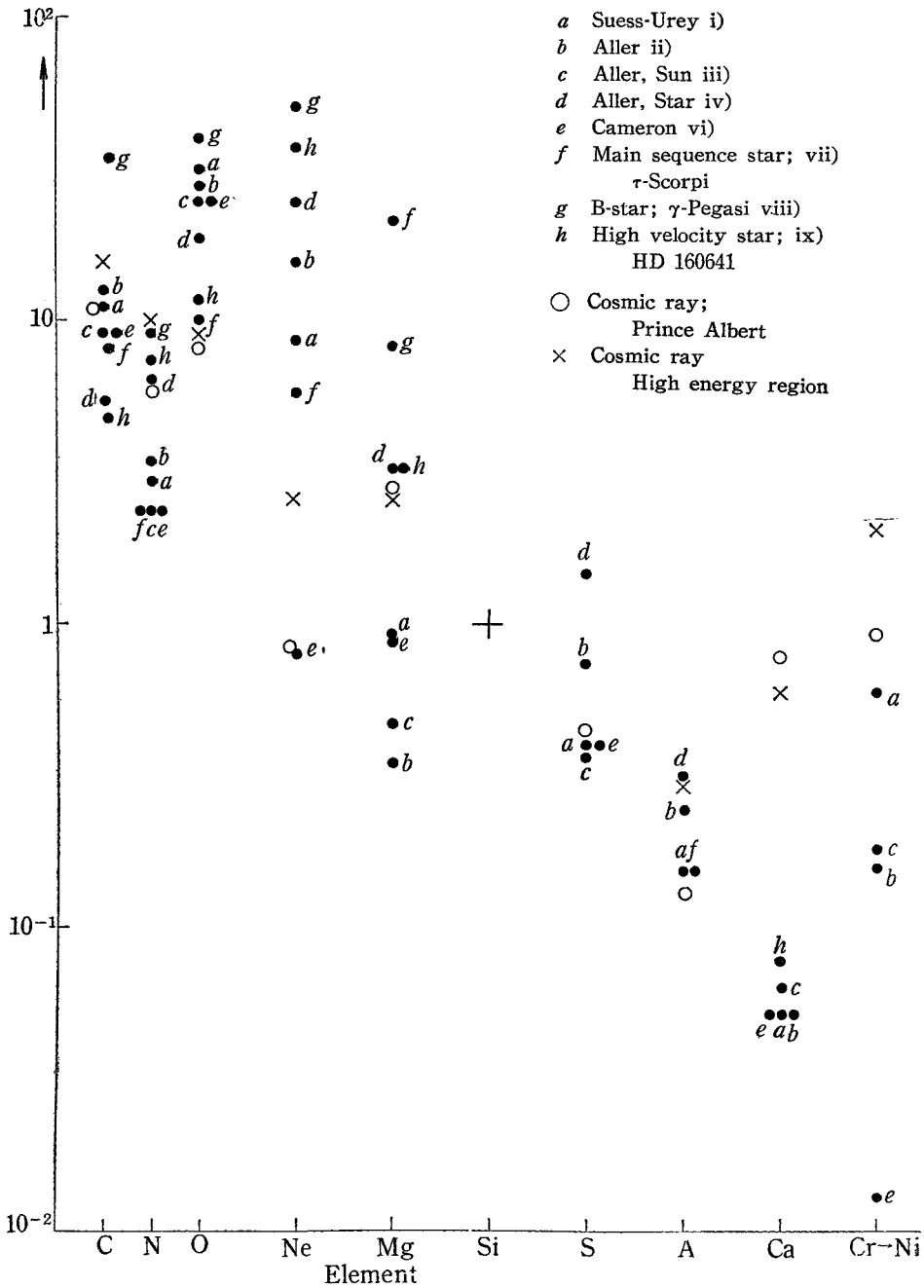

Fig. 3•2•1. Overall relative abundance of the elements of the various astronomical objects and cosmic rays. The abundance of silicon is taken as unit.

In the Figure considerable divergence is found among the data by different authors.* Results of the measurements for particular types of stars for which results are available are plotted in the same figure. For the cosmic ray abundance we present two sets of data, one being the low energy data by the present authors, and the other, the mean value of the high energy data by various authors. The difference between these two cosmic ray data is not significant beyond statistical errors. No overall good correlation to the cosmic ray data can be found for any sole type of astronomical object within, say, a factor of five.

3·2·2. *Overabundance of heavier components and supernovae origin*

For a particle to be accelerated up to the cosmic ray energy range by some electromagnetic process, the gain of kinetic energy must win in the competition with the ionization loss. The loss of energy is greater for heavier nuclei, so that heavier nuclei must be more difficult to be accelerated than lighter ones. Considering this difficulty of injection mechanism of heavy nuclei, one notices that the heavy nuclei, Ca and Fe groups are overabundant.** Unfortunately one cannot make the argument more quantitative, because at present one does not have enough information on the acceleration efficiency and injection mechanism, particularly its variation with charge.

The nuclei heavier than Ne, particularly the iron group, are synthesized under a high temperature condition; T is equal to or more than 10^9 °K. Such a high temperature is realized in the interior of a star only after exhaustion of hydrogen and helium which are burned up under conditions of lower temperatures. This means that the chemical composition of cosmic ray is similar to that of the interior matter of stars near the end of their evolutionary process. Thus the origin of cosmic rays must be looked for among stars which are in the advanced stage of evolution, and are, at the same time, active in the interior motion so that there are chances for the interior-matter to come out of the stellar atmosphere.

Supernovae origin theory proposed by Hayakawa[3206] has many favourable aspects. The supernovae are believed to be stars at the last stage of evolution. At the moment of its explosion, the temperature will get high enough so that most of the existing iron group elements and heavier

* The famous Suess-Urey abundance table is mostly based on the chemical analysis of meteorites. Aller gave another determination of chemical abundance from spectroscopic observation on the sun, early-type stars and planetary nebulae. Cameron recalculated the values of Suess and Urey's, adopting the value of Aller for the abundances of light and medium nuclei. The difference between the two methods is most significant in the abundance of Ne nuclei, and will be discussed later.

** As shown in § 3·1·3, considerable part of Ca nuclei may originate from fragmentation of Fe group in interstellar space. Therefore the most characteristic feature at the cosmic-ray source is, here, the overabundance of Fe group elements.

elements up to uranium are believed to be synthesized there. A large fraction of the interior matter will be ejected to the outer space by the vigorous motion of matter induced by the release of a tremendous amount of energy. We have already seen very high generation power of supernovae, and have an evidence for the existence of high energy electrons in the atmosphere of supernovae from the observation of radio noises in the Crab Nebula.[3207]

It is therefore interesting to see whether the observed element abundances of cosmic rays are consistent with the expected ones in the supernovae. A characteristic of element synthesis in the supernovae is that the nuclear synthesis is carried out under high temperatures, several times 10^9 °K or higher, and within a short period, a hundred of seconds or so. These rapid processes in supernovae are studied in detail by Hayakawa et al., in a separate paper in this issue. A general trend of the element abundances in cosmic rays seems to show no contradiction against their analysis on the rapid processes in supernovae.

3·2·3. *Abundances of medium weight nuclei and contributions of giant stars*

One is able to discuss in more detail the distribution of medium weight nuclei, because on the one hand the charge determination in cosmic ray measurement can be made quite accurately in this region and on the other hand the nuclear reactions governing this mass number region are studied in detail. From Fig. 3·2·1 one is able to see the overabundance of carbon and the underabundance of neon in cosmic rays compared with general cosmic abundances.

The carbon-to-nitrogen ratio is important because this quantity is closely related to the famous C-N cycle. Values of N/C ratio at the equilibrium of the C-N cycle are calculated and found to vary greatly according to temperature. The relative abundance of nitrogen increases rapidly as the temperature increases and it reaches a few hundred times that of carbon at around 6×10^7 °K. This shows that the C-N cycle is not among the reactions responsible for abundances of cosmic rays.

Among various kinds of stars, one finds several types of stars which show remarkable carbon overabundance. Carbon stars, Wolf-Rayet stars, are some of the known examples.[3203] It is believed that these stars have experienced a large amount of matter ejection and as a result their outer layers have been stripped off. If this is true, one may be able to consider that the inner core region of other giant stars will have more or less similar abundances as the above types of stars.

In the later stage of giant stars, He-burning process is going on in the interior region. $4n$-nuclei, C, O and Ne are produced, and values

of their relative abundances can be calculated, assuming various temperatures and helium densities. One is always able to find a certain set of conditions under which the abundance values agree with those of cosmic rays. The only question is whether these conditions really exist in nature. The above observation seems to suggest a positive answer for giant stars.

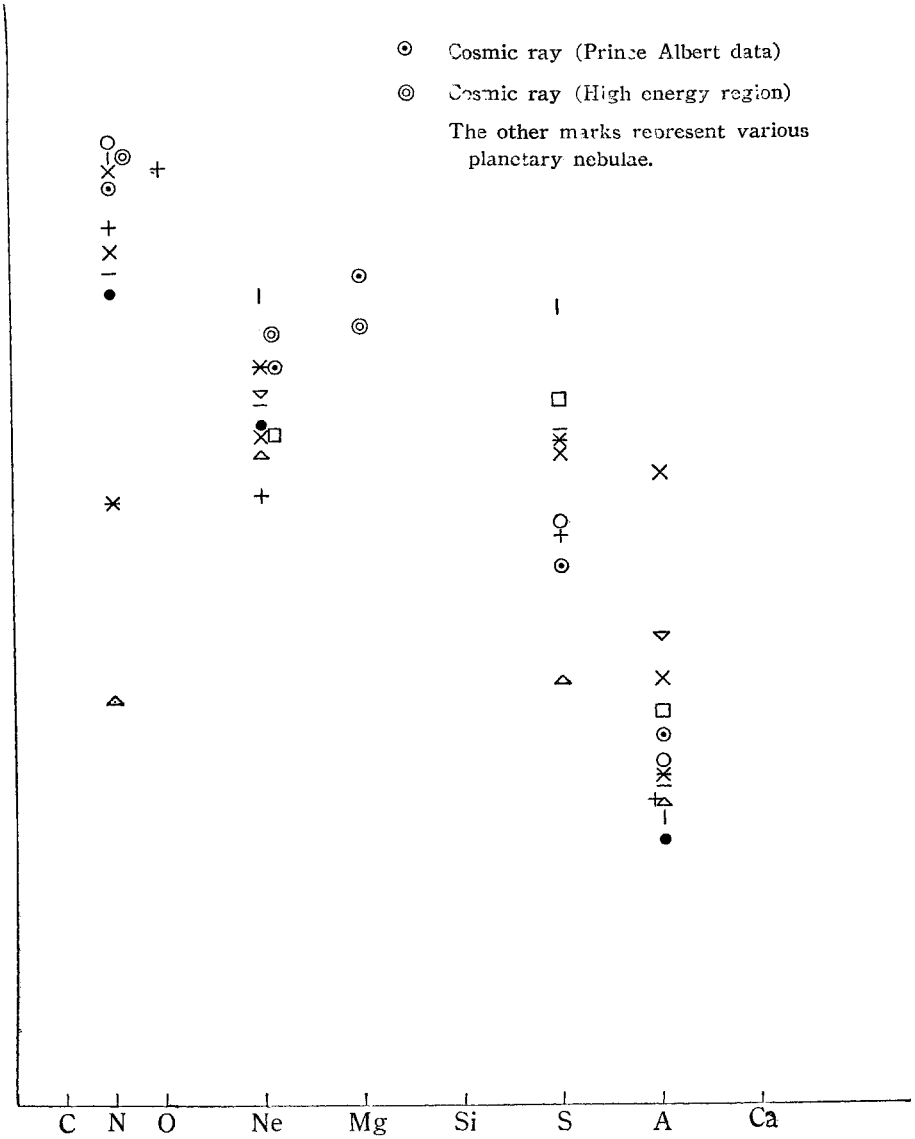

Fig. 3•2•2. Relative abundance of the elements in the cosmic rays and in the planetary nebulae observed by L. H. Aller.[3208] The abundance of oxygen is taken as unit.

Another interesting piece of information comes from observations on planetary nebulae.[3208] It is generally supposed that, as stated by Aller, a planetary nebula is produced by the ejection of matter—the rate of which sometimes reaches the value of about 10^{20}g/sec—from a central star which has departed from the main sequence stage and is at the pre-nova stage. In Fig. 3•2•2 a comparison is made between the cosmic ray data and the results of spectroscopic observation by Aller on about ten such nebulae. The observed values of Ne/O ratio seem to agree with each other and are definitely lower than these found in other ordinary types of stars. It is quite interesting that the relative abundances of N, O and Ne observed in those planetary nebulae are found to be quite stable from one nebula to another and at the same time very similar to those of cosmic rays.*

Coming to this situation, it becomes likely that at least two kinds of sources of cosmic rays at different stages of nuclear synthesis are operating, one for H-group and another for M-group. Hayakawa and his collaborators have already pointed out the importance of giant stars besides supernovae for cosmic ray proton and alpha-particle production and showed a consistency of their idea with estimated total amount of cosmic ray production in our Galaxy. It is now probable that H-group will mainly come from supernova outburst while M-group and lighter components will come from giant stars at the stage of He burning.

There is another way of interpretation, i.e., the interpretation assuming the supernovae as the only significant source of cosmic rays. The observed abundance of M-group has then to be interpreted as due to the rapid C-N-O cycle occurring in the outer layers of the supernovae. This possibility is discussed in detail by Hayakawa and others in a separate paper of this issue.

3•2•4. *Possible variation of charge spectrum with cosmic ray energy*

It has already been shown that the supernova will be an important source of heavy primaries and contributions from giant stars may not be negligible either. It is left an open question how much contributions come from other types of stars. Most plausibly, the production of cosmic rays is a phenomenon which will be found more or less in almost all types of stars.

It is expected that cosmic rays from different kinds of origins will have different element compositions and energy spectra. If one assumes that acceleration in the interstellar space is not important and the observed cosmic rays are simple sum of those coming from various origins, then one can expect that the shape of energy spectrum will be different for

* In Fig. 3•2•1 we find the Ne abundance given by Cameron is about one order lower than that of Suess-Urey's, while the solar abundance of Ne cannot be measured. Suess-Urey's determination of the abundance of Ne does not come from a direct observation of Ne, but from an interpolation between O^{16} and Mg^{24}.

each component. On the other hand, if acceleration by interstellar cloud is mainly responsible for building up the energy spectrum, then the charge spectrum will show different energy dependence from the above.

This expectation can be, of course, experimentally checked by observing the energy variation of relative intensity of various components. Unfortunately no such systematic observation has been made so far over a sufficiently wide range of energies. Between several hundred Mev and several Gev our observations show no significant variation. At higher energies, up to ~20 Gev/nucleon, there are observations by various authors. Collecting all existing informations, one may be able to conclude that the relative intensity of various components does not vary by more than a factor of two up to several tens of Gev. It should be mentioned that the comparison of charge ratios observed by different authors could introduce a large error. A systematic observation in a wide range of energies with a fixed method of charge determination is greatly required.

A variation of charge spectrum with energy in the vicinity of the earth may be created due to the secondary effects inflicted upon cosmic ray particles during their travel from the source to the earth. It is already estimated that cosmic rays traverse, in an average, about $4\,g/cm^2$ of matter before they are accelerated up to the concerned energy region from, say, several ten Mev and reach the earth. Appreciable contributions come from ionization loss and fragmentation which cosmic ray particles suffer during their passage.

A cosmic ray particle of velocity v and charge Z suffers ionization loss ΔE in its passage through $4\,g/cm^2$ of hydrogen gas,

$$\Delta E \sim 16\ \text{Mev} \cdot \frac{Z}{v^2} \cdot \text{per nucleon.} \qquad (3\cdot2\cdot1)$$

For VH-group this loss of energy is not negligible. If one could extend observation on VH-group down to 300~400 Mev at the air top with good statistics, one would be able to observe the effect of ionization loss through the comparison of energy spectrum of VH-group and other components. This will provide us a precious piece of information on the acceleration mechanism.

3·2·5. *Effect of fragmentation*

$4\,g/cm^2$ of matter is an estimated average passage of a heavy primary with energy of about one Gev/nucleon. For higher or lower energy particles the traversed thickness of matter can be different. One can point out two possible effects which will give rise to the energy dependence of traversed path length.

It will take longer time to accelerate particles to higher energy so that

higher energy particles will traverse larger thickness of matter than the lower energy ones. If the acceleration is obtained by successive small energy gains of approximately fixed fraction, this situation will be realized. Then, most plausibly, the traversed thickness t will be

$$t \sim \text{const} \cdot \ln(E/E_0), \tag{3·2·2}$$

where E_0 is about several tens of Mev.

Another effect comes from the diffusion of cosmic rays. Let the linear dimension of the system containing cosmic rays be L, and mean free path for scattering of cosmic rays be l. Then, from an analogy with the problem of random walk, one has

$$L \sim \sqrt{n}\, l, \tag{3·2·3}$$

where n is the number of collisions. Therefore, one has for the traversed thickness t

$$t \sim \text{const} \cdot (L^2/l^2). \tag{3·2·4}$$

The collision mean free path l is smaller for particles of lower energy. Thus one may suspect that lower energy particles will take longer time in diffusing out of the space, and accordingly will traverse larger thickness of matter than higher energy ones.

The above two possibilities are effective in opposite directions. No one knows the actual variation of traversed thickness t with particle energy which is a superposition of the above two and possibly other unknown effects. We have to wait and obtain the information on the energy dependence, $t(E)$, before settling the question.

Experimental information on $t(E)$ can be expected from a detailed study on the energy variation of various heavy primary components. Let the m-component nuclei have an absorption mean free path Λ_m, then the fraction of nuclei remaining undestroyed after the nuclear collisions during their travelling of $t(E)$ is $\exp(-t(E)/\Lambda_m)$. The ratio of the two, $-m$ and $n-$ components becomes

$$\frac{N_m(E)}{N_n(E)} = \text{const} \cdot \exp\left(-t(E)\left(\frac{1}{\Lambda_m} - \frac{1}{\Lambda_n}\right)\right), \tag{3·2·5}$$

assuming that the two components originate from the same source.

Light nuclei component is particulary interesting in the study of $t(E)$, because almost all light nuclei can be regarded as fragmentation products of other heavier nuclei. Its relative intensity is expressed as

$$\Sigma_m \frac{\Lambda_L}{\Lambda_L - \Lambda_m} \frac{\Lambda_m}{\lambda_m} N_m P_{mL} (e^{-t/\Lambda_L} - e^{-t/\Lambda_m}) \Big/ N_n e^{-t/\Lambda_n}. \tag{3·2·6}$$

A possible effect of $t(E)$ will appear here in the most unambiguous way.

§ 3·3. Solar modulation of the energy spectrum of heavy primaries

Our study on the Prince Albert Stack is the first and to date the only extensive investigation on the energy spectrum of various components in the low energy region. This work has made clear various interesting features of the energy spectrum of heavy primaries. One is able to conclude from their results that α-, M-, H- and VH-components appear to have the spectrum of the same shape for their energy per nucleon. The general shape of the spectrum, common to all components, is found to be such that a broad maximum lies at around 500 Mev/nucleon with a width of about 300 Mev/nucleon. At higher energies, the spectrum appears to fall according to power law, $(1+E)^{-\gamma}$ with $\gamma=1.0\pm0.2$.

A comparison with data of other authors provides the following interesting conclusions.

i) There seems to be time variation of the heavy primary intensity with considerable magnitude. The flux values measured in a period around 1957[3301] show good agreement with the results of the Prince Albert Project, while those obtained in a period 1954~55[3302] show systematically higher values by a factor of two or so. This change in the flux value is not due to a mere systematic error, but seems to indicate time variation following the solar activity. The high flux value obtained in 1954~55 corresponds to the period of minimum solar activity, while that of 1957~58 to the period of the maximum activity. Fig. 3·3·1 demonstrates this situation very clearly, and gives the comparison of the observed α-energy spectra obtained by various authors at different periods of the solar activities.[3303] In 1954, at the time of near minimum solar activity, the observed spectrum had a maximum at around 300 Mev/nucleon. These data should be compared with our observed

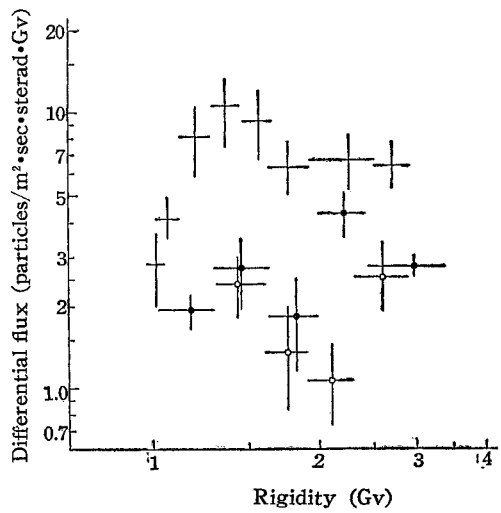

Fig. 3·3·1. Differential rigidity spectra of the alpha particles.

+ The spectrum obtained in June 18, 1954 at Saskatoon

⊕ The spectrum obtained in Sept. 1, 1957 at Minnesota by Freier et al.

● The spectrum obtained in Sept. 11, 1957 at Prince Albert

spectrum measured in 1957, when the solar activity was near maximum.* The shift of the position of maximum in the spectrum is clearly seen. Furthermore the intensity observed in 1957 is observed generally lower by a factor of two to three in comparison with that observed in 1954. This change in the α-spectrum during these three years is considered to be due to a change in the solar activity. Referring to the proposed theory of eleven-year solar modulation[3304)3305)] on cosmic rays, we shall discuss the interpretation of the change of energy spectrum of heavy primaries, with $Z \gtrsim 3$ by the reason stated in the footnote of this page.

There is one thing which we must mention here. Our observation was

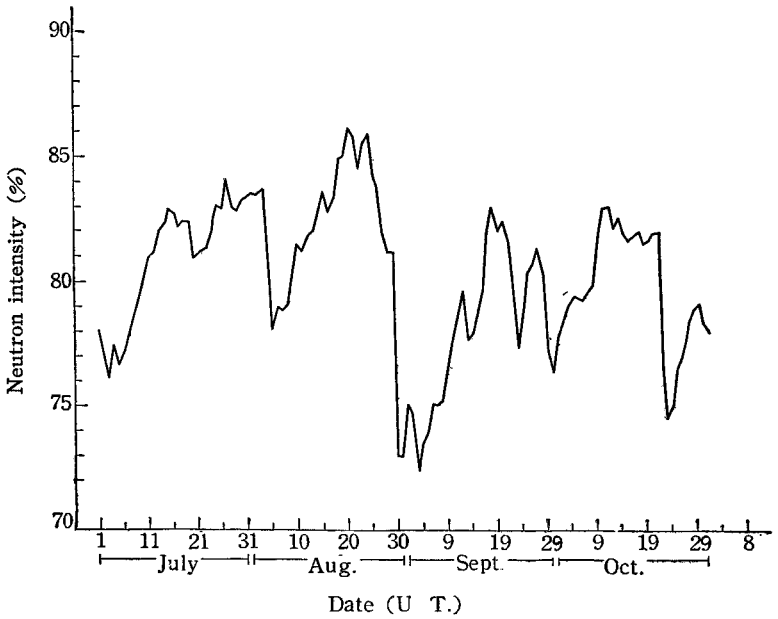

Locality of Mt. Washington Observation Station:

Height	=1957 m (806.0 mbar)
Geomagnetic latitude	=55.6°N
Cutoff rigidity	=1.9 Gv
UT for LT 0^h	=5 h

Fig. 3•3•2(a). Daily average neutron intensity at Mt. Washington normalized to the mean intensity for July-August, 1957.

* There is some evidence that alpha spectra in 1954 and 1957 both have two peaks around 200 Mev/nucleon and 600 Mev/nucleon, instead of only one peak at 400 Mev/nucleon ~600 Mev/nucleon, even though the statistical error of both data is quite large. If these two peaks really exist, and if the peak at lower energy is to be attributed to solar alpha particles, modulation of these two peaks must be separately analysed. For this reason, the comparison is made for the spectra of $Z \gtrsim 3$, in stead of making comparison between alpha spectra of different years.

made on 11th of Sept., 1957. On that day the data of the continuous observation of neutron intensity[3306] showed that the intensity of cosmic rays was just in the course of recovery from the large Forbush decrease, as shown in Fig. 3•3•2. It is therefore likely that some part of the reduction in our alpha intensity could be attributed to this Forbush decrease. However the neutron intensity observed at Mt. Washington[3307] (cutoff rigidity=1.9 Gv) was reduced by about 20% from 1954 to 1957, whereas the intensity of neutrons at the same station was reduced only by about 3% on that day compared with the average intensity from July to October in 1957. Thus, it is plausible that most part of the reduction should still be attributed to the 11-year solar cycle modulation.

ii) The relative abundances of various heavy primary components appear to be roughly constant as shown in § 2•2. When one compares the experimental values of the ratio of the intensities obtained by various authors, one finds that they scatter considerably, sometimes beyond the

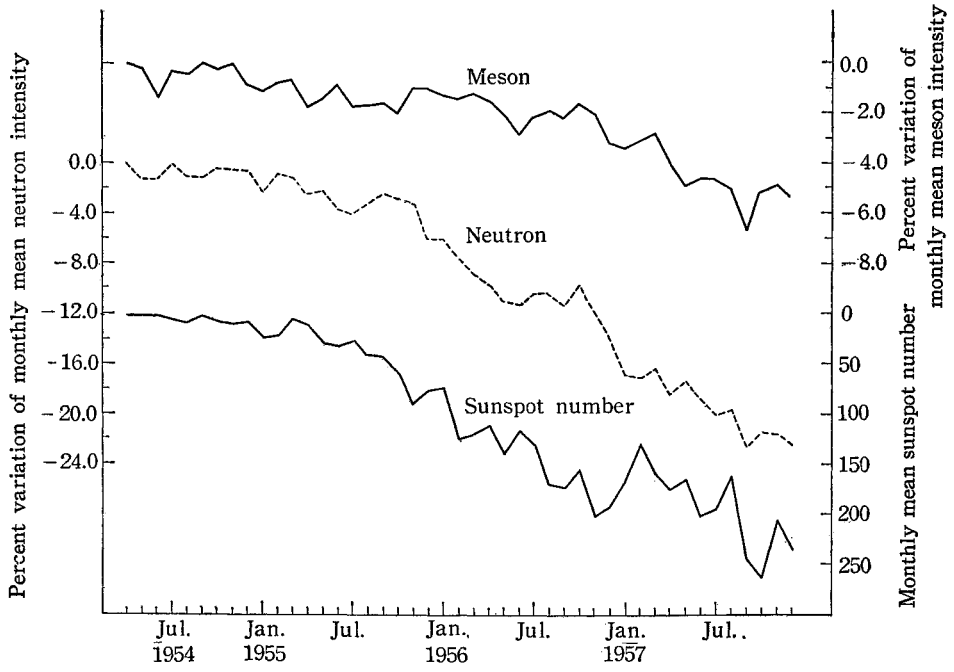

Locality of Ottawa Observation Station:

Height	=101 m (1004.0 mbar)
Geomagnetic latitude	=56.8°N
Cutoff rigidity	=1.7 Gv
UT for LT 0^h	=5 h

Fig. 3•3•2(b). Variation in monthly mean cosmic ray intensity at Ottawa throughout the period between April, 1954 and December, 1957. Monthly mean sunspot number is also illustrated.

quoted errors. But one finds no evidence for any systematic change of the ratio between the data obtained in periods of different solar activities, and within an energy interval of several hundred Mev to several Gev. Considering possible systematic errors in the charge determination, one might be able to conclude the constancy of the ratio within an error of 30%.

The above conclusions, particularly i), indicate that the heavy primary particles arriving at the earth are greatly affected by the activity of the sun. Phenomena of the time variation of general cosmic ray intensity with solar activity have been known for a long time, from the continuous observation of the intensity at ground stations. One finds now that the heavy primary component also shows a similar variation. Considering that heavy primaries originate not from the sun but from different types of stars, the main effect of the sun is not to produce cosmic rays but to modulate the intensity of the cosmic rays coming from outside of the solar system. One can suspect that corpuscular streams or plasma clouds emitted from the sun will accelerate, decelerate and scatter the cosmic ray particles from outside through the electromagnetic interaction, and modulate the intensity coming into the atmosphere.

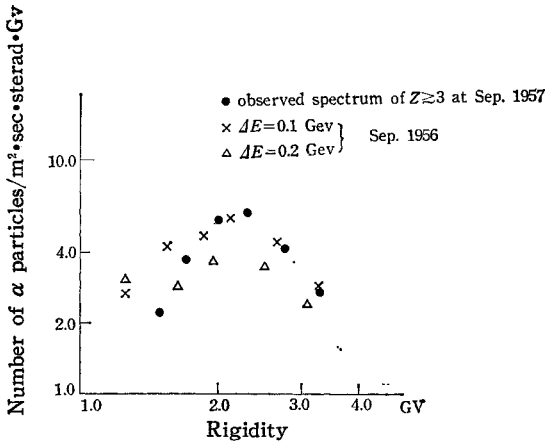

Fig. 3•3•3. Expected rigidity spectrum of primary particles in solar maximum, assuming that modulation is only caused by the electric field.

3•3•1. *Mechanism of solar modulation*

Recent developments in rocket techniques make it possible to observe directly the magnetic field in the interplanetary space far from the earth. The observation[3308] shows that magnetic field strength decreases as $1/r^3$

with distance r from the earth like a dipole field and reaches asymptotically a value of the order of 10^{-5} gauss to 10^{-3} gauss, which seems to be the value of the general interplanetary magnetic field. On magnetically quiet day this value is a few times 10^{-5} gauss, and on the disturbed day it sometimes increases beyond 10^{-4} gauss, and it fluctuates from day to day.

These fluctuating interplanetary magnetic fields are certainly due to the field attached to the neutral plasma clouds ejected from the sun. Therefore, the whole solar system is considered to be surrounded by such plasma clouds with a field of 10^{-5} to 10^{-4} gauss which were ejected sometimes in the past. Thus, the Davis cavity theory[3309] is rejected.

Let us consider a place far from the solar system, where the effect of the solar magnetic cloud is negligibly small, and let the rigidity spectrum of the cosmic ray at this position be $I_0(R)dR$, then $I_0(R)dR$ is the unmodulated cosmic ray.

In order to investigate the modulation effect on the above spectrum due to the magnetic cloud, we first have to assume the electric field caused by this cloud. Suppose a cosmic ray particle is degraded in energy by an amount ΔE, by this electric field, then a simple calculation shows that the rigidity of the particle, R, is reduced to a smaller value, R', given by the relation (R in Gv),

$$R'=[R^2+(A/Z)^2\Delta E^2-2\{(R^2+(A/Z)^2A^2)^{1/2}\}(A/Z)\Delta E]^{1/2}.$$

Furthermore the decrease in the intensity is expressed, following the Liouville's theorem, by the factor,

$$\left(\frac{R'}{R}\right)^2\frac{dR'}{dR}. \qquad (3\cdot3\cdot1)$$

These arguments are used in constructing a modulated spectrum from the spectrum in 1956, which is believed to be least affected by the solar activity.[3310] Calculations are made for several different values of ΔE and the results are compared with the observed spectrum in 1957, as shown in Fig. 3·3·3. One finds that, while some amount of reduction at a low rigidity side results from the expression (3·3·1), the shape of the spectrum is in

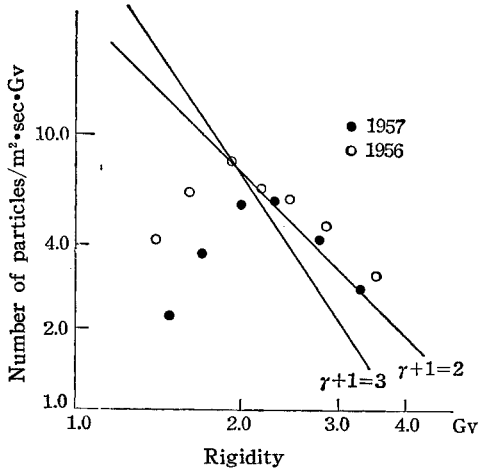

Fig. 3·3·4. Determination of exponent of the primary rigidity spectrum outside the solar system.

disagreement with the observational data. Thus one may conclude that reduction in the rigidity by the electric field, even if it exists, is quite small, and the effect of the electric field cannot explain the main features of the modulation of cosmic ray particles at the low energy side.

Next we consider the effect of magnetic field acting on cosmic rays. If the magnetic barrier surrounding the solar system is stationary in time, then the cosmic ray particles diffuse into the field, and the particles are filled up in the interplanetary space after a while. So, there occurs only a transient reduction of intensity within a short period, and after that, the intensity of cosmic rays will recover again to the normal level. Therefore, one must look for another associated reduction mechanism due to magnetic cloud, for instance, the case of nonstationary magnetic fields, mentioned by Parker.[3311]

3·3·2. *General argument on modulation by magnetic clouds*

So far, the theory of modulation by magnetic field seems most promising among all. Leaving details of assumed properties of magnetic clouds, one can construct phenomenological general arguments on the mechanism of modulation by magnetic fields and obtain several pieces of important information from the observed data. Comparison of this phenomenological approach with some of the proposed models will be discussed in Appendix 7.

Let us consider the barrier of magnetic field surrounding the solar system. We divide this barrier into n thin layers in such a way that in each layer the reduction of cosmic ray intensity is the same. The geometrical thickness of this layer will be in general not the same for all layers, but will depend on the strength of the magnetic field in each layer. Let the reduction factor, or the obscuration, in one layer be M. M is a function of the rigidity and also the velocity* of the particles. Then the total modulation factor B is given by

$$B=(1-M)^n. \tag{3·3·2}$$

If we take a large value for n, then

$$B\simeq e^{-nM}.$$

If we consider another condition of the barrier, with different thickness and different strength of the magnetic field, we have another modulation factor B' which is approximately given by

* Except for the proton component, M may be considered as a function depending only on the rigidity, because for other particles Z/A is almost 1/2.

$$B' \simeq (1-M)^{n'} \simeq e^{-n'M}, \tag{3·3·3}$$

with the same M and different n'. Thus the values of n must depend in a complicated way upon the features of magnetic field. Considering the fact that low rigidity particles are deflected more in a magnetic field than high rigidity ones, low rigidity particles are modulated more than high rigidity ones as is observed in Fig. 3·3·4. Therefore we can assume that M is a monotonically decreasing function of the rigidity R. Then, we may write

$$M \simeq 1/R^m \tag{3·3·4}$$

where m is a function of rigidity and also the velocity of the particles.

For the unmodulated spectrum, we write

$$I_0 dR \sim \frac{dR}{R^{\gamma+1}}, \tag{3·3·5}$$

where γ is a function of R. We know γ is a slowly increasing function of R and equal to 1.5 at several Gv.

From the formulae (3·3·3), (3·3·4) and (3·3·5), a modulated spectrum observed at the earth is given by

$$IdR \sim e^{-\frac{n}{R^m}} \frac{dR}{R^{\gamma+1}}. \tag{3·3·6}$$

Now we examine the decrease of intensity at the peak of the spectrum.

As shown in Fig. 3·3·4 the maximum always appears near 2 Gv. It is restricted only to a small region even if we compare the spectrum in 1956 with that in 1957, so that we may consider m to be nearly constant in the expression (3·3·4). A similar argument can also apply for the exponent of the unmodulated rigidity spectrum.

Thus the maximum of the spectrum appears at the rigidity R_0, satisfying the following equation,

$$\frac{mn}{R_0^{m+1}} - \frac{(\gamma+1)}{R_0} = 0, \tag{3·3·7}$$

obtained by differentiating (3·3·6). From this equation we get

$$\frac{n}{R_0^m} = \frac{\gamma+1}{m}. \tag{3·3·8}$$

Then at the maximum of the spectrum, the intensity is depressed by a factor,

$$e^{-(\gamma+1)/m}, \tag{3·3·9}$$

compared with the unmodulated spectrum.

It must be emphasized that, if we take the modulation factor as given in the expression (3•3•3), then the factor (3•3•9) is quite independent of the features of modulation.

Then if we draw a line, connecting the maximum of the spectrum observed at different times the slope of this line must coincide with that of the unmodulated spectrum. We apply the above argument to the spectra shown in Fig. 3•3•4, then we get

$$r=1.5\pm0.5. \qquad (3\cdot3\cdot10)$$

Thus the depression of the intensity and the shift of the rigidity at the maximum of the spectrum can be interpreted in terms of the exponent of the unmodulated spectrum.

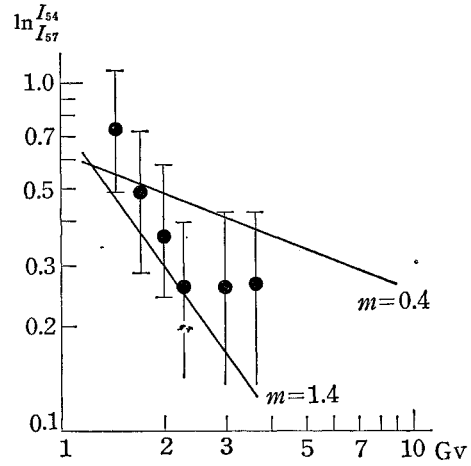

Fig. 3•3•5. Determination of modulation parameter, m.

Our next task is to determine the values of n and m in the expression (3•3•6), and to compare them with those obtained by a plausible modulation models presented till now.

Here we compare the spectra observed in 1956 and 1957. The intensity is reduced by a factor of

$$I_{56}/I_{57}=e^{-\frac{n_{56}-n_{57}}{R^m}} \qquad (3\cdot3\cdot11)$$

which is given by the expression (3•3•6).

Thus, if we derive the reduction factor (3•3•11) using the experimental data, and examine this factor about the dependence of the rigidity, we get information about the value of m.

Fig. 3•3•5 shows the result, and, from this, we get

$$m=0.9\pm0.5. \qquad (3\cdot3\cdot12)$$

As we get the values of m and r, we determine the value of n using the relation (3•3•7). The results are shown in Table 3•3•1.

In that Table, we derive the values of n for the lower and the upper limits of the values of r and m. In the Appendix, these figures of m and n are shown to be of right order of magnitude, if we make acceptable

assumptions on the features of magnetic clouds surrounding the earth.

Table 3•3•1.

	$\gamma=1.0$		$\gamma=2.0$	
	n_{56}	n_{57}	n_{56}	n_{57}
$m=0.4$	6.5	7.0	9.7	10.5
$m=1.4$	3.5	4.3	5.3	6.4

Acknowledgement

This experiment was started in Chicago during the stay of one of the authors (M. K.) in U.S.A. The authors would like to express their sincere thanks to late Professor M. Schein for having made it possible to perform this experiment and for his continuous interest and his support through the course of this work.

They are indebted to Professor S. Hayakawa for his critical discussions and encouragement throughout this work, and also wish to acknowledge to Professor T. Hatanaka and Professor M. Taketani and the members of the Galaxy Research Group for their encouraging advices.

Thanks are also due to the scanning staff of University of Chicago and to Mrs. E. Mikumo, Mrs. T. Moro-oka, Miss. K. Murakami, Mrs. Y. Nishimura and Mrs. T. Nishimura of Institute for Nuclear Study, University of Tokyo, for their skilful scanning and measurements. Dr. S. Naranan kindly read our manuscript before the publication, and gave us invaluable advices and corrected our English.

This work was partly supported by Nishina Memorial Foundation and Research Institute for Fundamental Physics, Kyoto University and one of the authors (K. Y.) was sponsored by Japan Society for the Promote of Science for his stay at Institute for Nuclear Study.

Appendix 1

Diagonalization of the fragmentation matrix

Fragmentations of primary nuclei are described by the differential equation

$$\frac{d\boldsymbol{\Phi}(x)}{dx}=\boldsymbol{F}\boldsymbol{\Phi}(x), \tag{A1•1}$$

where $\boldsymbol{\Phi}(x)$ is a vector in the "charge group space":

$$\boldsymbol{\Phi}(x) \equiv [\Phi_i(x)], \tag{A1·2}$$

$\Phi_i(x)$ being the flux value of the primary nuclei belonging to i-th charge group at the depth x of medium and $\boldsymbol{F}$ is the "fragmentation matrix":

$$\boldsymbol{F} \equiv [F_{ij}] \tag{A1·3}$$

$$F_{ij} \equiv -\frac{1}{\Lambda_j}\delta_{ij} + \frac{1}{\lambda_j}P_{ji} \tag{A1·4}$$

where P_{ji} is the "fragmentation parameter of j-th component with respect to i-th component", i. e., the mean number of resultant nuclei of i-th component when a nucleus of j-th component makes a nuclear collision with a nucleus of the matter, Λ_j and λ_j are the absorption mean free path and the collision mean free path, respectively, of the nuclei of j-th component, and there exists a relation between them:

$$\Lambda_j = \frac{\lambda_j}{1-P_{jj}} \,. \tag{A1·5}$$

If we assign a smaller suffix to a heavier component, $P_{ji}=0$ for $j>i$. Therefore the matrix $\boldsymbol{F}$ has the form,

$$\begin{bmatrix} \boldsymbol{K} & \boldsymbol{O} \\ \boldsymbol{L} & \boldsymbol{M} \end{bmatrix}, \tag{A1·6}$$

where $\boldsymbol{O}$ is a null matrix, for every division of rows and columns on the condition that $\boldsymbol{K}$ and $\boldsymbol{M}$ are square matrices. Now, a matrix of the form shown above can be transformed into the form,

$$\begin{bmatrix} \boldsymbol{K} & \boldsymbol{O} \\ \boldsymbol{O} & \boldsymbol{M} \end{bmatrix}, \tag{A1·7}$$

by means of the matrix of the form,

$$\begin{bmatrix} \boldsymbol{E}_1 & \boldsymbol{O} \\ \boldsymbol{X} & \boldsymbol{E}_2 \end{bmatrix}, \tag{A1·8}$$

where $\boldsymbol{E}$'s are unit matrices.

Therefore, by applying matrices of this form successively, we can diagonalize the matrix $\boldsymbol{F}$ by means of a certain matrix $\boldsymbol{T}$:

$$\boldsymbol{T}\boldsymbol{F}\boldsymbol{T}^{-1} = \boldsymbol{G}, \tag{A1·9}$$

where

$$G_{ij} = -\frac{1}{\Lambda_j}\delta_{ij} \,. \tag{A1·10}$$

Eq. (A1·1) can then be transformed into the form,

$$\frac{d}{dx}[\boldsymbol{T}\boldsymbol{\Phi}(x)]_i=-\frac{1}{\Lambda_i}[\boldsymbol{T}\boldsymbol{\Phi}(x)]_i, \tag{A1·11}$$

and we can obtain the solution directly:

$$[\boldsymbol{T}\boldsymbol{\Phi}(x)]_i=[\boldsymbol{T}\boldsymbol{\Phi}(0)]_i e^{-x/\Lambda_i}. \tag{A1·12}$$

Therefore, by recombining $\boldsymbol{\Phi}_i(x)$'s by means of $\boldsymbol{T}$ we have the quantities which vary with x according to the exponential laws.* $\boldsymbol{\Phi}(x)$ and $\boldsymbol{\Phi}(0)$ are obtained by the formulae

$$\boldsymbol{\Phi}(x)=\boldsymbol{T}^{-1}\boldsymbol{A}\boldsymbol{T}\boldsymbol{\Phi}(0) \text{ and } \boldsymbol{\Phi}(0)=\boldsymbol{T}^{-1}\boldsymbol{A}^{-1}\boldsymbol{T}\boldsymbol{\Phi}(x), \tag{A1·13}$$

where $\boldsymbol{A}$ is a matrix whose elements are

$$A_{ij}=e^{-x/\Lambda_i}\delta_{ij}. \tag{A1·14}$$

If one solves $\boldsymbol{\Phi}(x)$ or $\boldsymbol{\Phi}(0)$ directly from (A1·12) using the property of $\boldsymbol{T}$ that

$$T_{ii}=1, \tag{A1·15}$$

one will get the solution usually given in the literature.

Let

$$\Lambda_{ij}\equiv-(\Lambda_i^{-1}-\Lambda_j^{-1})^{-1}=\frac{\Lambda_i\Lambda_j}{\Lambda_i-\Lambda_j}. \tag{A1·16}$$

For $|\Lambda_{ij}^{-1}x|\ll 1$, the solution of $\Phi_i(0)$'s by means of Eq. (A1·13) is inconvenient for numerical treatment and the approximate solutions (2·1·5) given in § 2·1·1 are more adequate.

If $\boldsymbol{\Phi}(x)$ is a four-component vector:

$$\boldsymbol{\Phi}(x)\equiv\begin{pmatrix}\Phi_1(x)\\ \Phi_2(x)\\ \Phi_3(x)\\ \Phi_4(x)\end{pmatrix}, \tag{A1·17}$$

the matrix $\boldsymbol{T}$ has the form,

---

* Incidentally, this means that we can check the reliability of the data given by various observers and guess the most plausible set of fragmentation parameters by plotting the $[\boldsymbol{T}\boldsymbol{\Phi}(x)]_i$'s obtained in observations made at various depths in air during the same period of solar activity.

$$
\boldsymbol{T}=\begin{pmatrix}
1, & 0, & 0, & 0 \\
\frac{1}{\lambda_1}\Lambda_{21}P_{12}, & 1, & 0, & 0 \\
\frac{1}{\lambda_1}\left[\Lambda_{31}P_{13}+\frac{1}{\lambda_2}(\Lambda_{32}-\Lambda_{31})\Lambda_{21}P_{12}P_{23}\right], & \frac{1}{\lambda_2}\Lambda_{32}P_{23}, & 1, & 0 \\
\frac{1}{\lambda_1}\left[\Lambda_{41}P_{41}+\frac{1}{\lambda_2}(\Lambda_{42}-\Lambda_{41})\Lambda_{21}P_{12}P_{24}\right. & \frac{1}{\lambda_2}\left[\Lambda_{42}P_{24}\right. & \frac{1}{\lambda_3}\Lambda_{43}P_{34}, & 1 \\
\quad\left.+\frac{1}{\lambda_3}(\Lambda_{43}-\Lambda_{41})\Lambda_{31}P_{13}P_{34}\right. & \quad\left.+\frac{1}{\lambda_3}(\Lambda_{43}-\Lambda_{42})\Lambda_{32}P_{23}P_{34}\right], & & \\
\quad+\frac{1}{\lambda_3\lambda_2}(\Lambda_{43}\Lambda_{32}\Lambda_{21}+\Lambda_{41}\Lambda_{31}\Lambda_{21} & & & \\
\quad\left.-\Lambda_{42}\Lambda_{32}\Lambda_{21}-\Lambda_{43}\Lambda_{31}\Lambda_{21})P_{12}P_{23}P_{34}\right], & & &
\end{pmatrix}. \tag{A1·18}
$$

Incidentally, the matrix $\boldsymbol{T}^{-1}$ has the form,

$$
\boldsymbol{T}^{-1}=\begin{pmatrix}
1, & 0, & 0, & 0 \\
-\frac{1}{\lambda_1}\Lambda_{21}P_{12}, & 1, & 0, & 0 \\
-\frac{1}{\lambda_1}\Lambda_{31}\left(P_{13}-\frac{1}{\lambda_2}\Lambda_{21}P_{12}P_{23}\right), & -\frac{1}{\lambda_2}\Lambda_{32}P_{23}, & 1, & 0 \\
-\frac{1}{\lambda_1}\Lambda_{41}\left(P_{14}-\frac{1}{\lambda_2}\Lambda_{21}P_{12}P_{24}\right. & -\frac{1}{\lambda_2}\Lambda_{42}\left(P_{24}\right. & -\frac{1}{\lambda_3}\Lambda_{43}P_{34}, & 1 \\
\quad\left.-\frac{1}{\lambda_3}\Lambda_{31}P_{13}P_{34}\right. & \quad\left.-\frac{1}{\lambda_3}\Lambda_{32}P_{23}P_{34}\right), & & \\
\quad\left.+\frac{1}{\lambda_3\lambda_2}\Lambda_{31}\Lambda_{21}P_{12}P_{23}P_{34}\right), & & &
\end{pmatrix}. \tag{A1·19}
$$

In the most practical case of a three component $\boldsymbol{\Phi}(x)$:

$$
\boldsymbol{\Phi}(x)\equiv\begin{pmatrix}\Phi_H(x)\\ \Phi_M(x)\\ \Phi_L(x)\end{pmatrix}, \tag{A1·20}
$$

$\boldsymbol{T}$ is given by (A1·18) with the 4th row and 4th column removed and with the replacement of the suffices 1, 2, 3 by H, M, L, respectively.

In the case of the terrestrial atmosphere as the medium, the most probable values of the parameters are (cf. §2·1)

$$\lambda_H=19.0\ \mathrm{g/cm^2} \qquad \Lambda_H=27.1\ \mathrm{g/cm^2}$$

$$\lambda_M = 27.1 \text{ g/cm}^2 \qquad \Lambda_H = 31.9 \text{ g/cm}^2$$
$$\lambda_L = 31.6 \text{ g/cm}^2 \qquad \Lambda_L = 37.2 \text{ g/cm}^2, \tag{A1·21}$$

$$P_{HM} = 0.33, \qquad P_{HL} = 0.15, \qquad P_{ML} = 0.25, \tag{A1·22}$$

so that

$$\boldsymbol{T} = \begin{pmatrix} 1.00 & 0 & 0 \\ 3.13 & 1.00 & 0 \\ 4.39 & 2.07 & 1.00 \end{pmatrix} \tag{A1·23}$$

and

$$\boldsymbol{T}^{-1} = \begin{pmatrix} +1.00 & 0 & 0 \\ -3.13 & +1.00 & 0 \\ +2.09 & -2.07 & +1.00 \end{pmatrix}. \tag{A1·24}$$

A direct application of the diagonalization will be found in §1·1·1 and in Appendix 2.

Appendix 2

Ascent correction

Balloons take some time until reaching their ceiling heights. Let us calculate the fractions of the primary nuclei which enter into the stack during the ascent time. For simplicity, we shall treat only the case where the energies of the nuclei are sufficiently high and therefore no nuclei are stopped by ionization losses within the atmospheric depth which gives main contribution to the effect.

The rising of a usual plastic balloon can be approximated by a motion with constant upward velocity. Let the velocity be v, the time elapsed after launching be τ, and the height of the balloon at time τ be z, then

$$z = v\tau. \tag{A2·1}$$

The atmospheric depth, i.e., the amount of residual air x at height z, is described by the relation,

$$x = x_0 e^{-z/z_0}, \tag{A2·2}$$

where x_0 and z_0 are slowly varying functions of z (more precisely, they vary from day to day and place to place).

Now, considering that the collision mean free paths of heavy primaries are short, the values of x which we are interested in are smaller than 150 g/cm^2. For these values of x, quantities x_0 and z_0 are practically constant and are given by[A201]

$$x_0 = 1288\ \mathrm{g/cm^2}$$
$$z_0 = 6.38\ \mathrm{km}. \qquad \text{(A2·3)}$$

In this case we can derive the following formula from (A2·1) and (A2·2):

$$\frac{d\tau}{dx} = -\frac{z_0}{vx}. \qquad \text{(A2·4)}$$

Now, let the flux of a heavy primary component at depth x be $\Phi(x)$, and let us consider the case that $\Phi(x)$ decreases exponentially with depth according to the absorption mean free path Λ, then

$$\Phi(x) = \Phi(0)e^{-x/\Lambda}. \qquad \text{(A2·5)}$$

$F(x)$, the number per unit time of the nuclei of the above component which enter the stack at depth x fulfilling the scanning criteria, is, as will be seen in (1·1·4),

$$F(x) = k\Phi(x), \qquad \text{(A2·6)}$$

k being a numerical constant determined by the criteria and other conditions of the scanning.

Let X be the atmospheric depth of the ceiling height, m the air-equivalent of the amount of packing material above the stack, t the time of flight at the ceiling height, and $\overline{\sec\theta}$ the average of the secants of zenith angles of θ of the incident nuclei in question.

The fraction f of the nuclei which entered during the ascent with respect to those which entered during the ceiling flight is then given by

$$f = \frac{F(0)\int_0^{\tau(z)} e^{-\frac{x(\tau')+m}{\Lambda}\overline{\sec\theta}}d\tau'}{F(0)te^{-\frac{X+m}{\Lambda}\overline{\sec\theta}}} = \frac{1}{t}\int_0^{\tau(X)} e^{-\frac{x(\tau')-X}{\Lambda}\overline{\sec\theta}}d\tau'$$
$$= \frac{1}{t}\int_{1013}^{X} e^{-\frac{x-X}{\Lambda}\overline{\sec\theta}}\frac{d\tau'}{dx}dx \fallingdotseq \frac{1}{t}\int_x^{1013}\frac{z_0}{vx}e^{-\frac{x-X}{\Lambda}\overline{\sec\theta}}dx$$
$$= \frac{z_0}{vt}e^{\frac{X}{\Lambda}\overline{\sec\theta}}\int_{\frac{X}{\Lambda}\overline{\sec\theta}}^{\frac{1013}{\Lambda}\overline{\sec\theta}}\frac{e^{-y}}{y}dy \fallingdotseq \frac{z_0}{vt}e^{\frac{X}{\Lambda}\overline{\sec\theta}}\left[-\mathrm{Ei}\left(-\frac{X\overline{\sec\theta}}{\Lambda}\right)\right], \qquad \text{(A2·7)}$$

where[A202)]

$$-\mathrm{Ei}(-Y) \equiv \int_Y^\infty \frac{e^{-y}}{y}dy. \qquad \text{(A2·8)}$$

Now let $N(X+m)$ be the total number of tracks of the nuclei in question accepted in the scanning, $\Phi(X+m)$ be the true flux, and $\Phi'(X+m)$ be the flux value obtained without ascent correction, respectively, at the top of the emulsion stack. Then

$$\Phi(X+m)=\frac{N(X+m)}{kt(1+f)}\,, \tag{A2·9}$$

while

$$\Phi'(X+m)=\frac{N(X+m)}{kt}\,. \tag{A2·10}$$

The effect of ascent correction, $\Delta\Phi/\Phi'$, is then given by

$$\frac{\Delta\Phi}{\Phi'}(X+m)\equiv\frac{\Phi'(X+m)-\Phi(X+m)}{\Phi'(X+m)}=\frac{f}{1+f}\,. \tag{A2·11}$$

In the practical case of dealing with $\Phi_H(x)$, $\Phi_M(x)$ and $\Phi_L(x)$, $\Phi_M(x)$ and $\Phi_L(x)$ do not vary according to (A2·5). According to the result of Appendix 1, however, $(\boldsymbol{T\Phi})_H(x)$, $(\boldsymbol{T\Phi})_M(x)$ and $(\boldsymbol{T\Phi})_L(x)$ fulfil the condition. If we denote the respective fraction of the nuclei of these components which entered during the ascent by f_H, f_M and f_L, and the respective total number of the accepted tracks by $(\boldsymbol{TN})_H(x)$, $(\boldsymbol{TN})_M(x)$and $(\boldsymbol{TN})_L(x)$, where $\boldsymbol{N}(x)$ is a vector

$$\boldsymbol{N}(x)\equiv\begin{pmatrix}N_H(x)\\N_M(x)\\N_L(x)\end{pmatrix}, \tag{A2·12}$$

then

$$kt\boldsymbol{KT\Phi}(X+m)=\boldsymbol{TN}(X+m), \tag{A2·13}$$

where $\boldsymbol{K}$ is a matrix whose component is

$$K_{ij}=(1+f_i)\delta_{ij}\,, \tag{A2·14}$$

while

$$kt\boldsymbol{T\Phi}'(X+m)=\boldsymbol{TN}(X+m), \tag{A2·15}$$

where $(\boldsymbol{T\Phi}')_i(X+m)$ is the flux value without ascent correction.

Therefore,

$$\boldsymbol{\Phi}(X+m)=\frac{1}{kt}\boldsymbol{T}^{-1}\boldsymbol{K}^{-1}\boldsymbol{TN}(X+m) \tag{A2·16}$$

and

$$\boldsymbol{\Phi}'(X+m)=\frac{1}{kt}\boldsymbol{N}(X+m), \tag{A2·17}$$

so that

$$\begin{aligned}\frac{\Delta\boldsymbol{\Phi}_i}{\boldsymbol{\Phi}_i}(X+m)&\equiv\frac{\Phi_i'(X+m)-\Phi_i(X+m)}{\Phi_i'(X+m)}\\&=\frac{N_i(X+m)-(\boldsymbol{T}^{-1}\boldsymbol{K}^{-1}\boldsymbol{TN})_i(X+m)}{N_i(X+m)}\,.\end{aligned} \tag{A2·18}$$

In practical cases $f_i \ll 1$, and (A2·18) are approximately given by

$$\frac{\Delta\Phi_H}{\Phi'_H} = f_H ,$$

$$\frac{\Delta\Phi_M}{\Phi'_M} = f_M + 3.13(f_M - f_H)\frac{N_H}{N_M} ,$$

$$\frac{\Delta\Phi_L}{\Phi'_L} = f_L + 2.07(f_L - f_M)\frac{N_M}{N_L} + [4.39(f_L - f_M) - 2.09(f_M - f_H)]\frac{N_H}{N_L} . \qquad \text{(A2·19)}$$

If we are dealing with four charge groups, 1, 2, 3 and 4, the corresponding approximate expressions of $(\Delta\Phi_i/\Phi'_i)$'s are

$$\frac{\Delta\Phi_1}{\Phi'_1} = f_1 ,$$

$$\frac{\Delta\Phi_2}{\Phi'_2} = f_2 + A(f_2 - f_1)\frac{N_1}{N_2} ,$$

$$\frac{\Delta\Phi_3}{\Phi'_3} = f_3 + [B(f_2 - f_1) + C(f_3 - f_2)]\frac{N_1}{N_3} + D(f_3 - f_2)\frac{N_2}{N_3} ,$$

$$\frac{\Delta\Phi_4}{\Phi'_4} = f_4 + [E(f_2 - f_1) + F(f_3 - f_2) + G(f_4 - f_3)]\frac{N_1}{N_4} + [H(f_3 - f_2) + J(f_4 - f_3)]\frac{N_2}{N_4} + L(f_4 - f_3)\frac{N_3}{N_4} , \qquad \text{(A2·20)}$$

where

$$A \equiv \frac{1}{\lambda_1}\Lambda_{21}P_{12} ,$$

$$B \equiv \frac{1}{\lambda_1}\Lambda_{31}P_{13} - \frac{1}{\lambda_2\lambda_1}\Lambda_{31}\Lambda_{21}P_{12}P_{23} ,$$

$$C \equiv \frac{1}{\lambda_1}\Lambda_{31}P_{13} + \frac{1}{\lambda_2\lambda_1}(\Lambda_{32} - \Lambda_{31})\Lambda_{21}P_{12}P_{23} ,$$

$$D \equiv \frac{1}{\lambda_2}\Lambda_{32}P_{23} ,$$

$$E \equiv \frac{1}{\lambda_1}\Lambda_{41}P_{14} - \frac{1}{\lambda_2\lambda_1}\Lambda_{41}\Lambda_{21}P_{12}P_{24} - \frac{1}{\lambda_3\lambda_1}\Lambda_{41}\Lambda_{31}P_{13}P_{34} + \frac{1}{\lambda_3\lambda_2\lambda_1}\Lambda_{41}\Lambda_{31}\Lambda_{21}P_{12}P_{23}P_{34} ,$$

$$F \equiv \frac{1}{\lambda_1}\Lambda_{41}P_{14} + \frac{1}{\lambda_2\lambda_1}(\Lambda_{42} - \Lambda_{41})\Lambda_{21}P_{12}P_{24} - \frac{1}{\lambda_3\lambda_1}\Lambda_{41}\Lambda_{31}P_{13}P_{34}$$

$$+\frac{1}{\lambda_3\lambda_2\lambda_1}(\Lambda_{41}\Lambda_{31}-\Lambda_{42}\Lambda_{32})\Lambda_{21}P_{12}P_{23}P_{34}\,,$$

$$G\equiv\frac{1}{\lambda_1}\Lambda_{41}P_{14}+\frac{1}{\lambda_2\lambda_1}(\Lambda_{42}-\Lambda_{41})\Lambda_{21}P_{12}P_{24}+\frac{1}{\lambda_3\lambda_1}(\Lambda_{43}-\Lambda_{41})\Lambda_{31}P_{13}P_{34}$$

$$+\frac{1}{\lambda_3\lambda_2\lambda_1}(\Lambda_{43}\Lambda_{32}-\Lambda_{42}\Lambda_{32}-\Lambda_{43}\Lambda_{31}+\Lambda_{41}\Lambda_{31})P_{12}P_{23}P_{34}\,,$$

$$H\equiv\frac{1}{\lambda_2}\Lambda_{42}P_{24}-\frac{1}{\lambda_3\lambda_2}\Lambda_{42}\Lambda_{32}P_{23}P_{34}\,,$$

$$J\equiv\frac{1}{\lambda_2}\Lambda_{42}P_{24}+\frac{1}{\lambda_3\lambda_2}(\Lambda_{43}-\Lambda_{42})\Lambda_{32}P_{23}P_{34}\,,$$

$$L\equiv\frac{1}{\lambda_3}\Lambda_{43}P_{34}\,. \qquad \text{(A2·21)}$$

Appendix 3

On the effect of the capture of electrons by heavy primaries near the end of their tracks

In the course of the present analysis of stopped heavy primaries in our emulsions, the *range and integral delta-ray method* has been widely used for the determination of their charges and energies. Some details of this method are already described in § 1·2·4. As shown in that paragraph, the idea of this method is to use the similarity relation of the range versus integral delta-ray curves for various nuclei. Thus, if one experimentally finds this curve for a heavy primary with a known atomic number, one can determine the charge of the nuclei without referring to any detailed theory of the ionization loss. This similarity relation has in fact been proved for tracks of heavy primaries up to Si. On measuring the number of delta rays for nuclei heavier than Si, however, we found that this similarity relation does not hold. This situation is illustrated in Fig. A3·1, and we can see that the slope of the curve tends to increase with increasing atomic number of nuclei. To see more details of the situation, we draw the range versus delta-ray density curves in Fig. A3·2 instead of using the integral values of delta rays. One can see, from these data, that, for small ranges, delta-ray densities for heavy nuclei are smaller than the values estimated from the similarity relation. This difference appears to become more pronounced with increasing atomic number, even though the data show large statistical fluctuations.

The delta-ray density increases with increasing range, and after 1 mm range or so, it becomes almost constant. This plateau value is just the peak value of the density for a given value of Z, and it is proportional

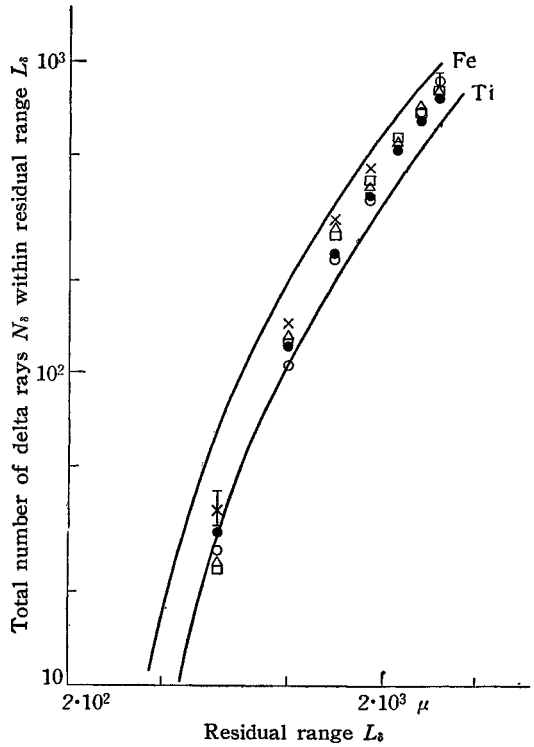

Fig. A3•1. The effect of the capture of electrons by heavy primaries, especially of the iron group, near the end of their tracks. Relation between residual range and integral delta-ray number.

○ ● △ × □ experimental data

— standard curves for Fe and Ti

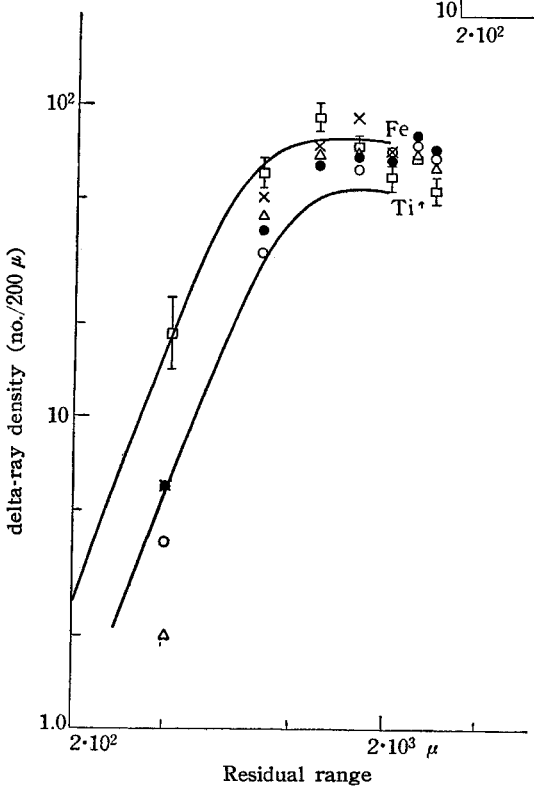

Fig. A3•2. Relation between residual range and differential delta-ray density.

○ ● △ × □ experimental data

— standard curves for Fe and Ti

to Z^2 as shown in § 1•2•4.

Comparing the plateau value of the delta-ray density of each track with the standard one, we tentatively determine the charge of the track. For an illustration, all the data plotted in Fig. A3•2 are shown to lie within the limit of $Z=25\pm2$. Thus, these tracks may be interpreted to be due to nuclei of iron group. Next, we calculate the mean values of these data, and the result is also shown by the curve in Fig. A3•3 comparing with the standard one. This procedure is made in order to minimize the statistical fluctuation of the data, and from these two curves, we can clearly see the depression of the delta-ray density of high Z track for small values of the range.

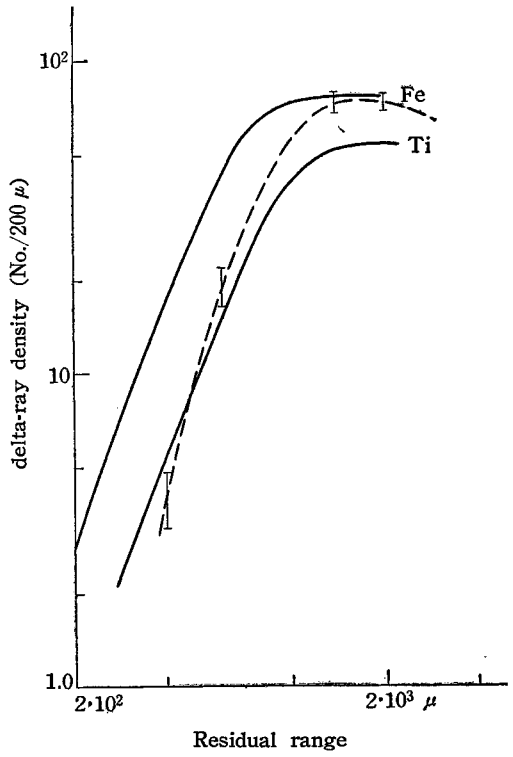

Fig. A3•3. Relation between residual range and differential delta-ray density.
—— standard curves for Fe and Ti
--- mean values of the data

To maintain the similarity relation, one must shift the curve for these tracks by an amount of $200\pm50\mu$. Similar procedure can also be applied to other nuclei after tentative determination of the charge of tracks.

The heavy primary with a velocity of the order of its K shell electron's tends to capture the electrons in the traversed material. Thus the particle behaves as though it had less charge, and the ionization loss becomes smaller compared with that of the original charged particle. This results in some increase in the range of the particle. The shift of the range *vs.* delta-ray density curves for high Z particles can be interpreted in this way.

The study of this range extension has also been made by Heckman and others[A301] using heavy ion beams from Hilac in Berkeley. In their work, they used C, N, O, Ne and A beams, each of energy 10 Mev/nucleon. As the velocity of the K shell electron is approximately given by $Z/137$, they get completely stripped ion beam only for C, N and O nuclei. Thus, a complete

analysis can be made only for nuclei up to O. However, from the general theoretical consideration of this range extension, they find the mass and charge dependence of this quantity, and it is given by

$$R_{ext}=CMZ^{2/3}, \qquad \text{(A3•1)}$$

where C is expected to be a monotonically and slowly increasing function of Z. From the results of the experiments, they get the value of C, and it is given by 0.22.

Now we can calculate the range extension of Fe or Ca beam, assuming that the relation (A3•1) holds up to these heavy nuclei. The results are shown in Table A3•1 along with our data. Considering the fact that the constant C in (A3•1) is a monotonically, slowly increasing function of Z as mentioned above, the agreement between the two is quite satisfactory.

Table A3•1

	$R_{ext}=0.22MZ^{2/3}$	Our experimental data
C	5 μ	
Ca	70 μ	100±50 μ
Fe	100 μ	200±50 μ

The charge determinations of the stopped very heavy particles are thus made as follows:

1. Tentative charge determination is made by using the plateau delta-ray density value.
2. The mean values of the several data of tracks with similar charges are compared with the standard one, and then the value for the shift to maintain the similarity law is obtained.
3. Using the above value of shift, the integral delta-ray curve is constructed and the charge is again determined using the similarity relation.

Appendix 4

Calculation of nucleus-nucleus collision cross-sections according to a simple optical model

The collision cross-section, σ_{it}, of a nucleus of mass number A_i with another nucleus of mass number A_t can usually be approximated by the semi-empirical formula (2•1•7):

$$\sigma_{it}=\pi r_0^2(A_i^{1/3}+A_t^{1/3}-b)^2, \qquad \text{(A4·1)}$$

which is derived from geometrical consideration plus some phenomenological corrections. The mass-number dependence of nuclear radii as well as the numerical value of $r_0\sim 1.45\times 10^{-13}$cm, is based, as is well known, upon the experiments of nucleon-nucleus collision.

The adjustable parameter b may be considered as a phenomenological expression of the opacity of the nuclei, and in the usual heavy primary work, this value is determined from the experimental collision mean free paths of heavy primaries in emulsions or in other material such as glass or carbon plates sandwiched in between emulsion sheets. Bradt and Peters[A401] are the first to propose the expression (A4·1), and from the observed collision mean free paths of various nuclei in glass plates of nuclear emulsions, they get

$$b=1.17.$$

In the energy region of several Gev/nucleon, this value is consistent with those obtained in other later measurements made in nuclear emulsions.[A402]

In this appendix, however, we give another way of obtaining σ_{it}.

According to the simple optical model[A403] a nucleus can be considered as an opaque material with a distribution of absorption coefficient $\bar{\sigma}\rho(r)$ corresponding to the density distribution $\rho(r)$, where $\bar{\sigma}$ is the mean value of neutron-proton and proton-proton total scattering cross section in the nucleus. To apply this model to nucleus-nucleus collision, we assume an incident nucleus as a nucleon beam distributed according to the density distribution $\rho(r)$ of the incident nucleus.

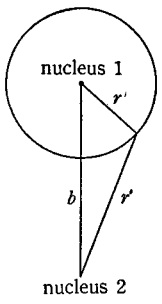

Fig. A4·1. The definition of variables of Appendix 4.

We define a cylindrical coordinate system (z, r, θ) with the origin at the center of the target nucleus 1, and take the incident direction of the nucleus 2 as z-axis. Then the opacity $\kappa(b)$ of the ring area at impact parameter b (Fig. A4·1) is

$$\kappa(b)=1-\exp\left\{\bar{\sigma}\int_0^{2\pi}\int_{-\infty}^{\infty} n_2(r')t_1(r)r\,dr\,d\theta\right\}, \qquad \text{(A4·2)}$$

where the number density, $n_2(r')$, of the incident nucleon beam at a distance r' from the center of nucleus 2 is expressed as

$$n_2(r')=\int_{-\infty}^{\infty}\rho_2(\sqrt{(r')^2+z^2})\,dz \qquad \text{(A4·3)}$$

and the path length $t_1(r)$ expressed in units of the number of nucleons is

given by

$$t_1(r)=\int_{-\infty}^{\infty}\rho_1(\sqrt{r^2+z^2})dz, \tag{A4·4}$$

and $(r')^2=b^2+r^2-2br\cos\theta$. The cross section, Σ, of nucleus-nucleus collision is expressed as

$$\Sigma=2\pi\int_0^{\infty}\kappa(b)bdb. \tag{A4·5}$$

The total cross section of nucleon-nucleon scattering at 2.5 Gev is about 37 mb which is the average of the value 47 mb for proton-proton scattering and the value 27 mb for proton-neutron scattering,[A404] and at 500 Mev the average is 31 mb.[A405] The effect of Pauli principle for bound nucleon is about 5 % at 500 Mev and, therefore, in the case of nucleus-nucleus collision $\sigma_{eff}=0.95\ \sigma_{free}=30$ mb is the effective collision cross section of a particular nucleon in the incident nucleus with a particular nucleon in the target nucleus.

The density distribution of various nuclei is investigated by the analysis of attenuation and total cross section of nucleon-nucleus collision in terms of the optical model, and we adopt the results obtained at the higher energy region.[A405)A406] We take the following two extreme assumptions of density distribution; (1) uniform distribution from $r=0$ to $r=R$ and (2) Gaussian distribution characterized by a constant a. Coor et al.[A406] show that $R=1.38A^{1/3}$, $a=0.63A^{1/3}+0.3$ for the respective assumptions:

$$\text{(i)}\qquad \rho(r)=A\Big/\left(\frac{4}{3}\pi r^3\right)\quad \text{for}\quad 0\leqq r\leqq R=1.38A^{1/3}$$
$$=0\qquad\qquad\qquad \text{for}\quad r>R. \tag{A4·6}$$

$$\text{(ii)}\qquad \rho(r)=\frac{A}{(a\sqrt{\pi})^3}\exp(-r^2/a^2);\ a=0.63A^{1/3}+0.3. \tag{A4·7}$$

Some authors have indicated that the nuclear density distribution has a tapered shape.[A406)A407]

For Gaussian distribution (A4·7), the integration (A4·5) with $\kappa(b)$ given in (A4·2) can be performed analytically, and the result is given by

$$\Sigma_G=\pi(a_1^2+a_2^2)\left[\gamma+\ln\frac{A_1A_2}{\pi(a_1^2+a_2^2)}-\mathrm{Ei}\left(-\frac{A_1A_2}{\pi(a_1^2+a_2^2)}\right)\right], \tag{A4·8}$$

where γ is Euler's constant and is equal to 0.57, and $-\mathrm{Ei}(-x)=\int_x^{\infty}\frac{e^{-t}}{t}dt$. The Ei-term is almost negligible in this case. Collision mean free paths are calculated for the known chemical composition of G5 emulsion taking $\bar{\sigma}=37$ mb and 30 mb, for $E=2.5$ Gev/nucleon and for $E=0.5$ Gev/nucleon,

respectively, and taking the experimental collision cross section for protons reported in A404) and A405). The results which are tabulated in Table A4•1 are excellently consistent with experimental results at higher energy. The calculated energy dependence is only 5%. The discrepancy with the experimental results at lower energy may be explained by unvisible peripheral collisions (where only neutrons are emitted).

Table A4•1. Experimental and calculated values of collision mean free path of heavy primaries.

	Medium	Mean energy in Gev/nuc.	L-nucleus (Be)	M-nucleus (N)	H-nucleus (Mg)	VH-nucleus (Cr)
Experimental	emulsion	~3	14.3±1.2cm	13.2±0.7cm	10.1±1.5cm	8.4±0.7cm
Calculated	emulsion	2.5	15.6	13.5	10.6	8.3
Experimental	emulsion	~0.7	18.7±2.1	16.2±1.3	12.1±1.4	
Calculated	emulsion	0.5	16.2	14.0	10.7	
Calculated	air	2.5	38.2 g/cm²	27.6 g/cm²	21.6 g/cm²	13.9 g/cm²
Calculated	air	0.5	40.0	28.6	22.4	14.4

Collision mean free paths of various nuclei in the air are calculated and listed also in Table A4•1.

For uniform density distribution (A4•6), expression cannot be analytically integrated. Rough estimation can be made as follows. If two nuclei collide with an impact parameter $b=R_1+R_2-\Delta R$, overlapped section area is $\sim\Delta R\sqrt{(1/2)\Delta R(R_1R_2)/(R_1+R_2)}$ and the mean thickness of each nucleus of these parts are $(4/3)\sqrt{2R_1\Delta R}$ and $(4/3)\sqrt{2R_2\Delta R}$, respectively. The mean frequency of nucleon-nucleon collisions in this case is given by

$$f=\bar{\sigma}nt, \tag{A4•9}$$

where

$$n=\Delta R\sqrt{\frac{1}{2}\frac{R_1R_2}{R_1+R_2}\Delta R}\frac{4}{3}\sqrt{2R_2\Delta R}\cdot\rho$$

$$t=\frac{4}{3}\sqrt{2R_1\Delta R}\cdot\rho$$

$$\rho=A\Big/\frac{4\pi}{3}(1.38A^{1/3})^3=0.114\times10^{39}\ \mathrm{cm}^{-3}.$$

We can easily determine ΔR_1 for which f is equal to 1. The cross section of nucleus-nucleus collision can be roughly estimated as

$$\Sigma_U\simeq\pi b_1^2+2\pi b_1R_1\left(1-\frac{1}{e}\right), \tag{A4•10}$$

where $b_1=R_1+R_2-\Delta R_1$. The results do not very much differ from those of the Gaussian model, but, as will be physically expected, the energy dependence is smaller in (A4•10) than in (A4•8).

Appendix 5

Extrapolation procedure where both fragmentation and ionization are taken into account

For obtaining the flux value of heavy primaries at the top of atmosphere and further at the source of the cosmic ray, one must apply correction for their interaction with atoms in the medium, as mentioned at the beginning of Chap. 2. The one is the correction for break-up of the heavy primary due to its nuclear collision, and the other is the correction by ionization loss. One can put the latter out of consideration, if one concerns only on the integral fluxes or the higher energy part of the spectra in which ionization loss in the medium can be safely neglected. Here, we consider a correction for ionization loss to be applied for the differential spectrum in the lower energy region.

In this lower energy region the effect of both ionization and nuclear collision processes on the spectrum is connected with each other as will be shown later with Eq. (A5·2). In many cases, however, we can separately apply two kinds of corrections as the simplest and sufficient approximation as proved in the following way. One can correct the energy of observed particle by calculating their ionization loss in the atmosphere to get the spectrum at the top of atmosphere at first, and then next, correct the effect of break-up by the nuclear interaction in the atmosphere. This approximation is sufficient in M- and H-components at the energy we concerned, in which fragmented particles from the higher charge group can be considered as a minor correction. But this is not the case for L-component in which fragmented particles give a main contribution.

Let us consider the diffusion equation for the differential spectrum $N_j(x, E)$ of j-th group in the atmosphere. The increase of the flux caused by the shift of energy resulted from ionization loss is given by

$$\frac{\partial(N_j(x, E)\cdot w_j(E))}{\partial E},$$

where $w_j(E)$ is ionization loss rate for the i-element in the medium and is Z_i^2/A_i times that for proton, $w(E)$. Thus we get

$$\frac{\partial}{\partial x}N_j(x, E) = -\frac{1}{\Lambda_j}N_j(x, E) + \frac{\partial}{\partial E}(N_j(x, E)\cdot w_j(E)) + S_j(x, E). \tag{A5·1}$$

The solution of Eq. (A5·1) is given by

$$N_j(x, E) = N_j(0, E)\frac{w(E_x^j)}{w(E)}e^{-x/\Lambda_j} + e^{-x/\Lambda_j}\int_0^x S_j(x', E_{x-x'}^j)\frac{w(E_{x-x'}^j)}{w(E)}e^{x'/\Lambda_j}dx', \tag{A5·2}$$

where E_x^j is the energy of the particle with the residual range of $x+R_j(E)$, and $R_j(E)$ is the residual range of the j-element with energy E, i.e.,

$$R_j(E_x^j)=R_j(E)+x.$$

The source function $S_j(x,E)$ is given by

$$S_j(x,E)=\sum_{i<j}\frac{P_{ij}}{\lambda_i}N_i(x,E).$$

When the depth x is not large compared with the mean free path for $i\to j$ collision, λ_j/P_{ij}, the method of successive approximation is useful to get the solution of (A5·2). They are given by

$$N_j^{(0)}(x,E)=N_j(0,E_x^j)\frac{w(E_x^j)}{w(E)}e^{-x/\Lambda_j}$$

$$N_j^{(1)}(x,E)=\sum_{i<j}\frac{P_{ij}}{\lambda_i}\frac{1}{w(E)}e^{-x/\Lambda_j}\int_0^x N_i(0,\{E_{x-x'}^j\}_{x'}^{i})w(\{E_{x-x'}^j\}_{x'}^{i})e^{-x'/\Lambda_{ij}}dx'$$

$$N_j^{(2)}(x,E)=\sum_{k<i}\sum_{i<j}\frac{P_{ki}}{\lambda_k}\frac{P_{ij}}{\lambda_i}\frac{1}{w(E)}e^{-x/\Lambda_j}$$

$$\times\int_0^x dx'e^{-x'/\Lambda_{ij}}\int_0^{x'}dx''e^{-x''/\Lambda_{ki}}\cdot N(0,\{(E_{x-x'}^j)_{x-x''}^{i}\}_{x''}^{k})\cdot w(\{E_{x-x'}^j)_{x'-x''}^{i}\}_{x''}^{k}),\qquad\text{(A5·3)}$$

where

$$\Lambda_{ji}^{-1}=\Lambda_i^{-1}-\Lambda_j^{-1}$$

and

$$R_i(\{E_x^j\}_y^i)=R_i(E_x^j)+y$$

and so on.

This procedure is applied to our data to get the spectra at the top of atmosphere, and in our case the difference between (A5·3) and <separate> approximations is less than 2%.

In the case of propagation of particles in the intersteller hydrogen gas of 4 g/cm² thickness, however, the difference is more than ~13% in L-component at energy ~250 Mev/nucleon and ~5% for 450 Mev/nucleon.

Appendix 6

Spallation of nucleus by proton bombardment

There are several published data on the radiochemical studies of the spallation products of proton bombardment on Cu, Al, and other medium weight nuclei. Interpolating the yield value of product isotopes in the nuclear chart by the evaporation theory, one can construct a relation for the mass number variation of the spallation products in some cases. Figs. A6·1 and

A6•2 show such curves for the cases of Al and Cu targets[A601), A602)] with varying bombarding proton energy.

The data of Cu can be used for constructing the fragmentation parameters for the VH-group (iron group).

One notices in this case that the variation of yield curves with energy is rather remarkable. It can be imagined that large energy transfer to the nucleus occurs through meson production in the nucleon cascades so that

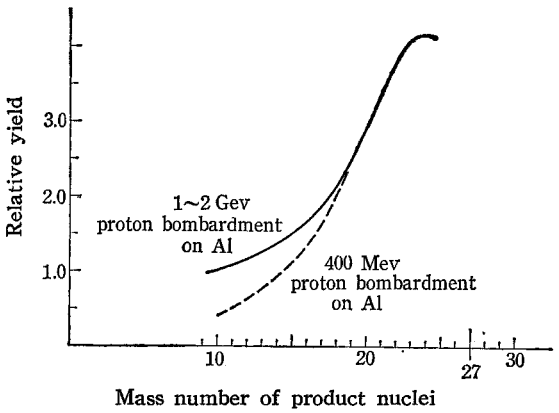

Fig. A6•1. The expected mass number distribution of the spallation product from proton bombardments on Al.

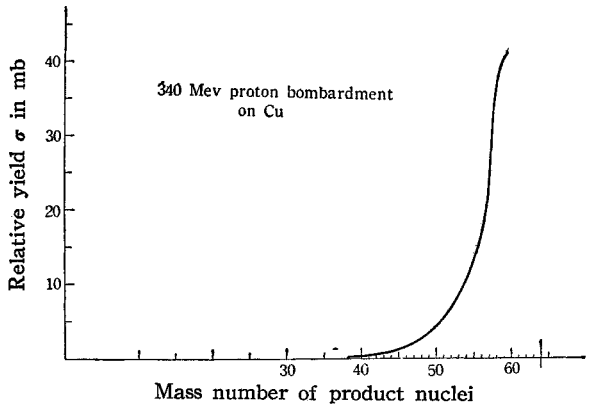

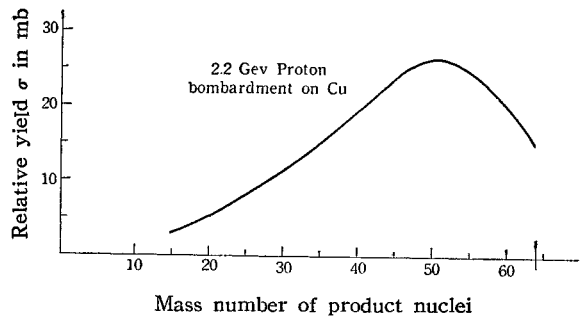

Fig. A6•2. The expected mass number distribution of the spallation products from proton bombardment on Cu.

the energy variation of spallation will be rather large only up to 1 Gev. For practical purposes the yield curve of Cu-data can be approximated by a Gaussian function.

$$F(A)=\text{const}\cdot\exp(-(A-A_0+a)^2/2a^2),$$

where A_0 and A are the mass number of initial and final nuclei. The numerical value of a is

$$a=\begin{cases}14 & \text{for } 2 \text{ Gev}\\ 3 & \text{for } 340 \text{ Mev.}\end{cases} \qquad \text{(A6·2)}$$

The fragmentation parameters of H-group can be inferred from the data of Al. In this case, the energy variation of the yield curve is not so large. It seems that the classical evaporation model is not valid for a nucleus as light as Al.

The break-up process of a medium nucleus can be studied from some measured reactions. The followings are the published experimental data of the concerned reactions.[A6·3] Since most of these are found to be almost constant in our energy regions, the table shows only the value for 1 Gev.

Table A6·1.

Target	Reaction	Cross section	Fraction to total
C^{12}	Be^7	10.6 mb.	5.3%
	Li^8	0.6 (at 340 Mev)	0.3
	C^{11}	23.4	12.0
N^{14}	C^{11}	20.6	9.8
	N^{13}	10.9	4.9
O^{16}	C^{11}	10.3	4.3
	N^{13}	7.5	3.1
	O^{15}	37.0	15.0

Appendix 7

Acceleration of the cosmic ray particles associated with the 11-year solar cycle modulation and Parker's model of the modulation phenomena

Suppose a perfect reflecting barrier, a, for the cosmic ray particles far away from the solar system, so that near the barrier the spectrum of cosmic rays can be considered the same as the unmodulated spectrum I_0dR.

We define a rather small region, b, as that region in which modulated spectrum is observed. Thus intense magnetic clouds exist only inside b.

Then the total energy of cosmic rays inside a including b will be increased by collisions with magnetic clouds as predicted by the Fermi acceleration mechanism.[A702] Inside b, however, we are observing only the reduced cosmic ray intensity. Therefore the energy of the cosmic rays between the regions a and b must be increased.

Thus, if we observe reduced intensity of cosmic rays on the earth, and if it is not due to the absorption phenomena, there must be acceleration associated with this reduction.

Based on a particular modulation model, we can calculate the order of magnitude of this acceleration of the particles. Parker's model[A701] of outward sweeping magnetic barrier seems to be one of the most promising for the interpretation of the modulation. In his model, particles colliding on this barrier from the outside diffuse into this magnetic field, but some fraction, μ, of them are driven back to the outside because the barrier is moving in the outward direction. On the other hand, almost all the particles colliding on the barrier will escape from b due to the same reason.

Thus, finally the intensity of the cosmic rays is reduced by a factor of $1-\mu$, and this is just the modulation factor B given in § 3•3. From these arguments it is now clear that a fraction, μ, of the particles makes head-on collision with the barrier. Thus, by the application of the Fermi's acceleration mechanism, cosmic ray particles get the energy per unit time

$$\Delta E \simeq S\int(1-B)f(E, V)Ej(E)dE, \qquad \text{(A7•1)}$$

where $j(E)$ is the differential energy spectrum of cosmic rays, S and V the surface area and the velocity of the barrier, respectively, and $f(E, V)$ Fermi's acceleration factor. f is given by

$$\begin{aligned} f &\sim V/c \quad \text{at extreme relativistic region,} \\ f &\sim 2V/c \quad \text{at non-relativistic region.} \end{aligned} \qquad \text{(A7•2)}$$

If we take

$$\begin{aligned} &V \sim 10^8 \text{ cm/sec}, \\ &S \sim 4\pi(10 \times \text{sun-earth distance})^2, \\ &B \sim 1/2, \end{aligned} \qquad \text{(A7•3)}$$

then we get

$$\Delta E \sim 10^{26\sim27} \text{ Gev/sec.} \qquad \text{(A7•4)}$$

This figure is one or two orders higher than that averaged for the case of the unusual Forbush increase which is estimated by Hayakawa[A703] to be

$10^{24\sim25}$ Gev/sec.

It is natural to consider that each star in the Galaxy is the source of such outward sweeping magnetic clouds, so that it can be considered as a source of acceleration for the cosmic ray particles. If we assume that about 10^{11} stars in the Galaxy have barriers similar to that of the sun in size, then the total amount of the energy gain by the above process is given by

$10^{37\sim38}$ Gev/sec,

which is still smaller than that demanded for the total cosmic ray acceleration.*

The detailed figures of these contributions from various stars are given and discussed in § 3•3.

Now we return back to the problem of the physical meaning of the quantities n and m introduced in § 3•3.

In his outward sweeping model, Parker has shown that the modulation factor is given by

$$B=e^{-\frac{3V}{v}\int\frac{dr}{\lambda}}, \tag{A7•5}$$

where λ is the scattering mean free path of the particles.

As shown in § 3•3, we introduce the modulation factor of the form

$$B\simeq e^{-n/R}, \tag{A7•6}$$

where we assume that n does not depend on R, R being the rigidity of the particle.

Then, if we compare our expression (A7•6) with Parker's expression (A7•5), we get

$$m=\frac{R}{v}\frac{d}{dR}v-R\frac{d}{dR}\ln\int\frac{dr}{\lambda} \tag{A7•7}$$

and

$$n=\frac{3R^m V}{v}\int\frac{dr}{\lambda}. \tag{A7•8}$$

As v is given by

$$v=\frac{Rc}{\left(R^2+\left(\frac{A}{Z}\right)^2\right)^{1/2}}, \quad (R \text{ in Gv}),$$

we get the rigidity dependence of the scattering mean free path of the particles from the expression (A7•7) if we have a complete data about the 11-year variation of the rigidity spectrum of cosmic rays. As shown in § 3•3, we get $m=0.9\pm0.5$, and since the value of $(R/v)(dv/dR)$ is $+0.5$

* The figure is estimated as 10^{42} Gev/sec.

around $R=2$ Gv, we get

$$\lambda \sim R^{0.4\pm0.3}.* \qquad \text{(A7·9)}$$

Next we discuss the absolute values of n listed in the Table 3·3·1 relating the features of the magnetic clouds by the expression (A7·8). As shown in that Table, n had values ranging from 5 to 10 in 1957, and had a slightly smaller value in 1956. Assuming that the thickness of the barrier is about 10 times the sun-earth distance and $V\sim10^3$ km/sec, we get

$$\lambda \sim 10^{11} \text{ cm}. \qquad \text{(A7·10)}$$

The radius of curvature of particles with rigidity 2 Gv in the field strength of 10^{-4} gauss is $7\cdot10^{11}$ cm. Thus referring to the slight rigidity dependence of λ in (A7·9), all figures of n and m are interpreted in terms of outward sweeping disordered magnetic fields with the strength of 10^{-5} to 10^{-4} gauss which extend up to a distance of about 10 times sun-earth distance. These are the commonly accepted figures, and this analysis of the experimental data is just complementary to the work of Hayakawa, Koshiba and Terashima[A704] and Terashima.[A705]

References

0001) P. Freier, E. J. Lofgren, E. P. Ney, F. Oppenheimer, H. L. Bradt and B. Peters, Phys. Rev. **74** (1948), 213.

0002) S. Hayakawa, K. Ito and Y. Terashima, Suppl. Prog. Theor. Phys. **6** (1958), 1.

0003) H. Aizu, Y. Fujimoto, S. Hasegawa. M. Koshiba, I. Mito, J. Nishimura, K. Yokoi and M. Schein, Phys. Rev. **116** (1959), 436; *Proc. Moscow Cosmic Ray Conf.* (1960) III, 96; Phys. Rev. **121** (1961), 1206.

1101) W. R. Webber, Suppl. Nuovo Cim. **8** (1958), 532.
J. Linsley, Phys. Rev. **101** (1956), 826.
F. B. McDonald, Phys. Rev. **104** (1956), 1723.
P. Meyer, Phys. Rev. **115** (1959), 1734.
E. P. Ney and D. M. Thon, Phys. Rev. **81** (1951), 1069.
T. Stix, Phys. Rev. **95** (1954), 782.

1102) C. J. Waddington, Phil. Mag. **2** (1957), 1059.
R. Cester, A. Debenedetti, C. M. Garelli, B. Quassiati, L. Tallone and M. Vigone, Nuovo Cim. **7** (1958), 371.
M. Koshiba, G. Schultz and M. Schein, Nuovo Cim. **9** (1958), 1.

1103) W. R. Webber, Suppl. Nuovo Cim. **8** (1958), 532.

1104) M. Rich and R. Madey, University of California Radiation Laboratory Report UCRL-2301, (1954).

1105) W. H. Barkas, University of California Radiation Laboratory Report UCRL-ZN-991-REV (unpublished).

1201) B. Rossi and K. Greisen, Rev. Mod. Phys. **13** (1941), 240.

1202) C. O'Ceallaigh, Phil. Mag. **42** (1951), 1032.

1203) P. H. Fowler and D. H. Perkins, Phil. Mag. **46** (1955), 587.

* If we assume an ordered magnetic field. λ may be approximated as a gyro-radius of the particle, so that $\lambda\sim R$. Other extreme case is that of discrete clouds with strong magnetic field. In this case we may approximate λ to be independent of R.

1204) W. A. McKinley and H. Feshbach, Phys. Rev. **74** (1948), 1759.
1205) H. L. Bradt and B. Peters, Phys. Rev. **74** (1948), 1828.
1206) N. F. Mott, Proc. Roy. Soc. **124** (1929), 425.
1207) D. R. Corson and A. O. Hanson, Ann. Rev. Nucl. Sci. **3** (1953), 67.
1208) J. Nishimura, Research in Elementary Particle Physics, Vol. IV, *Experimental Nuclear and Cosmic Ray Physics*, p. 225, Iwanami Pub. Co. (1954) (in Japanese).
M. Miyagaki, *Thesis, University of Osaka* (1956).
De Marco et al. also put the method into practice independently, and recently the Indian Group made extensive use of the method:
A. de Marco, A. Milone and M. Reinharz, Nuovo Cim. **1** (1955), 1041 (in Italian).
S. Biswas, P. J. Lavakare, K. A. Neelakantan and P. G. Schukla, *Proc. Moscow Cosmic Ray Conf.* (1960) III, 102.
1209) H. H. Heckman, B. L. Perkins, W. G. Simon, F. M. Smith and W. H. Barkas, Phys. Rev. **117** (1960), 544.
1210) L. Voyvodic, *Progress in Cosmic Ray Physics* (North-Holland Publishing Company, Amsterdam, 1954), Vol. II, 215.
1211) M. F. Kaplon, B. Peters, H. L. Reynolds and D. M. Ritson, Phys. Rev. **85** (1952), 295.
1212) D. H. Perkins, Phil. Mag. **41** (1950), 138.
1213) V. Y. Rajopadhye and C. J. Waddington, Phil. Mag. **3** (1958), 19.
2101) P. S. Freier, G. W. Anderson, J. E. Naugle and E. P. Ney, Phys. Rev. **84** (1951), 322.
R. E. Danielson, P. S. Freier, J. E. Naugle and E. P. Ney, Phys. Rev. **103** (1956), 1075.
R. E. Danielson and P. S. Freier, Phys. Rev. **109** (1958), 151.
V. Bisi, R. Cester, C. M. Garelli and L. Tallone, Nuovo Cim. **10** (1959), 881.
2102) M. V. K. Appa Rao, S. Biswas, R. R. Daniel, K. A. Neelakantan and B. Peters, Phys. Rev. **110** (1958), 751.
2103) C. J. Waddington, Progress in Nuclear Physics **8** (1960), **1**.
2104) Y. Hirashima, Nuovo Cim. **12** (1959), 1.
2105) P. S. Freier, G. W. Anderson, J. E. Naugle and E. P. Ney, Phys. Rev. **84** (1951), 322.
2106) J. H. Noon and M. F. Kaplon, Phys. Rev. **97** (1955), 769.
2201) P. H. Fowler, C. J. Waddington, P. S. Freier, J. Naugle and E. P. Ney, Phil. Mag. **2** (1957), 157.
2202) See 0003)
2203) S. F. Singer, Suppl. Nuovo Cim. **8** (1958), 342.
2204) See 1102)
2205) See 2103)
2206) P. S. Freier, E. P. Ney and C. J. Waddington, Phys. Rev. **113** (1959), 921.
2207) C. J. Waddington, Suppl. Nuovo Cim. **8** (1958), 518.
P. L. Jain, E. Lohrmann and M. W. Teucher, Phys. Rev. **115** (1959), 654.
3101) See 0002)
3102) V. Y. Rajopadhye and C. J Waddington, Phil. Mag. **3** (1958), 19.
P. H. Fowler, R. R. Hillier and C. J. Waddington, Phil. Mag. **2** (1957), 293.
3103) R. Cester, A. Debenedetti, C. M. Garelli, B. Quassiati, L. Tallone and M. Vigone, Nuovo Cim. **7** (1958), 371.
3104) A. H. Rosenfeld, R. A. Swanson and S. D. Warshaw, Phys. Rev. **103** (1956), 413.
3201) M. Taketani, T. Hatanaka and S. Obi, Prog. Theor. Phys. **15** (1956), 89.
3202) E. M. Burbidge, G. R. Burbidge, W. A. Fowler and F. Hoyle, Rev. Mod. Phys. **29** (1957), 547.
3203) G. R. Burbidge and E. M. Burbidge, Handbuch der Physik **51**, *Stellar Evolution.*
3204) See 0002)
3205)
(i) H. E. Suess and H. C. Urey, Handbuch der Physik **51**, *Die Häufigkeit der Elements in den Planeten und Meteoriten.*

(ii) L. H. Aller and J. Jugaku, *Report to Cleveland Meeting of A. A. J.*
(iii), (iv), (v) L. H. Aller, Handbuch der Physik **51**, *The Abundance of the Elements in the Sun and Stars.*
(vi) A. G. W. Cameron, Astrophys. J. **129** (1959), 676.
(vii) L. H. Aller and J. Jugaku, Suppl. Astrophys. J. **3**, (1957), No. 25.
(viii) L. H. Aller and J. Jugaku, Suppl. Astrophys. J. **4**, (1959), No. 38.
(ix) See 3202)
3306) S. Hayakawa, Prog. Theor. Phys. **15** (1956), 111.
3207) I. S. Shklovski, Dokl. Akad. Nauk, SSSR **90** (1953), 983.
3208) L. H. Aller, Astrophys. J. **125** (1957), 84.
3301) P. S. Freier, E. P. Ney, and C. J. Waddington, Phys. Rev. **114** (1959), 365.
3302) F. B. McDonald, Phys. Rev. **116** (1959), 462.
P. Meyer, Phys. Rev. **115** (1959), 1734.
3303) P. H. Fowler, P. S. Freier and E. P. Ney, Suppl. Nuovo Cim. **8** (1958), 492.
C. J. Waddington, Nuovo Cim. **6** (1957), 748.
F. B. McDonald, Phys. Rev. **104** (1956), 1723.
L. R. Davis, H. M. Caulk and C. Y. Johnson, Phys. Rev. **101** (1956), 801.
P. J. Duke, *Proc. Moscow Cosmic Ray Conf.* (1960) III, 89.
3304) Cf. L. I. Dorman, *Cosmic Ray Variation* (State Publishing House for Technical and Theoretical Literature. Moscow, 1957).
3305) Y. Terashima, Prog. Theor. Phys. **23** (1960), 1138.
3306) *Cosmic Ray Intensity during the IGY* (National Committee for the IGY, Science Council of Japan, Tokyo), No. 1 (1959).
A. G. Fenton, K. B. Fenton and D. C. Rose, Can. J. Phys. **36** (1958), 824.
3307) J. A. Lockwood, Phys. Rev. **112** (1958). 1750.
3308) P, J. Coleman, Jr., Leverett Davis and C. P. Sonett, Phys. Rev. Letters **5** (1960), 43.
3309) L. Davis, Phys. Rev. **100** (1955), 1440.
3310) D. Evans, *Proc. Moscow Cosmic Ray Conf.* (1960) III, 92.
3311) E. N. Parker, Phys. Rev. **103** (1956), 1518; **110** (1958), 1445.
A201) B. Rossi, *High-Energy Particles* (Prentice-Hall Inc., Englewood Cliffs, N. J.), 2nd Ed. (1956), p. 544.
G. B. Beiser, R. C. Haymes and S. A. Korff, *Research Ballooning Project Report* (New York University, 1960).
A202) E. Jahnke and F. Emde, *Tables of Functions* (Dover Publications, New York), 4th Ed. (1945), p. 1.
A301) See 1209)
A401) H. L. Bradt and B. Peters, Phys. Rev. **77** (1950), 54.
A402) See 3102) and 3103)
A403) I. Fernbach, R. Serber and T. B. Taylor, Phys. Rev. **75** (1949), 1352.
A404) F. F. Chen, C. P. Leavitt and A. M. Shapiro, Phys. Rev. **103** (1956), 211.
A405) F. F. Chen, C. P. Leavitt and A. M. Shapiro, Phys. Rev. **99** (1955), 857.
A406) T. Coor, D. A. Hill, W F. Hornyak and L. W. Smith, Phys. Rev. **98** (1955), 1369.
A407) R. W. Williams, Phys. Rev. **98** (1955), 1387.
A601) G. Friedlander, J. Hudis and R. Wolfgang, Phys. Rev. **99** (1955), 263.
A602) G. Friedlander, J. M. Miller, R. Wolfgang, J. Hudis and E. Baker, Phys. Rev. **94** (1954), 727.
A603) The authors are grateful to Dr. K. Ito for offering us his unpublished review article on these high energy reactions.
A701) See 3310)
A702) E. Fermi, Phys. Rev, **75** (1949), 1169.
A703) See 0002)
A704) S. Hayakawa, M. Koshiba and Y. Terashima, *Proc. Moscow Cosmic Ray Conf.* (1960) III, 181.
A705) See 3305)